The Role of Heat Shock Protein A4 (HSPA4) in the Heart

Dissertation

for the award of the degree
"*Doctor rerum naturalium*"
of the Georg-August-Universität Göttingen

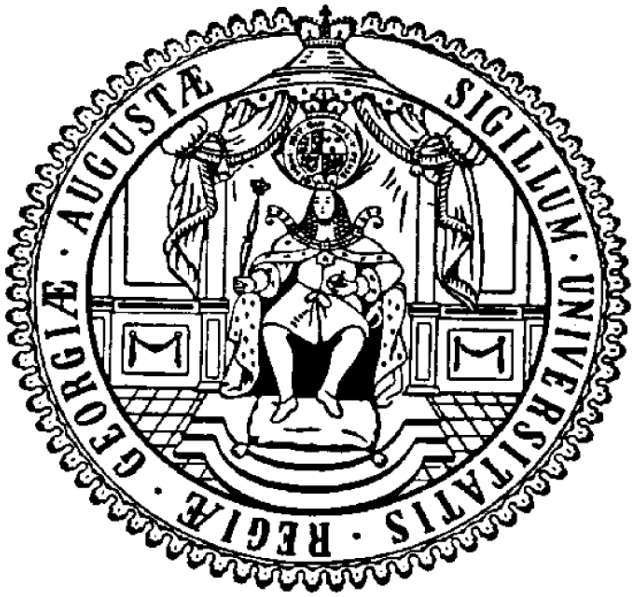

within the doctoral program Molecular Medicine
at the Georg-August University School of Science (GAUSS)

submitted by

Daniel Marques Rodrigues
born in Brilon, Germany

Göttingen, November 2022

Thesis Committee Members

Prof. Dr. med. Karl Toischer (1st reviewer)
Cardiology and Pneumology
University Medical Center Göttingen

Prof. Dr. rer. Nat. Susanne Lutz (2nd reviewer)
Pharmacology and Toxicology
University Medical Center Göttingen

Prof. Dr. rer. Nat. Michael Thumm
Cellular Biochemistry
University Medical Center Göttingen

Extended committee Members

Prof. Dr. med. Ralf Dressel
Institute of Cellular and Molecular Immunology
University Medical Center Götingen

Prof. Dr. med. Elisabeth Heßmann
Gastroenterology and GI-Oncology
University Medical Center Götingen

Dr. rer. physiol. Shiv Singh
Gastroenterology and GI-Oncology
University Medical Center Götingen

Date of oral examination: 02.02.2023

Affidavit

I hereby declare that I have written the dissertation

“The Role of Heat Shock Protein A4 (HSPA4) in the Heart”

independently with no other aids or sources than quoted.

_____

Daniel Marques Rodrigues
Göttingen, 30.11.2022

List of Publications

- Elkenani, Manar, Amal Z. Barakat, Torsten Held, Daniel Marques Rodrigues, Sherok Mobarak, Surabhi Swarnka, Ibrahim M. Adham, and Belal A. Mohamed. "Heat shock protein A4 ablation leads to skeletal muscle myopathy associated with dysregulated autophagy and induced apoptosis." *Journal of translational medicine* 20. no. 1 (2022): 1-10.

- Mohamed, Belal A., Manar Elkenani, Sherok Mobarak, Daniel Marques Rodrigues, Karthika Annamalai, Moritz Schnelle, Michael Bader, Gerd Hasenfuss, and Karl Toischer. "Hemodynamic stress-induced cardiac remodelling is not modulated by ablation of phosphodiesterase 4D interacting protein." *Journal of cellular and molecular medicine* 26, no. 16 (2022): 4440-4452.

- Kaiser, Franz, Zhiyi Lv, Daniel Marques Rodrigues, Jan Rosenbaum, Timo Aspelmeier, Jörg Großhans, and Karen Alim. "Mechanical model of nuclei ordering in Drosophila embryos reveals dilution of stochastic forces." *Biophysical journal* 114, no. 7 (2018): 1730-1740.

Zusammenfassung:

Nicht-ischämische Kardiomyopathien können durch genetische Mutationen, aber auch durch zytotoxische Einflüsse von Chemotherapeutika und die Ansammlung fehlgefalteter Proteine verursacht werden.

Bei Mäusen, bei denen das Hitzeschockprotein A4 (HSPA4) ausgeschaltet wurde, wurden Muskeldystrophie, juvenile Mortalität und Wachstumsverzögerung sowie konzentrische Herzhypertrophie festgestellt. Die Überexpression von HSPA4 hat ein Gleichgewicht in der Proteinqualitätskontrolle bewahrt und eine hypertrophe Entwicklung der linken Herzkammer verhindert. Das lückenhafte histologische Muster der Fibrose in mutierten Herzen deutet auf eine Unterbrechung der Signalübertragung hin, die vermutlich auf eine Unterbrechung der Gap Junction zurückzuführen ist. Es ist anzunehmen, dass HSPA 4 im Herzen eine wichtige Rolle spielt, um die Aggregation von Proteinen zu verhindern und den Abbau durch das autophagische System zu fördern.

Darüber hinaus wurden Mäuse, die mit Doxorubicin behandelt wurden, vor den proteotoxischen Nebenwirkungen dieser Behandlung geschützt, indem HSPA4 im Herzen überexprimiert und anschließend mit einer akuten tödlichen Dosis des Medikaments belastet wurde. Hier konnten die geschädigten Proteine durch eine erhöhte HSP70:HSPA4-Chaperon-Effizienz und vermutlich durch Chaperon-vermittelte Autophagie stabilisiert werden.

Die Chaperon-vermittelte Autophagie ist ein HSPA70- und damit auch HSPA4-abhängiger Prozess, der die Integrität der lysosomalen Membran, die Ansäuerung und den autophagischen Fluss umfasst. Ob dieser Prozess einen anderen Nukleotidaustausch erfordert und ob HSP70:HSPA4 daran beteiligt ist, muss noch herausgefunden werden.

Andererseits könnten die DOX-induzierte mitochondriale Schädigung und die gestörten autophagischen Prozesse zu einem metabolischen Ungleichgewicht in den Kardiomyozyten führen und ein eher fötales Genprogramm fördern, das atrophische Wege initiiert, die zum "Winterschlaf" der Kardiomyozyten führen. Die ATP-unabhängigen Holdase-Fähigkeiten von HSPA4 könnten ROS-geschädigte mitochondriale Proteine stabilisieren. Im Gegensatz dazu würde eine erhöhte autophagische Clearance einen größeren Pool an Aminosäuren bereitstellen, die katabolisiert werden könnten.

Darüber hinaus führte der überschüssige HSPA4-Proteinpool bei den mit AAV9-HSPA4 behandelten Kontrollmäusen nicht zu einer Hyperaktivierung des Proteinabbaus durch UPS oder autophagische Clearance. Dies deutet darauf hin, dass der Überschuss bei umgekehrten Umbauprozessen therapeutisch wirken könnte. Die HSP70:HSPA4-Chaperon-vermittelte Autophagie könnte in diesem Zusammenhang von Vorteil sein, und es wäre interessant, die zeitabhängige proteostatische Wirkung, die der autophagische Abbau zu haben scheint, weiter zu untersuchen.

Es bedarf weiteren Forschungen, den unzureichenden Proteinpool durch Überexpression zu ersetzen, um die Herzfunktion zu verbessern. Die Stärkung der Proteinstabilität und der Autophagie könnte als adjuvante Therapie zu kardiotoxischen Chemotherapeutika wie Doxorubicin von Vorteil sein. Es müssen jedoch noch weitere Experimente durchgeführt werden, bevor eine Schlussfolgerung gezogen werden kann. Letztendlich scheint die Überexpression von HSPA4 positive Auswirkungen auf die Proteinhomöostase im Herzen zu haben, und gentherapeutische Eingriffe könnten vielversprechende neue Perspektiven für die Zukunft bieten.

Abstract:

Non-ischemic cardiomyopathies may be caused by genetic mutations but may also result from cytotoxic influences of chemotherapeutic drugs and the accumulation of misfolded proteins.

Heat shock protein A4 (HSPA4) knockout mice have been shown to have muscular dystrophy, juvenile mortality and growth retardation, and concentric cardiac hypertrophy. Overexpression of HSPA4 has preserved a balance in protein quality control and avoided hypertrophic development of the left ventricle. The patchy histological pattern of fibrosis in mutant hearts suggests pauses in signal transmission, presumably due to gap junction disconnection. In the heart, it may be assumed that HSPA 4 is essential for preventing the aggregation of proteins and promoting degradation by the autophagic system.

Additionally, mice treated with doxorubicin were protected from the proteotoxic side effects of this treatment by overexpressing HSPA4 in the heart, after which they were stressed with an acute lethal dose of the drug. Here the damaged proteins could be stabilized by increased HSP70:HSPA4 chaperoning efficiency and presumably chaperone-mediated autophagy.

Chaperone-mediated autophagy is an HSPA70 and, therefore, also HSPA4 dependent process that encompasses lysosomal membrane integrity, acidification, and autophagic flux. If this process requires different nucleotide exchange and if HSP70:HSPA4 is involved has yet to be discovered.

On the other hand, the DOX-induced mitochondrial damage and disrupted autophagic processes could lead to a metabolic imbalance in the cardiomyocytes, promoting a more fetal gene program initiating atrophic pathways that lead to cardiomyocyte “hibernation” The ATP-independent holdase abilities of HSPA4 could stabilize ROS-damaged mitochondrial proteins. In contrast, an increased autophagic clearance would provide an increased pool of amino acids that could be catabolized.

Furthermore, excess HSPA4 protein pool did not lead to hyperactivation of protein degradation by either UPS or autophagic clearance in AAV9-HSPA4 treated control mice. This suggests excess could be therapeutic in reverse remodeling processes. The HSP70:HSPA4 chaperone-mediated autophagy could be beneficial in this context, and it would be interesting to investigate further the time-dependent proteostatic effect Autophagic degradation seems to have.

It needs further research to supplement the insufficient protein pool with overexpression to improve cardiac function. Strengthening protein stability and autophagy could be advantageous as an adjuvant therapy to cardiotoxic chemotherapeutics like doxorubicin. Still, further experiments must be tested before drawing a conclusion if this holds.

Ultimately, HSPA4 overexpression seemed to have beneficial effects on protein homeostasis in the heart, and gene therapeutic interventions might hold promising new prospects for the future.

Table of Contents

List of Figures

Abbreviations

Activating Transcription Factor 6 (ATF6) _____ 19

Adeno associated virus 9 (AAV9) _____ VII

Analysis of variance (ANOVA) _____ 29

Ankyrin3(AnkG); _____ 16

ATP and peptide-binding protein in germ cells 1(APG-1) _____ 13

ATP and peptide-binding protein in germ cells-2(APG-2) _____ 13

ATPase Sarcoplasmic/Endoplasmic Reticulum Ca2+ Transporting 2 (SERCA) _____ 5

Autophagy Related 12 (Atg12) _____ 26

Autophagy Related 13 (ATG13) _____ 25

Autophagy Related 5 (Atg5) _____ 25

BCL2 Apoptosis Regulator (BCL2) _____ 16

BCL2 Associated Athanogene (BAG3) _____ 12

BCL2 Associated Athanogene 1 (BAG-1) _____ 10

BCL2 Interacting Protein 3 (Bnip3) _____ 25

1. Introduction

1.1. An overview about Cardiomyopathies

Cardiomyopathies are a heterogeneous group of non-coronary heart diseases, including dilated cardiomyopathy (DCM), hypertrophic cardiomyopathy (HCM), restrictive cardiomyopathy (RCM), and more recently, arrhythmogenic cardiomyopathy [Goodwin 1961, Corrado 2017]. DCM encompasses cardiac enlargement with a typical ventricular wall thickness and varying extent of fibrosis that eventually progresses into heart failure [McKenna 2017]. Familial DCM can be caused by mutations in various genes encoding proteins in the sarcomere, cytoskeleton, ion channels, nuclear envelope, and mitochondria, but most commonly, mutations in sarcomeric protein Titin [Herman 2012]. Outside of the inherited disease, viral-induced myocarditis can lead to DCM years after the acute infection has passed [Trachtenberg 2017]. Furthermore, cardiac toxins are an important cause of DCM. The most common is dietary alcohol, but notably also chemotherapeutic drugs [Bozkurt 2016]. HCM shows concentric hypertrophy along with fibrosis and obstruction of the ventricular blood flow [Nishimura 2017]. Familial cases can be caused by mutations in the myosin heavy chain gene and other sarcomeric proteins, and ventricular fibrillation is the most common cause of death in HCM [Maron 2000].

Arrhythmogenic cardiomyopathies can be caused by mutations in intercellular adhesion molecules, for example, plakophilin 2 (PKP2) and desmoplakin (DSP) [Thiene 2015]. Initially only associated with right ventricular disease progression, the involvement of the left ventricle and heart failure increased in recognition [Corrado 2017].

Restrictive cardiomyopathies reduce the flexibility of the heart muscle, and the first example was described in familial amyloid heart disease [Pilebro 2016]. Cardiac amyloidosis is caused by misfolded proteins forming aggregated cytotoxic fibrils and ultimately leading to the progression of heart failure [Muchtar 2017].

1.2. Cardiac remodeling and transition to heart failure

Cardiac remodeling was defined at the beginning of this century as a group of molecular, cellular, and interstitial changes that manifested clinically as changes in size, mass, geometry, and function of the heart after injury and was categorized into adaptive/physiological or maladaptive/pathological remodeling [Cohn 2000]. The frequent asymptomatic progression makes the disease hard to detect, and it can eventually lead to heart failure, with only 50 % of diagnosed patients surviving for five years [Liu 2014]. Cardiac remodeling entails a metabolic switch and alterations in mitochondrial function in every cell type of the heart, namely, cardiomyocytes, fibroblasts, endothelial cells, and leucocytes **(Figure 1.2.0)**.

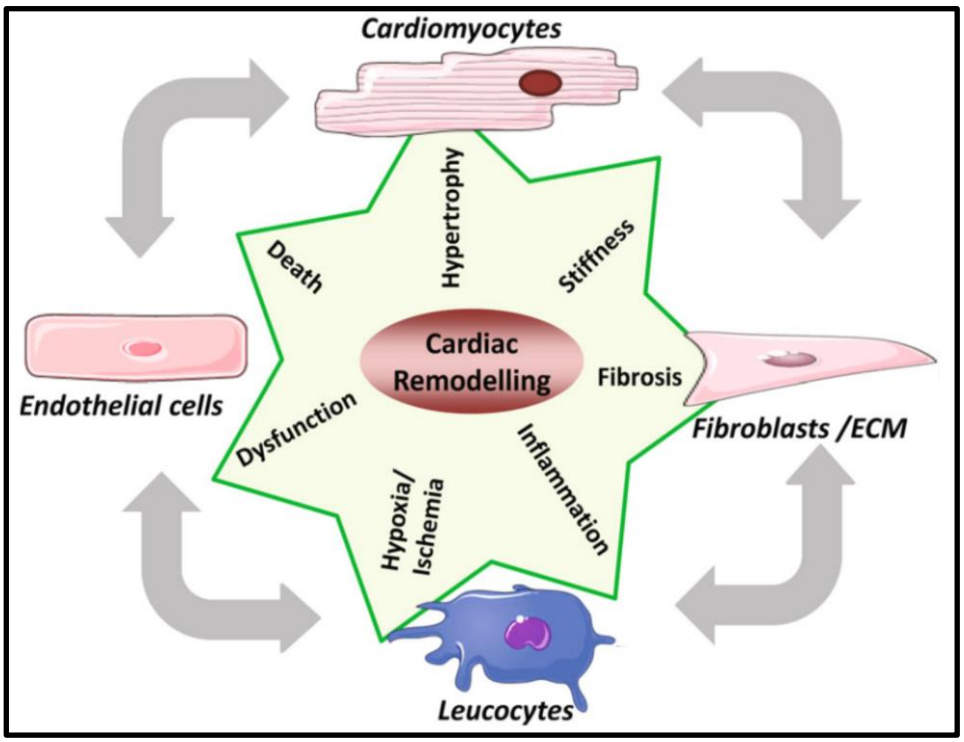

Figure 1.2.1: ***Crosstalk between cell types in cardiac remodeling.***

The organ of the heart is composed of various cell types interacting with each other. A complex cellular network adapts to the increased force in response to stress by strengthening cardiomyocytes via hypertrophy. Eventually, the response turns maladaptive transdifferentiating fibroblasts into myofibroblasts, increasing extracellular matrix (ECM) production. The developing fibrosis and cardiac stiffness cause an inflammatory response involving cytokines, eventually leading to hypoxic conditions, further promoting apoptosis of endothelial vessel cells promoting the cycle leading to cardiac dysfunction. (Adapted from Gonzales *et al.*, 2020)

The main consequence of pathological remodeling is the development of cardiac dysfunction, rooted in cellular and molecular changes to a more fetal gene program in response to prolonged stress or injury [Zornoff 2009]. In response to increased wall tension, cardiomyocytes undergo a differential hypertrophic thickening or elongation depending on whether the stretch is induced by pre- or afterload [Toischer 2010]. Consequently, the cardiomyocytes secrete natriuretic peptides ANP and BNP to lower blood pressure [Goetze 2020]. Cardiac troponins are released after cardiomyocyte injury or death and are a robust indicator of cardiac dysfunction [Kociol 2010]. One of the molecules produced by hypertrophic cardiomyocytes is growth differentiation factor-15 (GDF-15), which is involved in cardiac hypertrophy, fibrosis, and endothelial dysfunction [Wesseling 2020].

Other cell types than cardiomyocytes are affected in the remodeling process as well. The excretion of pro-fibrotic factors will affect cardiac fibroblasts, activating or transdifferentiating them into myofibroblasts, leading to increased secretion of collagen fibers into the ECM and inducing cardiac fibrosis. Here an excessive deposition of primarily collagen type I & III occurs [López 2021]. In the two-step maturation process of collagen fibrils, lysyl oxidase (LOX) family proteins play a crucial role and are another biomarker for increased cardiac stiffness [Yang 2016]. These fibers are involved in the regulation of apoptosis, the restoration of pathological deformations, the maintenance of the alignment of myocardial structures and stability during contraction, and the expression of cytokines and growth factors [Zannad 2010]. Increased ECM stiffness

may further perpetuate cardiac fibroblasts' activation and promote a pro-fibrotic milieu. The dysregulation of any of these processes can contribute to cardiac fibrosis and therefore stiffening of the ventricle and can be a predictor for mortality in cardiac dysfunction patients [López 2015].

One-third of cardiac cells belong to the microvascular endothelium, which shares its own cardiovascular risk factors [Camici 2020]. The endothelial layer not only separates blood from tissue but also communicates with leucocytes permeating an immune response [Shu 2019]. In fact, the peptide endothelin 1 (ET1), the most potent vasoconstrictor, is excreted by the endothelial cells and promotes cardiac hypertrophic response to mechanical stimuli [Jankowich 2020]. Finally, while macrophages are part of the cells represented in a healthy heart, an influx of immune cells occurs during cardiac remodeling, leading to the excretion of a wide array of pro- and anti-inflammatory cytokines [Steffens 2020. Swirski 2018].

Other than these cells directly forming the organ of the heart, the neurohormonal systems of the sympathetic nervous system and the renin-angiotensin-aldosterone system are involved in cardiac remodeling [Sayer 2014]. Their activation leads to altered gene expression and, ultimately, changes in the geometry of the heart. Ventricular wall thickness, cavity diameter, and ventricle shape can be affected [Norton 2002]. In the last two decades, the ventricular substructure of cardiac muscle fibers into basal and apical loops, each with distinct contraction and relaxation intervals needed for physiological ejection, has been misaligned after cardiac remodeling [Buckberg 2015]. The contraction-relaxation intervals are governed by neurohormonal stimulation, fiber alignment, and the homeostasis of calcium release from the sarcoplasmic reticulum. Here during systole and uptake during diastole, essential proteins like L-type calcium channels, ryanodine receptor, calsequestrin, and SERCA-2a are involved [Luo 2013].

The contractile myosin proteins are composed of a pair of the heavy chain (alpha and beta) and two pairs of light chains. The MHC-alpha isoform is primarily found in atrial cardiomyocytes. In contrast, the MHC-beta isoform is found in the ventricular cells of the human heart. During cardiac remodeling, an isoform switch in ventricular cells can occur a weakening contraction [Maytin 2002]. One potential cause of cardiac fibrosis is the infiltration of the heart by immune cells upon injury, leading to the re-expression of fetal genes, activation of metalloproteinases, and proliferation of fibroblast, as well as apoptosis of cardiomyocytes [Epelman 2015]. Another trigger of fibroblast activation and cardiomyocyte damage is the chronic energetic deficit during remodeling, leading to a switch from fatty acid to glucose metabolism and the increased production of reactive oxygen species [Azevedo 2013]. Cardiac remodeling can result from pressure or volume overload and possible loss of functional cardiomyocytes, but also proteinopathies were found to progress the cardiac remodeling since mice that express aggregate-prone cardiomyocytes show progressive cardiac remodeling [Pattinson 2008].

In cardiac remodeling, the typical cardiomyocyte structures are rearranged as a chronic maladaptive process, leading to progressive ventricular dilatation, myocardial hypertrophy, fibrosis, and diminished cardiac performance arising from cardiomyocyte death and fibrosis [Pfeffer 1990]. Cardiomyopathy, valvular dysfunction, and chronic hypertension cause pressure or volume overload and load-induced remodeling [Gottlieb 2012]. The initial cardiac hypertrophy is an adaptive response improving function and reduces stress on the ventricular wall, which will turn maladaptive under chronic stress [Swynghedauw 1999]. The prolonged hypertrophy and induced fibrosis disrupt microcirculation, tissue hypoxia, and apoptosis [Osterholt 2013, De Boer 2003]. Therefore, reversing cardiac hypertrophy and fibrosis is a major goal for therapeutic advances [Tarazi 1985, Schmieder 1996]. Autophagy plays a crucial role in

maintaining physiological protein homeostasis in the heart and is differentially regulated in the pressure overload model [Nakai 2007]. In the initial compensatory phase, autophagic activity is lowered as b-adrenergic stimulation that induces cardiac hypertrophy was shown to inhibit autophagy [Pfeifer 1987]. Along these lines, induction of autophagy by Rapamycin treatment, which inhibits the upstream regulator mTORC, prevents cardiac hypertrophy in the TAC model [Ha 2005]. During pressure overload, the epigenetic micro-RNA miR-212 and miR132 were upregulated and acted as anti-autophagic factors by targeting the transcription factor FoxO3. If these micro RNAs were inhibited, hypertrophy was prevented [Ucar 2012]. Therefore, a lowered autophagic activity precedes the initialization of the hypertrophic response and can be prevented by inducing the autophagic pathway. In contrast to these findings, the histone deacetylase inhibitor trichostatin-A prevented cardiac hypertrophy by suppressing the remodeling-induced hyperactivation of the autophagic system [Cao 2011]. Ultimately balanced protein quality control and degradation processes are essential components in the physiological function of the heart **(Fig 1.2.2)**.

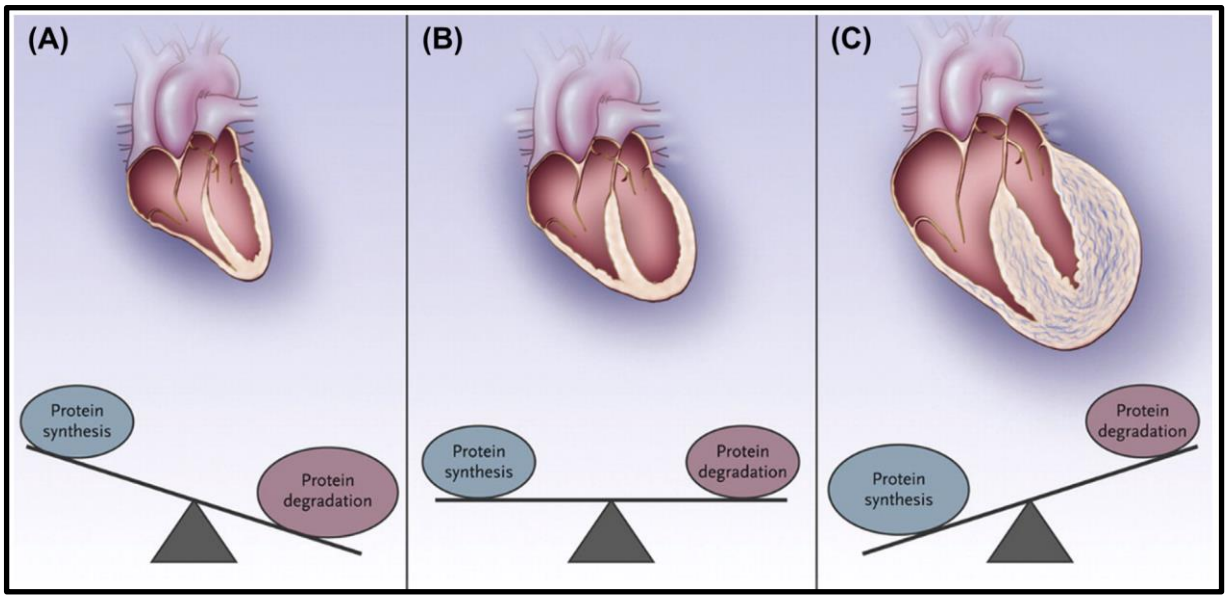

Figure 1.2.2 Morphological changes in cardiac remodeling

Protein synthesis and degradation must be fine-tuned in the heart to maintain balance. Under normal physiological function, an equilibrium in protein quality control is achieved (B). During mechanical unloading, for example, in the zero-G environment and bedridden patients, the heart muscle atrophies, which means that more protein is degraded than synthesized, but it is often a reversible process after an average load is recovered (A). During high periods of stress, the heart muscle compensates with the thickening of the ventricular walls as cardiac hypertrophy develops (C). The higher need for functional proteins increases the synthesis, and metabolic stress overburdens protein degradation systems. Additionally, cardiac fibrosis develops in chronically hypertrophic hearts, which is irreversible. Eventually, the heart muscle decompensates by dilating in volume and losing functionality leading to heart failure. (Figure adapted from Harvey and Leinwand 2014)

1.3. Protein quality control is regulating protein homeostasis

The disruption of protein homeostasis(proteostasis) is the focus of more and more research as the aggregation of proteins is recognized in numerous degenerative diseases [Hipp 2014]. Proteostasis is especially interesting in post-mitotic cells like cardiomyocytes, as they generally cannot compensate for damage via asymmetric cell division since the heart has a minimal regenerative potential [Rujano 2006]. In addition, the initiation of the cell cycle is suppressed because a more fetal gene program expressing genes like c-myc are involved in proliferation and apoptosis [Evan 1995]. Because of this and to deal with misfolded proteins, stringent quality control systems have evolved, including chaperone heat shock proteins, degradation in the ubiquitin-proteasome system, and autophagic-lysosome-directed degradation **(Fig 1.3.1)**. These systems will work independently or in concert with each other to ensure the balance between protein synthesis and degradation [Willis 2013].

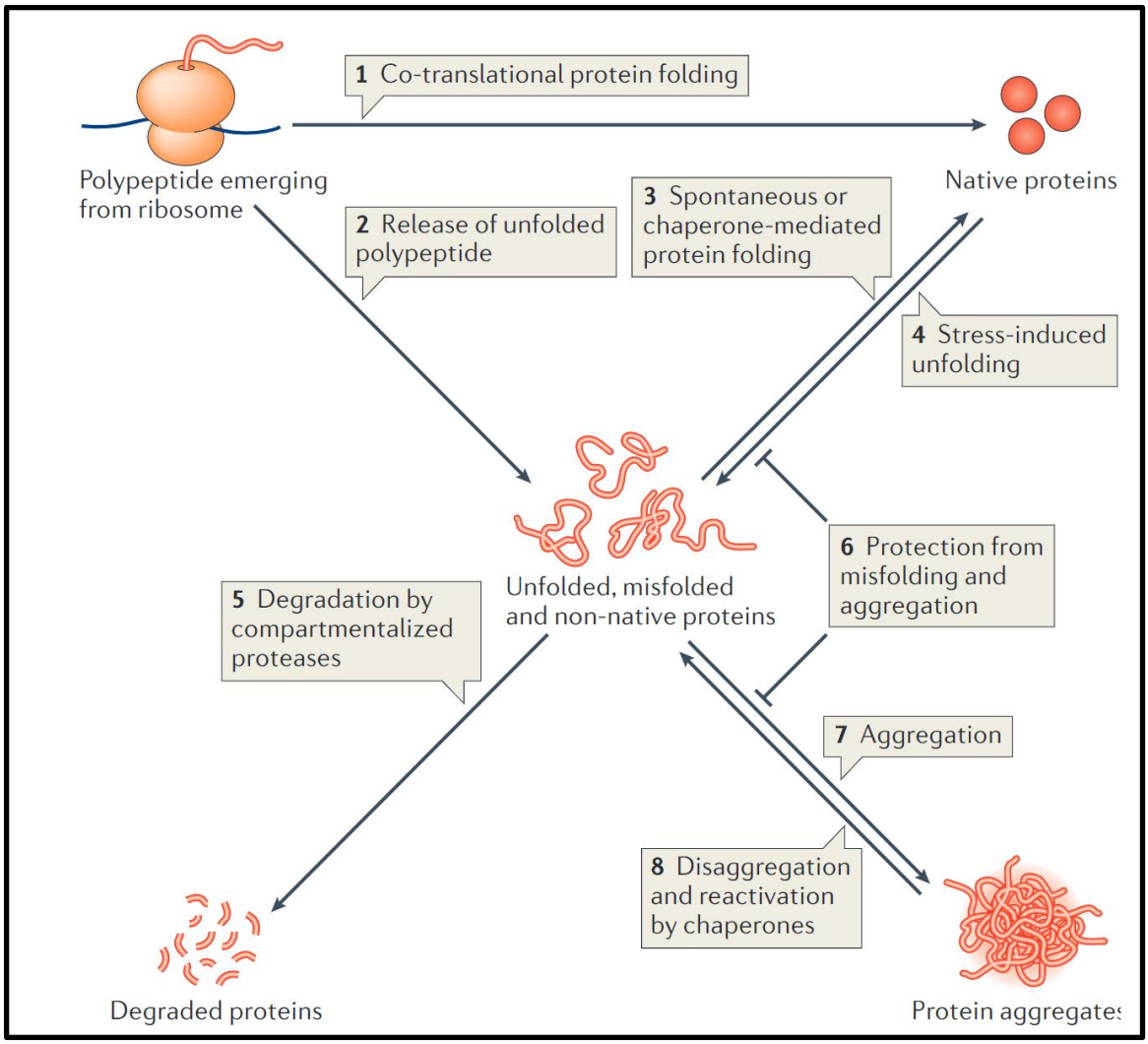

Figure 1.3.1The multitude of functions that chaperone heat shock proteins perform.

Tertiary protein structure is essential for the physiological function of any protein in the cell. During translation, the polypeptide is supported by chaperones to be folded into a native structure [1] or remains unfolded [2]. If the conditions are ideal, the proteins can undergo spontaneous folding. Otherwise, chaperones are recruited again to support the folding process [3]. Under stressful conditions, for example, high tensile forces or prolonged hypoxia, proteins can lose their tertiary structure [4]. Suppose these proteins stay misfolded for a prolonged time. In that case, they will be marked by selective ubiquitinates and are guided to the cell's recycling system, namely the proteasome, a tunnel-like structure of multiple subunits of proteases [5]. Another function of chaperones is to support the native structure of proteins and prevent misfolding or aggregation [6]. Aggregation can occur if the number of misfolded proteins outweighs the available chaperones, and the proteasome is overburdened [7]. If the protein quality control is recovered or more chaperones are expressed, chaperones can assist in the disaggregation of protein aggregates, returning them to physiological function [8] (figure adapted from Doyle 2013).

Chaperones classically act first in interacting with the hydrophobic domains of newly synthesized proteins to stabilize and prevent aggregation. Typically, increased stress by misfolded proteins leads to dissociating heat shock factor-1 (HSF1) from HDAC6

and HSP90. HSF-1 then translocates to the nucleus and leads to the expression of other chaperones like HSP70. HSP40, HIP, and HOP, forming the HSC70 complex, which will assist in refolding the cargo **(Fig 1.3.2)** [Trüe 2012].

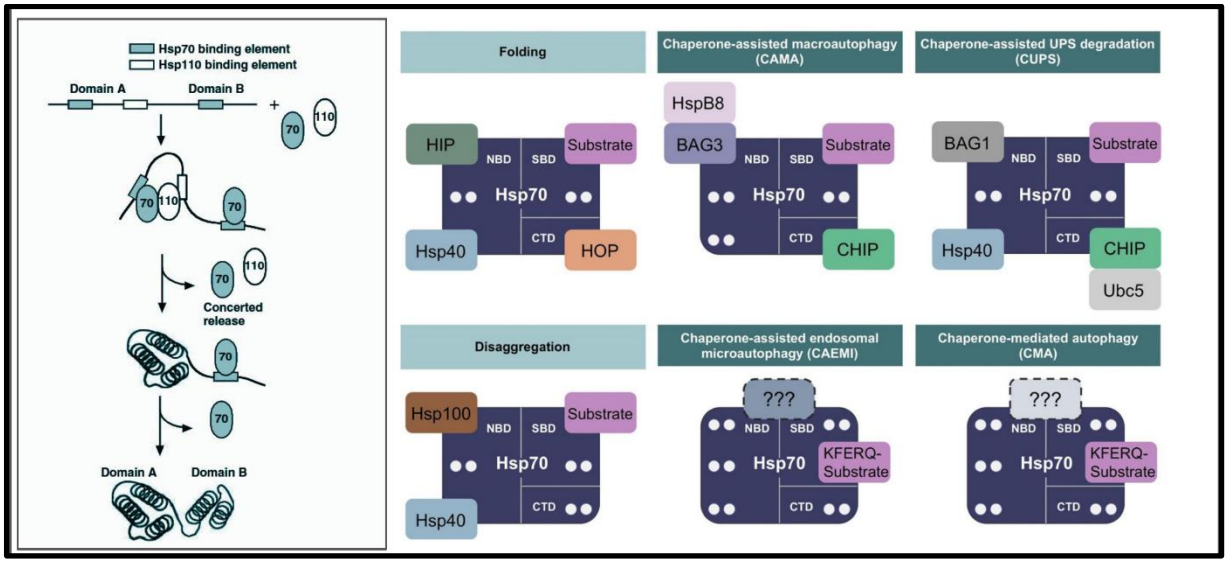

Figure 1.3.2 HSP70 as an adaptor complex linking protein quality control processes

HSP70 acts with HSP110 in the heteromeric complex to refold non-native cargo, each molecule binding to different domains on the target. Additional co-chaperones HSP40 and HIP regulate the ATP to ADP exchange, while HOP is a substrate-stabilizing co-factor. HSP70 was also shown to disaggregate misfolded proteins with the assistance of HSP100 and HSP40. HSP70 is a modular link between the ubiquitin-proteasome system. At the same time, bound to the co-factor BAG1 and an active ubiquitin ligase CHIP by Ubc5 and the macroautophagy system, where a BAG1 to BAG3 shift occurs supported by HspB8 and inactivated CHIP. Hsp70 is also suspected of recognizing the specific hydrophobic amino acid sequence KFERQ, hidden in natively folded proteins, to guide the misfolded cargo toward endosomes or autophagosomes directly. Still, the involved co-chaperones need to be better defined in this case. [Fernandez-Fernandez 2017; Dragovic 2006]

This complex is highly modular, making it a versatile machine and master regulator in protein degradation [Fernàndez-Fernàndez 2017]. If proteins cannot be refolded, the chaperones again play a distinct role as BAG-1 and carboxy terminus HSP-70 interacting protein (CHIP) are recruited to the HSC70. While CHIP acts as a ubiquitin ligase marking the cargo for degradation, BAG-1 has a ubiquitin-like domain acting as a direct link between HSC70 and the proteasome leading to chaperone-assisted UPS-degradation (CUPS) [Esser 2004]. The cargo is transported to the proteasome, a complex of proteases forming a cavity hydrolyzing the misfolded protein and releasing

the amino acids to be recycled, making it essential for proteostasis [Wang 2014]. If these direct degradation mechanisms are overloaded and the proteins form structures too large to be degraded by the ubiquitin proteasome system (UPS) **(Figure 1.3.3**), the surface of the aggregates is ubiquitylated. This modification is further recognized by sequestosome-1(P62/SQSTM1) and transported with the help of the motor protein dynein to perinuclear centrosomes to form aggresomes [Johnston 1998]. The aggregates are then removed via autophagic protein degradation, where P62 acts as an adaptor between the ubiquitylated aggregate and the autophagosome-related Microtubule Associated Protein 1 Light Chain 3 Beta (LC3B)-II. The aggregate is engulfed in the autophagosome, fusing with endosomes and lysosomes, and the cargo is degraded [Gottlieb 2010].

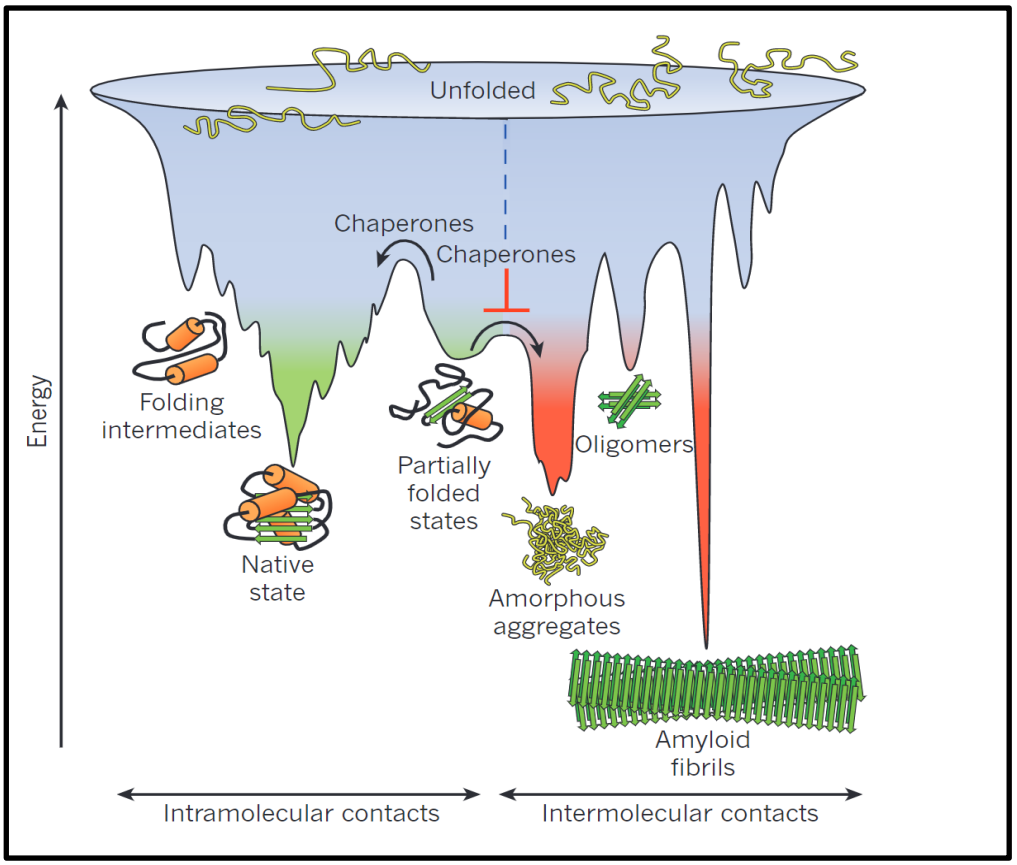

Figure 1.3.3 The physiological tertiary structure of proteins depends on the energetic state of the polypeptide

Proteins follow the entropic law of the universe, and the molecules will have a higher probability of staying in low energetic states. The unfolded confirmation has the highest entropy and will

spontaneously tangle into partially folded states. Under normal conditions, chaperone heat shock proteins will act as a catalyst for the partially folded proteins to overcome the energetic hill into folding intermediates and, finally, the native state, which is energetically stable. In the absence of chaperones, or instead, if the chaperone pool is exhausted, unfolded proteins can clump into amorphous aggregates energetically as stable as the native form. These aggregates are then either stored in perinuclear aggresomes, degraded via the autophagosomal system, or disaggregated by chaperones and returned to their physiological function. The exception here is pre-amyloid proteins which often form oligomeric structures which, under prolonged stress, form amyloid fibrils. These fibrils are energetically stable and, therefore, difficult to remove from the cytoplasm via the protein quality control system. (Figure adapted from Hartl 2011)

BAG1 and BAG3 are co-chaperones and nucleotide exchange factors of HSC70 that are involved in protein quality control and the induction of macroautophagy [Gamerdinger 2009]. Interestingly, BAG3 knockout mice were shown to develop a very similar phenotype to the HSPA4 knockout mice used in this study, as they showed early lethality and skeletal muscle myopathy [Homma 2006, Elkenani 2022]. These parallels raise the question of whether HSPA4 has similar HSC70 modulating capabilities compared to the BAG family of co-chaperones and if that lead to a similar disease progression.

1.4. Current knowledge about HSPA4

Heat shock protein A 4 is a class of proteins that protect the cell from stress-induced damage [Subjeck 1982]. The mammalian protein was first described as a novel member of the HSP70 protein family named HSP70RY in a human B-cell line [Fathallah 1993]. It was then reclassified to the newly formed HSP110 protein subfamily as ATP and peptide-binding protein in germ cells-2(APG-2) in mouse testis determined by sequence homology **(Fig 1.4.1)** [Yoon 1995]. The HSP110 family of proteins consists of three mammalian homologs, namely APG-1(HSPA4L); APG-2(HSPA4), and HSP110/105(HSPH1), which are structurally closely related to the HSP70 and Glucose-regulated protein 170 (GRP170) Family [Easton 2000]. Typically, proteins related to the HSP70 family it has an N-terminal ATPase domain followed by

a peptide-binding domain and an acidic c-terminal domain. Unlike other members in the HSP110 subfamily, HSPA4 is not inducible via traditional heat shock procedure and might therefore have a role under non-stress conditions as it is constitutively expressed [Kaneko 1997].

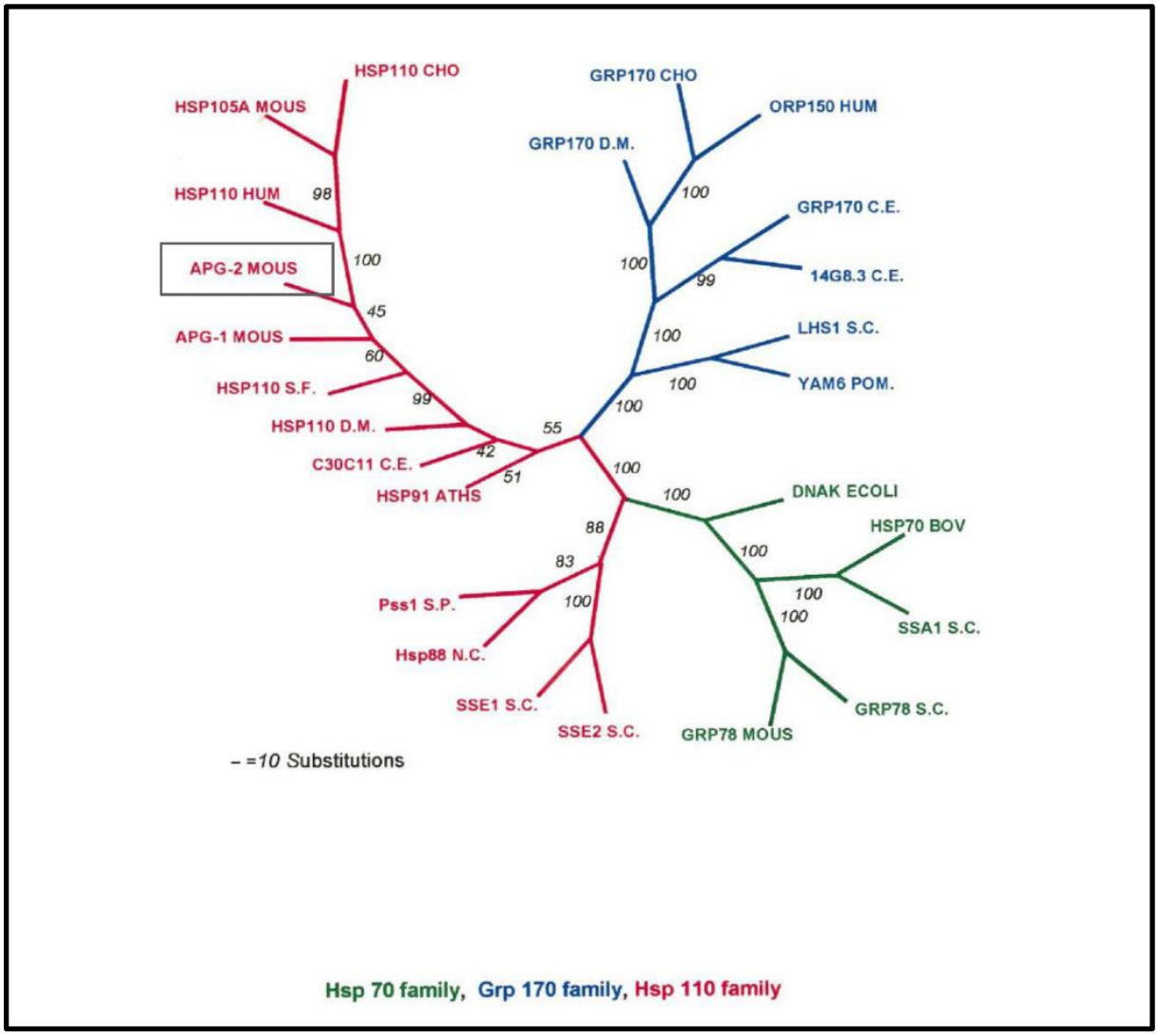

Figure 1.4.1 Identification of HSPA4 in the phylogenetic tree of the HSP70 family

The HSP70 chaperone family is diverse, with five main chaperones (green) interchangeably called HSP70 in literature. The GRP170 family comprises seven members and is associated with chaperoning at high ribosomal areas, especially the endoplasmatic reticulum. Finally, the HSP110 sub-family consists of at least 13 known ornithological members with three homologs in the mouse and humans, namely HSP105(HSPH1); APG-1(HSPA4L), and APG-2(HSPA4). (Adapted from Easton 2000)

In the last decade, HSPA4 was the focus of multiple animal models and was identified as a biomarker in various cancers [Fen 2020]. It was discovered that HSPA4 is upregulated in rat hippocampus after ischaemic injury and is expressed after radiation-induced stress in neurons [Kang 2002; Lee 2002]. HSPA4 was also found to be upregulated in human hepatocellular carcinomas alongside other HSPs. Here a Luciferase refolding assay was used to determine the chaperoning capabilities of HSPA4, revealing a robust anti-aggregating function without the ability to refold proteins on its own, suggesting a co-chaperone role [Gotoh 2004]. Recently, the nucleotide exchange function of HSPA4 to HSC70 was confirmed *in silico*. Furthermore, the acidic C-terminal domain was revealed to have a crucial role in association and dissociation with the complex **(Fig 1.4.2)** [Cabrera 2019].

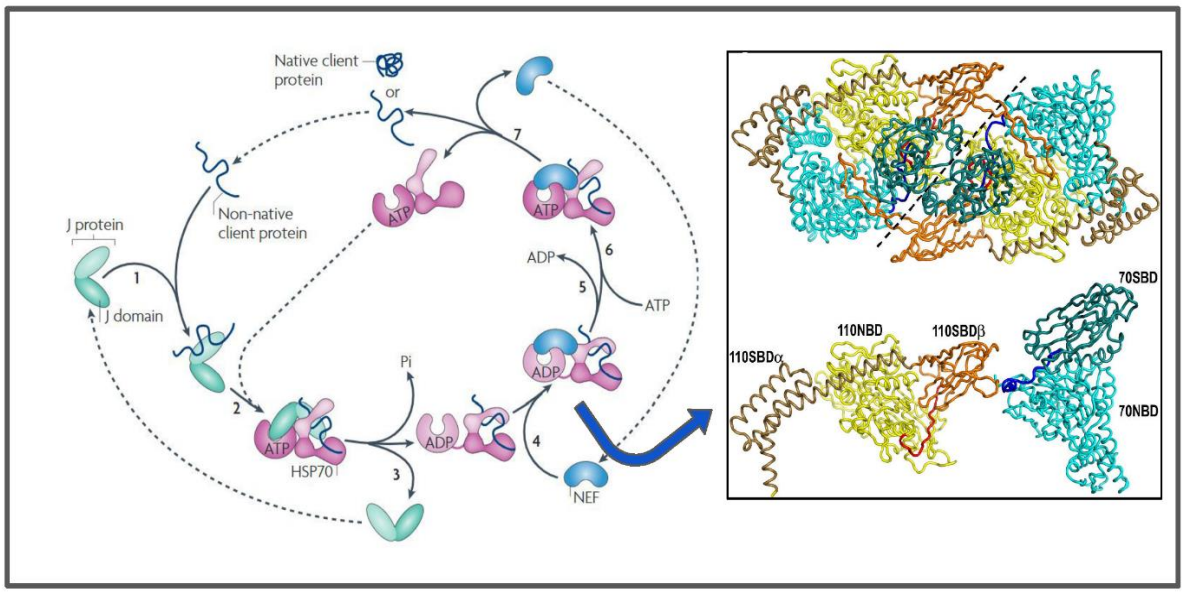

Figure 1.4.2 Chaperoning function of HSP70:HSP110 complex

The non-native client protein is held and prevented from aggregation by J-proteins (e.g., HSP40)[1] and is then loaded on the HSP70 complex [2]. The interaction of J-protein with HSP70 hydrolyses ATP and leads to a conformational change closing the molecular lid of HSC70 [3]. The cargo is then stabilized by the recruitment of nucleotide exchange factor HSP110(e.g., HSPA4) [4]. The HSP70:HSP110 complex is formed (infobox), further stabilizing the cargo, and ADP is exchanged from higher affinity to the nucleotide-binding domain on HSP110 [5]. At the same time, ATP is loaded onto HSP70. opening the molecular lid [6]. The recruitment of co-chaperones (e.g., HIP:HOP, Bag1:Bag3) replaces HSP110 on the complex, leading to dissociation of the cargo, which is either refolded or marked for proteasomal or autophagic degradation[7]. (Adapted from Schuermann 2008 and Kampinga 2010)

Even though HSPA4 is not upregulated after heat shock, it is hypothesized to change cellular distribution under stress conditions, binding to junction protein ZO-1(TJP1). It might therefore play a role in membrane integrity [Tsapara 2006].

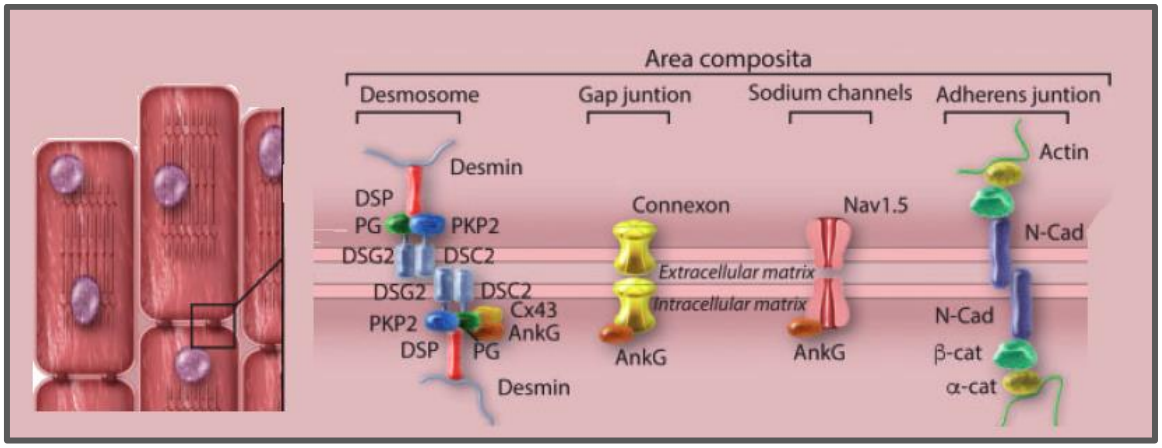

Figure 1.4.3 Schematic representation of the area composita

The *area composita* is a unique myocardial structure with high molecular complexity to ensure the ideal force propagation through the cardiac fiber. It harbors an ensemble of desmosomes, connecting the sarcolemma intracellularly [Desmin; Desmocollin2(DSC2); Desmoglein2(DSG2); Plakoglobin(PG); Plakophilin(PKP2); Desmoplakin(DSP); Ankyrin3(AnkG); Connexin43(Cx43)], as well as adherents junctions [Actin; alpha-Catenin(a-cat); beta-Catenin(b-cat); Cadherin 2(N-Cad)] to connect the cytoskeletal structures. Additionally, a high amount of connexons (connexin43 homohexamer) and voltage-gated sodium channels NaV1.5 serve as focal points for charged ion transfer. (Figure adapted from Hoorntje & Rijdt 2017)

A follow-up study revealed that tight junction formation in epithelial MDCK cells was retarded by HSPA4 knockdown under physiological conditions, possibly hinting at a redundant chaperoning or catalytic function on membrane-associated proteins of the *area composita* **(Fig 1.4.3)** [Aijaz 2007]. Furthermore, HSPA4 has an anti-apoptotic role by leading to the upregulation of BCL2 Apoptosis Regulator (BCL2) and Twist Family BHLH Transcription Factor 1 (Twist1) in fibroblasts involved in refractory inflammatory bowel disease preventing fibroblast cell migration [Adachi 2015] [Sakurai 2015]. Similarly, in a murine breast cancer model, B-Cells invading the lymph nodes formed autoantibodies against the chaperone and promoted metastasis [Gu 2019].

The HSP110 family chaperone HSPA4 was protective against H_2O_2-induced oxidative stress after overexpression in murine BCR/ABL B-cells and increased proliferation

thereof, underlining the importance of HSPA4 in high protein turnover processes [Feng 2010]. Recently, in a human *placenta accreta* study focusing on vessel endothelial cells, overexpression of HSPA4 in the HUVEC cell line promoted angiogenesis [Li 2022]. The previous findings of HSPA4 on proliferation were strengthened in one of the first HSPA4 knockout mouse lines, where spermatogenesis was disrupted without this chaperone [Held 2011]. The follow-up study on this mouse line revealed the extent of cardiac hypertrophy alongside interstitial fibrosis and accumulation of polyubiquitinated proteins in cardiac tissues, suggesting impairment in protein quality control [Mohamed 2012]. This work utilizes the same HSPA4 KO mouse line and aims to elucidate further the chaperone's role in the heart's homeostasis.

1.5. Clinical relevance of proteinopathies in heart failure progression

Proteinopathies primarily manifest with neurological symptoms, except for systemic amyloidosis [Mukherjee&Soto 2017, Olzscha 2011, Falk 1997]. While proteinopathies are often seen in this neurological context, a surprising development in Huntington's disease is that heart failure is the leading cause of death [Lanska 1988]. The pathophysiology of the disease is often thought to be responsible for cardiac side effects instead of direct cardiotoxicity of the misfolded protein. Nonetheless, proteotoxic stress can be induced by the gain of function diseases such as type 2 diabetes and more aggregation-prone mutants, e.g., in desmin-related cardiomyopathies. The age-related development of atrial fibrillation, cardiac hypertrophy, and cardiomyopathy have been linked to the imbalance in protein homeostasis (proteostasis) [Wiersma 2016, Brundel 2006]. In cystic fibrosis, it is unclear whether hypoxemia and pulmonary hypertension or the loss of function of the associated CFTR gene are the sources of cardiac deterioration. The loss of function

was found to impact Ca2+ balance in cardiomyocytes and affect the contraction rate [Sellers 2010]. Another example of mutated proteins inducing proteotoxic stress is mutations of presenilin-1(Psen1) and presenilin-2(Psen2), both markers associated with familial Alzheimer's disease, which were also found in a screening of DCM-patients [Li 2006]. Knockout of Psen1 in mice showed severe cardiac malformations, and knockout of Psen2 resulted in a lack of inhibition of the sarcoplasmic ryanodine receptor leading to systolic dysfunction giving these genes similarly essential functions for the heart [Nakajima 2004, Takeda 2005]. Many mutations found in inherited cardiomyopathies, like in the cardiac genes MYBPC3, MYH7, TNNI3, TNNT2, TPM1, and TTN, were hypothesized to have resulted in a gain of function that would lead to malignant interactions and aggregations of proteins [Lim 2001]. Interestingly, instead of forming protein aggregates, the mutations lead to the excessive degradation of sarcomeric proteins, inducing the development of hypertrophic cardiomyopathy [Henning 2017]. The loss of function mutation of SCN5A, the alpha subunit of the Nav1.5 sodium channel, led to Brugada Syndrome and was shown to be ameliorated by increased expression of proteostasis-related genes [Li 2017].

Atrial fibrillation is one of the most common cardiac arrhythmias and leads to the structural remodeling of atrial cardiomyocytes and, ultimately, the degradation of the sarcomeric cytoskeleton [Brundel 2006]. Experimental models and clinical atrial fibrillation showed tachypacing-induced post-translational modification by HDAC6, specifically deacetylated alpha-tubulin leading to rearrangement of the microtubule network. [Zhang 2014]. Furthermore, small HSPB is upregulated, supporting the cytoskeletal structure and preventing G-actin conversion to F-actin stress fibers preserving contractile function [Brundel 2006 - KE 2011].

In mice, the induction of cardiac hypertrophy via pressure overload showed proteotoxic stress, autophagic protein degradation, and the formation of aggregated proteins and

progressed cardiac remodeling [Tannous 2008]. Therefore, proteostasis plays a vital role in the development of heart failure as an imbalance is shown to progress the disease in acquired cardiomyopathies [Bozi 2016, Ma 2015, Lakatta 2015]. Several therapeutic approaches exist to modulate protein quality control in the cell **(Fig 1.4.1)**. The Receptors IRE1α, ATF6, and PERK become or activate transcription factors initiating protein-clearing associated genes and can be therapeutically interfered with. Finally, the ubiquitin-proteasome system and upstream factor HDAC6 are targets for therapy. Finally, autophagic initiation and chaperone stress response can be modified accordingly.

Treatment of proteotoxic stress is vital in cardiotoxic side effects after cancer therapy, and continuous ROS production from radiotherapy or chemotherapy can influence cardiovascular disease development [Ping 2020]. Even though recent technological advances in intensity-modulated radiation therapy seek to lower these side effects, heart disease remains a concern [Schlaak 2020]. Especially patients with breast or lung cancer receive radiotherapy near the heart, as well as Hodgkin's lymphoma patients who receive high doses of radiation to the whole body [Loap 2020. Jacob 2018]. In the same fashion, chemotherapeutic agents induce cardiomyopathy by increasing ROS production and mitochondrial damage [Fradley 2017, Hassan 2018]. Alkylating agents like cyclophosphamide, idarubicin, and doxorubicin are known for their induction of ROS production. They are, therefore, interesting targets in the proteotoxic context, especially since many childhood cancer survivors are now aged to be at risk for cardiovascular diseases [Chen 2020].

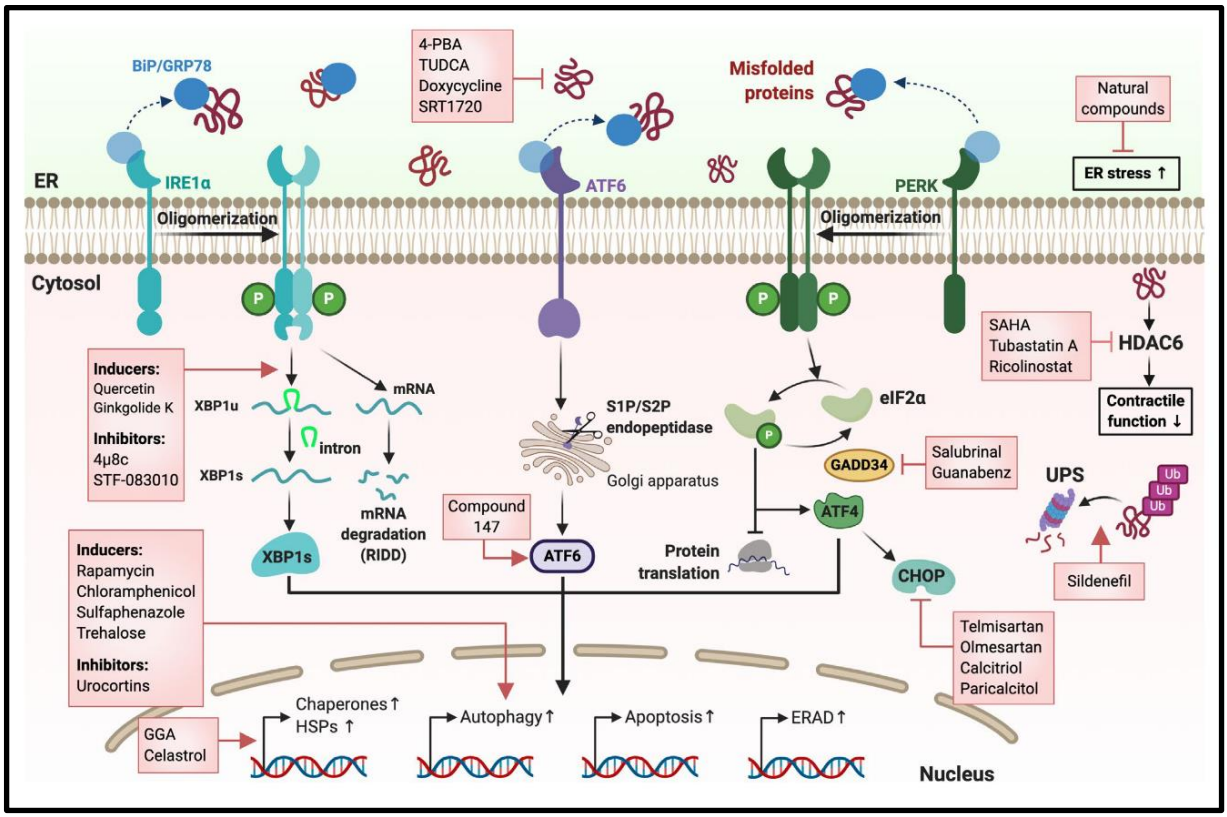

Figure 1.5.1 Schematic overview of therapeutic interventions in proteotoxic stress

Endoplasmatic reticulum (ER) chaperones BIP/GRP78 support freshly synthesized proteins that are yet to be folded or misfolded due to cardiac stress. The chemical chaperones 4-PBA, TUDCA, Doxycycline, and SRT1720. can ameliorate the increasing ER stress, which would lead to the activation of receptors IRE1α, ATF6, and PERK. IRE1α oligomerization leads to autophosphorylation and cleavage of unspliced XBP1u into XBP1s. Quercetin/Ginkgolide K promotes this cleavage leading to improved hemodynamics, while 48c and STF-08 inhibit the receptor from attenuating inflammation. ATF6 is cleaved into an active transcription factor by S1P/S2P endopeptidases and can be induced by Compound147 to increase cardiac pump function. PERK also oligomerizes and autophosphorylates, promoting eIF2α phosphorylation, which attenuates general protein translation. Salubrinal and Guanabenz prevent dephosphorylation by inhibiting GADD34, reducing hypertension, and attenuating cardiac hypertrophy. Phosphorylated eIF2α activates ATF4 and the downstream target CHOP, a master apoptosis regulator. The inhibition of CHOP by Telmisartan; Olmesartan; Calcitriol, and Patricalcitol, reduce mitochondrial dysfunction in oxidative stress responses. The transcription factors XPB1s, ATF6, and ATF4, promote the expression of several genes involved in HSP/Chaperones, Autophagy, Apoptosis, and ER-associated protein degradation (ERAD). SAHA, Tubastatin A, and Ricolinostat inhibit HDAC6, prevent accumulation of ubiquitylated proteins and improve cardiac function. In the same notion, Sildenafil promotes the degradation of proteins by inducing the UPS. Larger aggregates are cleared in autophagic processes induced by Rapamycin, Chloramphenicol, Sulfaphenazole, and Trehalose and can be inhibited with Urocortins. Geranylgeranylacetone (GGA) and Celastrol induce HSP expression improving clearance of aggregates, improving cardiac function, and reducing cardiac hypertrophy and remodeling. [Adapted from Diteepeng 2021]

1.6. Doxorubicin in the context of cardiotoxicity

Doxorubicin is a potent chemotherapeutic drug with fulminant cardiotoxic side effects that are still poorly understood [McGowan 2017]. Doxorubicin is known to inhibit Topoisomerase-2 and DNA replication. It is of the anthracycline family and is widely used in 1/3rd of breast cancer patients, 2/3 of elderly lymphoma, and 2/3 of childhood cancers with limiting cumulative dose-dependent cardiotoxicity [Giordano 2012, Nabhan 2015, Chihara 2016]. The origin of cardiotoxic side effects is still being researched, but it was reported that the increase of reactive oxygen species alongside mitochondrial damage plays a significant role [Tsang 2004]. Later it was revealed that the direct inhibition of topoisomerase-2-beta, a prominent isoform of cardiomyocytes in the adult heart, in a UPS-dependent manner contributed to the cardiac damage [Yi 2007].

The efficacy of Doxorubicin on cancer cells stems not only from the inhibition of TOPII in rapidly dividing cells but also from the mitochondrial damage in highly metabolic active cells [Zhang 2009]. However, the post-mitotic nature of cardiomyocytes, which also have high energy demands, makes them prominent targets for toxic side effects as doxorubicin derivates accumulate in the heart in a cumulative dose-dependent manner [Tacar 2013] **(FIG 1.6.1)**. The enzymes Nitric oxide synthase (NOS) and nicotinamide adenine dinucleotide phosphate-oxidase (NOX) play an essential role in the Dox-induced production of ROS [Damiani 2016]. Dox also interacts with iron forming DOX-Fe_2+ complexes that lead to further radical production. The radicals damage DNA and proteins and extensively peroxidize lipids, contributing to significant cellular damage and death. The positively charged iron complexes primarily target negatively charged mitochondrial membranes causing DOX-induced lipid peroxidation [Miura 1995].

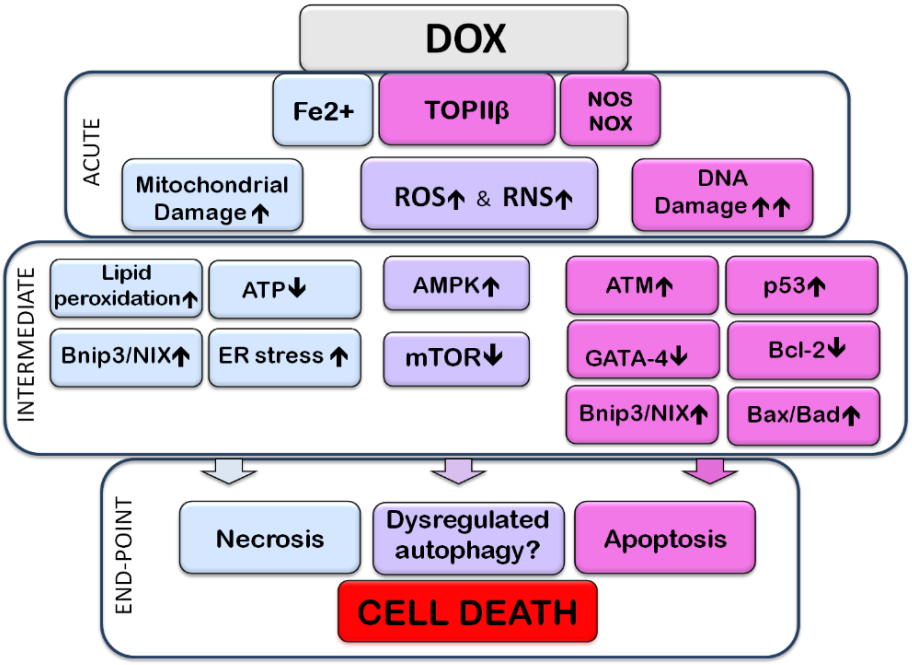

Figure 1.6.1 Doxorubicin toxicity leads to cell death in cardiomyocytes.

The immediate or acute effects of anthracycline doxorubicin on the cell are the localization into the nucleus and the inhibition and proteasomal degradation of topoisomerase II beta (TOPIIb). The interaction with NOS, NOX and Fe2+ leads to the generation of reactive oxygen and reactive nitrogen species (ROS/RNS) that damage mitochondria and DNA, as well as proteins and lipids. The intermediate toxicity of DOX affects multiple pathways. The increased lipid peroxidation and Fe2-DOX intermediates lead to lowered ATP production and ER stress, assessed by the increase in stress marker Bnip3/NIX, eventually leading to pyroptosis & ferroptosis. The DNA damage leads to increased expression of transcription factors ATM and GATA-4, which induce p53 activation and BCL-2 / BAX switch on the mitochondrial membrane starting the apoptotic cascade in the cell. Furthermore, AMPK activation results from reduced ATP levels and inactivates mTOR, the inhibitor of the autophagic pathway. Interestingly, at the same time, DOX raises the pH of lysosomes and therefore prevents physiological degradation of autophagosomes resulting in dysregulation of autophagy. (Adapted from Koleini and Kardami 2017).

The peroxidation of mitochondrial membrane proteins leads to lowered ATP Furthermore, Dox-induced DNA damage, mediated by TOPIIβ inhibition, significantly alters the nuclear and mitochondrial transcriptome leading to the down-regulation of mitochondrial biogenesis [Tokarska-Schlattner 2009]. The low ATP levels from mitochondrial fission and dysfunction, as well as the inflammatory response to ROS production, lead to a catabolic response of the myocardium and the expression of the pro-atrophic factor Tripartite Motif Containing 63 (MuRF1) **(Fig 1.5.2)** MURF1 is a muscle-specific E3 ubiquitin ligase that rapidly degrades muscle fibers by

ubiquitinating muscle actin and myosin-heavy and light chains, leading to atrophy and reduced muscle function [Clarke, 2007; Cohen, 2009; Polge 2011]. Interestingly, DOX also inhibits mTORC1, which is upstream of the glucocorticoid receptor, further affecting the catabolic response [Yu 2020].

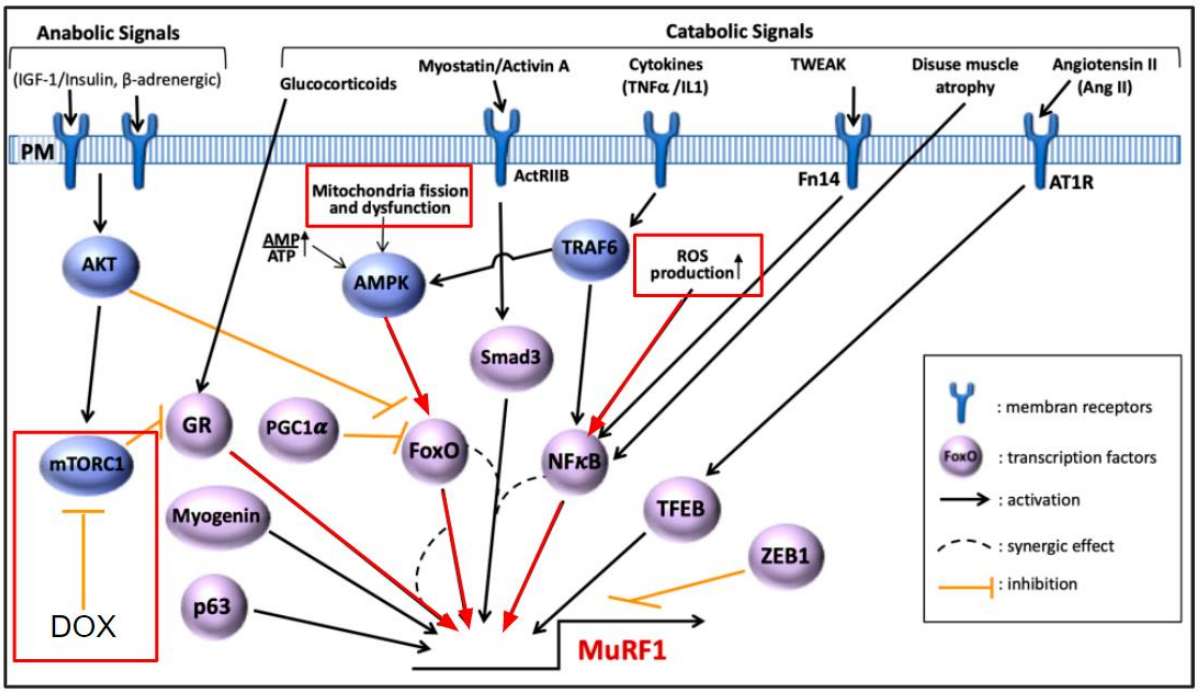

Figure 1.6.2 Upstream pathways of the pro-atrophic factor MuRF1

The expression of the ubiquitin ligase MuRF1 is associated with multiple upstream pathways. The most important pathways here stem from catabolic signals involved in neurohormonal and inflammatory anti-hypertrophic signaling. Here NfkB and FoxO are the best-described transcription factors of MuRF1 while also being activated by ROS production and mitochondrial dysfunction, both caused by acute doxorubicin administration. Furthermore, anabolic signaling leads to activation of the AKT-mTORC1 cascade inhibiting the glucocorticoid receptor (GR) and, therefore, MuRF1 activation. It was shown that doxorubicin inhibits mTORC1 activation giving another possible way of inducing MuRF1 expression and induction of acute cardiac atrophy. (Adapted from Peris-Morena 2020)

The DOX-induced DNA damage leads to the up-regulation of tumor suppressor protein p53 and is reported to suppress the transcription of GATA-4, a cardioprotective transcription factor [Park 2011]. An important effector of Dox-induced cell death is Bnip3, and the similar protein, Bnip3L/NIX, which are effectors of apoptosis and was also reported to play regulatory roles in the autophagic pathway [Dhingra 2014]. DOX can also lead to Bcl-2 phosphorylation, inhibiting the Bcl-2/Beclin1 interaction and facilitating autophagy initiation [Velez 2011]. Interestingly, recent research revealed an

inhibiting effect on autophagy by de-acidification of lysosomes [Li 2017]. Indeed, the effect of DOX on autophagy is more complex and leads to dysregulation, further disrupting protein quality control **(Figure 1.5.3).**

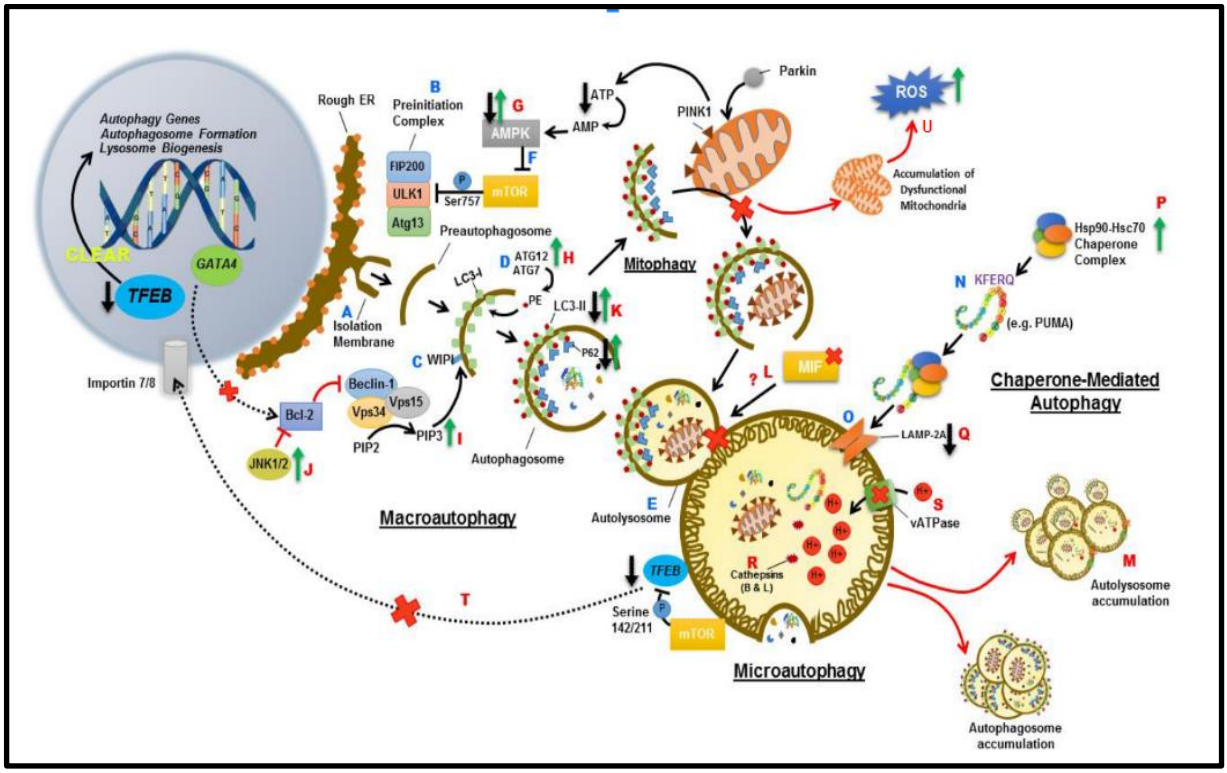

Figure 1.6.3 Doxorubicin renders cardiomyocytes vulnerable to proteotoxicity by dysregulating autophagy:

To initiate macroautophagy, mTOR signaling leads to the ULK1-FIP200-ATG13 complex, isolating a piece of ER-derived membrane (A; B). Furthermore, ULK1 phosphorylates Beclin-1 and activates the Vps34-Vps15 complex, which induces PI3 kinase catalysis leading to the recruitment of WIPI protein to the autophagosomal membrane (C.) WIPI also recruits LC3B-I to the autophagosomal membrane, which is lipidated by Atg5 to Atg12 (D). The ubiquitin-P62/SQSTM1 cargo binds to LC3B-II, is engulfed in the autophagosome, and fuses with the lysosome to form the autolysosome (E). Doxorubicin disturbs the AMPK and Akt mTOR signaling leading to the dysregulation of downstream autophagosomal function (F; G). DOX treatment increases ATG5-12 and LC3B-II autophagosomal content and p62 accumulation (H; K). Additionally, DOX promotes PI3K activity by decreasing BCL-2, the negative regulator of Beclin-1(J, I). On the other hand, DOX has been found to suppress MIF, which is likely a critical factor in autophagosome-lysosome fusion, and has been found to suppress lysosomal function by deactivating cathepsins through alkalinizing the lysosomal lumen leading to autolysosome accumulation (L, M, R, S). Chaperone-mediated autophagy is a selective degradation of proteins mediated by the HSP70 complex and lysosomal pore protein LAMP2A (N, O). While HSC70 is increased after DOX treatment, LAMP2A is down-regulated, leading to suppression of CMA (P, Q) TFEB is regulated during fasting by mTOR to promote lysosome production, and is depleted after DOX treatment, therefore, disrupting autophagy-related gene expression (T) The dysregulation in autophagy prevents the degradation of damaged mitochondria, which accumulate and further lead to increased ROS production ultimately causing cardiomyocyte dysfunction (U). [Adapted from Barlett et al. 2017]

It was shown that up-regulating autophagy prior to DOX treatment by administration of

Rapamycin, an mTOR inhibitor used to stimulate autophagy, rescued mice from Dox-induced cardiomyopathy [Xu 2013]. Ultimately, the dysregulation of protein quality mechanisms significantly impacts doxorubicin-induced cardiotoxicity, making it a promising target for HSPA4 chaperoning as a therapeutic intervention.

1.7. Aims of the Study:

Previously, our lab described genomic knockout of HSPA4 in 129SV mice. Here a dysfunction in spermatogenesis alongside skeletal muscle dystrophy was found. Additionally, the mice developed basal cardiac hypertrophy alongside interstitial fibrosis and impaired protein quality control in the form of aggregated proteins in left ventricular tissue. This work aims to elucidate further which role HSPA4 plays in the protein quality control of the heart and whether the knockout rescue of HSPA4 expression in the heart can prevent the hypertrophic phenotype, possibly by clearing protein aggregates in cardiomyocytes. The animals were injected with cardiotropic AAV9-HSPA4 vector six weeks before expected cardiac hypertrophy. The morphology and function of the heart were monitored via echocardiography at the different staged post-AAV application, and organ morphology was analyzed at the point of sacrifice. To further assess the left ventricular function, the global longitudinal strain was utilized as an early marker for systolic dysfunction. On the histological level, the relative area of cardiac interstitial fibrosis and the average cardiomyocyte size was determined. Finally, the role of HSPA4 in protein degradation processes of the ubiquitin-proteasome system and autophagy was investigated.

Furthermore, the expression of HSPA4 was found to be increased in pressure-overloaded hearts in mouse models and from samples of left ventricular tissue of patients with aortic stenosis [Mohamed 2012]. Hence, it is intriguing to investigate whether increasing HSPA4 expression could defend the heart from detrimental cardiac remodeling and enhance cardiac function., possibly by reducing stress to hypertrophic cardiomyocytes through increased chaperone function. In this part of the study, HSPA4 was overexpressed using a cardiotropic AAV9 vector, and the animals were stressed via transverse aortic constriction (TAC). Several parameters were analyzed to verify the pressure overload model's progression. First, the flow reserve was measured after TAC to ensure a successful operation. During the experiment, the probability of survival was determined, and the cardiac function was monitored via echocardiographic determination of the left ventricular ejection fraction. At the point of sacrifice, the organ morphology of the lung and heart was determined. Finally, markers of protein degradation in the UPS and autophagy system were measured to assess the role of HSPA4 in cardiac remodeling following pressure overload.

In the last part of this study, the cardiotoxic side effects of acute anthracycline treatment were investigated. Doxorubicin is a potent chemotherapeutic drug with a limiting cumulative dose-dependent cardiotoxicity, which is believed to stem from the inhibition of the cardiac isoform Topoisomerase 2B. Furthermore, it is known to inflict mitochondrial damage due to increased oxygen species, leading to the deacidification of lysosomes involved in protein degradation. Even though HSPA4 does not affect DNA damage directly, the buffering of misfolded protein damaged by reactive oxygen species and an improvement in chaperone-mediated autophagy is a promising prospect to be improved by HSPA4 chaperoning capabilities. In this experiment, HSPA4 was overexpressed via heart tissue directed AAV9, and the animals were

stressed with an acute doxorubicin dose known to be lethal after one week. During the experiment, the animals were monitored for severe weight loss, and the probability of survival was determined.

Additionally, the heart function and morphology were measured via echocardiography and organ morphology at the point of sacrifice. Early morphological changes after acute doxorubicin treatment are expected to lead to cardiac atrophy, which is assessed with the left ventricular wall thickness and average cardiomyocyte size. Finally, blockage of autophagic processes was assessed molecularly in immunoblots and immunofluorescence.

2. Methods

2.1. Statistical analysis

Data were expressed as mean ± SD, and ROUT outlier test 1 % was performed. Differences among groups were tested by Student's t-test, 1-way ANOVA or 2-way ANOVA where appropriate. A P-value of 0.05 was considered to be significantly different. GraphPad Version 9.3 was used for the statistical analysis.

2.2. Animals

Hspa4 KO mice were generated previously, and breeding was continued for this study [Held 2011].

Held et al. replicated PAC (RPCIP711P18115Q2) that encompassed the Hspa4 gene locus, obtained from the 129/Sv background genomic library in Berlin, Germany. They targeted the initiation codon ATG, found in Exon 1, and substituted it with the PGK-neo cassette. The 6 kb SpeI/XhoI and 4.5 kb BamHI/EcoRI genomic fragments, comprising the sequences of the 5'-flanking region and intron 1 of Hspa4, were separated from the PAC clone and inserted on both sides of the Pkg-neo cassette within the pPNT vector. The targeting vector was cut with NotI and employed to introduce genetic material into RI ES cells. The recombined ES cells were examined for homologous recombination through Southern blot analysis. Genomic DNA was isolated from ES cells, digested using XbaI, separated on 0.8% (w/v) agarose gels, and transferred onto a nylon membrane (Amersham Pharmacia). A 0.7 kb fragment situated at 30 of the targeting vector was amplified, labeled radioactively, and utilized as a probe for the Southern blot analysis. Successfully targeted ES cell clones were injected into blastocysts

derived from C57BL/6J mice and transferred into pseudo-pregnant DBA/Bl6 females to generate chimeric mice. The chimeric founders were bred with C57BL/6J mice to produce heterozygous Hspa4+/- mice, which were then intercrossed to obtain homozygous Hspa4-/- mice. Genotyping of mice was conducted by PCR amplification of DNA from the tail. A 535 bp PCR product derived from the wild-type allele was identified using primer F1: 50-GATCACGGGAAGT-GAGTGGT-30 and R1: 50-GAGCGGGAGTGAGACAGTTC-30. The targeted allele produced a 274 bp product with primer F1: and primer PGK 50-GGATGTGGAATGTGTGCGAGG-30. The thermal cycling consisted of 35 cycles of denaturation at 94 °C for 30 s, annealing at 55 °C for 30 s, and extension at 72 °C for 30 s.

All animal trials underwent assessment and received endorsement from the Institutional Animal Care and Utilization Committee at the University of Göttingen.

In this investigation, we examined the effects of Hspa4 knockout (KO) on the 129/Sv genetic background. The Institutional Animal Care and Utilization Committee of the University of Göttingen reviewed and approved all animal experiments conducted as part of this thesis. All animals involved in this research were kept under usual laboratory conditions, following a 12-hour light/dark cycle, and provided with unrestricted food and water. C57BL/6N mice were obtained from Charles River, while all other mice were generated internally. Animals were housed in groups of five and given a period of 1-2 weeks to acclimate before any interventions took place.

2.3. Transthoracic echocardiography

The echocardiography was performed by Marcel Zoremba and Sabrina Koszewa from the SFB1002 service team, employed by the Cardiology and Pneumology department of the University Medical Center Göttingen.

The echocardiography was performed using the Vevo 2100 system equipped with an MS-400 30 MHz transducer (VisualSonics). The cardiac function and measurements of the mice were assessed according to the methodology previously outlined by Pistner et al. in 2010. In the case of transverse aortic constriction (TAC) surgery, the flow rate through the aorta was determined using echocardiography employing a 20 MHz transducer (MS-250). To conduct the echocardiography, the mice were anesthetized with isoflurane (1-2%) and their skin was prepared by applying hair removal lotion. Brief sequences of the heart and respiratory rate were then captured in B-mode, either in the long axis or short axis view, and in M-mode using the mid-papillary view. Echocardiographic M-Mode images were investigated using the LV-trace application of VevoLab software (version 3.1.0).to determine heart dimensions, including left ventricular anterior wall thickness in diastole, left ventricular posterior wall thickness in diastole, and left ventricular diameter in diastole, as well as left ventricular ejection fraction, fractional shortening, and global longitudinal strain. Significance, unless otherwise indicated, was calculated using One or Two-Way ANOVA in Graphpad Software v9.3.0.

2.4. Induction of hemodynamic overload

TAC surgical operation were performed by Sabrina Koszewa or Sarah Zaffar from the SFB 1002 service team.

A surgical procedure called transverse aortic constriction (TAC), which has been before explained by Rockman et al. (1991), Hu et al. (2003), de Almeida et al. (2010),

and Toischer (2010), was performed on mice 8-10 weeks old. The mice were divided into two groups: Sham and TAC. Before the surgery, the mice were given anesthesia through an injection in the abdominal cavity using a small amount of a sodium chloride solution (0.9%) containing Medetomidine (0.5 mg/kg), Midazolam (5 mg/kg), and Fentanyl (0.05 mg/kg). A small incision, about 1-1.5 cm long, was made near the upper chest. Then, a thin blunt needle was placed on the aorta and tied with a thread (6-0 polyviolene) in between two branches of the aortic arch. In the Sham group, the procedure was the same except that the aorta was not constricted. The incision was closed with stitches. After the surgery, the anesthesia was reversed by injecting a sodium chloride solution (0.9%) containing Atipamezole (2.5 mg/kg) and Flumazenil (0.1 mg/kg) under the skin. Pain relief was provided by injecting Buprenorphine (0.05-0.1 mg/kg) under the skin at a standard dose. The mouse was placed on a warm pad to recover. Three days later, the constriction of the aorta was checked using echocardiography. The mice received pain medication (carprofen) for three days after the surgery, and their health condition was monitored daily. At 1, 4, and 8 weeks after the surgery, the mice underwent echocardiography for analysis. They were then euthanized for further examination of their hearts at a molecular level or for histological analysis.

2.5. Heart dissections

The mice were put to sleep using isoflurane and then humanely euthanized by cervical dislocation. Before dissecting the mice, their body weight was recorded. The chest was opened, and the heart was carefully removed from the body and placed in a clean saline solution. To clear any remaining blood, a blunted needle with a size of 21-gauge was inserted into the aorta and securely fixed. Sterile saline was then

passed through the needle in the opposite direction, rinsing away any remaining blood. The heart was weighed, and the atria (upper chambers) and right ventricle were removed. The left ventricle was weighed again before being rapidly frozen using liquid nitrogen. Lastly, the tibia bone was dissected, and its length was measured using an electronic gauge to account for differences in body size.

2.6. In-silico oligonucleotide design

Eurofins synthesized the oligonucleotides. The primers for the RT-qPCR were designed using Primer-BLAST, an online tool. The settings for Primer-BLAST were adjusted to specify the desired product size (100-200 base pairs), ensure that the primers do not span across different parts of the gene, include introns if possible, and select Mus musculus (mouse) as the organism. Splice variants were also allowed.

The genotypes of the genetically modified mice were determined by performing PCR using the primers listed in Table 2.1. MangoTaqTM Polymerase from Bioline (BIO-21078) was used for the PCR reactions. To extract the genomic DNA (gDNA), small pieces of tail samples were placed in a solution called DirectPCR-Tail lysis buffer (Viagen Biotech, #102-T) and left overnight. Then, Proteinase K was added and the samples were heated at 55 °C with gentle agitation according to the manufacturer's instructions. Proteinase K was deactivated by heating the samples at 85 °C for 45 minutes. The samples were prepared as described in Table 2.2 and programmed as specified in Table 2.3. The PCR reactions and a 100 base pair DNA ladder (Thermo Fischer, SM1153) were separated by gel electrophoresis for 45 minutes at 120 volts using a 2% agarose gel in a buffer called TBE (45 mM Tris-borate, 1 mM EDTA).

The gel was then imaged using the BioRad Gel Doc XR+ system with the ethidium bromide setting.

Table 2.1 Genotyping Reaction

Reagents	Volume(µl)
5x reaction buffer	4.0
MgCl2 (50mM)	1.5
dNTPs (100mM)	0.5
Forward Primer (10pmol/µl)	1.0
Reverse Primer (10 pmol/µl)	1.0
gDNA	1.5
H2O (to 20 µl)	10.3
Mango-Taq polymerase	0.2

Table 2.2 Genotyping Protocol

Step	Temp.(°C)	Time
Initi.Denaturation	95	3 min
Denaturation	95	30sec
Annealing	60	30sec
Elongation	72	30sec
Final Elongation	72	5min

2.7. Quantitative real-time PCR

The RNeasy Fibrous tissue Mini kit (Qiagen, 74704) was used according to the manufacturer's manual, to isolated RNA from left ventricular heart tissue.

20 mg of left ventricular heart tissue was added to 350 µl of RLT buffer + DTT and homogenized with a 5mm stainless steel bead (Qiagen, 69990) for 5 min at 50 hz Tissue Lyser LT (Qiagen, 85600). Cellular debris was removed at 10.000g for 5 min. The supernatant was mixed with 350 µl of 70 % Ethanol and loaded onto a silica column. The column was washed once with 700 µl RW1 and twice with 500 µl RPE, after which the column was incubated with RNAse-free water for 5 min at RT, and RNA was eluted. The RNA concentration was measured on a nanodrop spectrophotometer, and 1000ng of RNA was transcribed using an iScript Reverse Transcriptase kit(BioRad) according to manufacturer instructions. 10 ng of cDNA was mixed with BioRad SsoAdvanced universal SYBR Green supermix and 10 µM primer pair mix in a 96-well hardcover plate. PCR program as follows: 3 min 95°C initial denaturation; 10sec 95° denaturation; 30 sec 60°C annealing; repeated for 45 cycles; melt curve from 55-95°C in 0.5°C steps Cycle 40x with 30 sec @ 95°C and 30 sec @ 60°C.

2.8. Protein Isolation and Western Blot

20 mg of left ventricular heart tissue was added to 500 µl Pierce RIPA buffer (Thermo Fischer, 89900) supplemented with complete protease inhibitors (Sigma, 000000011873580001) and with added phosphatase inhibitor PhosSTOP(04906837001) and a 5-7 mm stainless steel bead(Qiagen, 69990) for homogenization at 4°C for 5 min at 50 hz in Tissue Lyser LT (Qiagen, 85600). The homogenates were incubated for 1 hr on ice, and the cellular debris was removed at 10.000g centrifugation at 4°C for 15min. The supernatant was transferred, and protein concentration was measured via standard BCA assay procedure (Thermofisher-Pierce™ BCA Protein Assay Kit). Samples were prepared with Lämmli loading dye(BioRad #1610747) for 5min at 95°C. The protein was separated in a TGX Stain-

Free Fast Cast Acrylamide 10 % SDS-PAGE from Biorad(#1610183) at 200V for 40 minutes, and the gel was blotted onto a Transblot Turbo mini-size nitrocellulose membrane in a BioRad Transblot Turbo for 3 minutes at 20V. The membrane was blocked in 5 % milk TBST (0.1 % Tween20) for 45minutes, followed by an incubation of the primary antibody in 1 % milk TBST overnight at 4 °C. The blot was washed for 3x5 minutes in TBST and incubated in HRP-conjugated secondary antibody for 1 hour at RT. The membrane was washed 3x5 minutes in TBST and developed with SuperSignal West Femto PLUS Chemiluminescent Substrate using the Gel Doc XR+system.

2.9. Hematoxylin & Eosin Staining

Left ventricular tissue was embedded in paraffin and cut into 5 µm thick sections. The slides were incubated for 30 minutes at 60°C and deparaffinized in xylol for 10 minutes twice. The tissue was hydrated in an ascending alcohol series (100 %>70 %>50 %>30 %>H2O) for 5 minutes each. The sections were stained in Hematoxylin for 2 minutes and de-stained in distilled water until they ran clear. The Sections were then stained in Eosin for 1 minute and cleared with distilled water. The slides were dehydrated in an ascending ethanol series (H2O>30 %>50>70 %>100 %) and cleared in xylol before being mounted with synthetic resin (H-5000)

2.10. Picro Sirius Red & Fast Green Staining

Left ventricular tissue was embedded in paraffin and cut into 5 µm thick sections. The slides were incubated for 30 minutes at 60°C and deparaffinized in xylol for 10 minutes twice. The tissue was hydrated in an ascending alcohol series (100 %>70 %>50 %>30 %>H2O) for 5 minutes each. The tissue was then covered with Picosirius Red

combined with fast green dye and incubated for 1 hour, washed until cleared, dehydrated twice in 100 % ethanol, and mounted in synthetic resin (H-5000). The sections were then imaged in a light microscope, and the relative fibrotic area was calculated utilizing ImageJ software.

2.11. Wheat Germ Agglutinin (Collagen) Staining

Left ventricular tissue was embedded in paraffin and cut into 5 µm thick sections. The slides were incubated for 30 minutes at 60°C and deparaffinized in xylol for 10 minutes twice. The tissue was hydrated in an ascending alcohol series (100 %>70 %>50 %>30 %>H2O) for 5 minutes each. Next, the tissue was covered with Alexa 555 conjugated wheat gluten agglutinin solution and incubated in the dark for 60 minutes. Afterward, the sections were washed three times for 5 minutes in PBS and mounted with aqueous mounting medium Antifade-Gold+Dapi. Sections were imaged under the fluorescent microscope, and around 120 cells per sample were analyzed utilizing ImageJ software.

2.12. Immunofluorescence

Left ventricular tissue was embedded in paraffin and cut into 5 µm thick sections. The slides were incubated for 30 minutes at 60°C and deparaffinized in xylol for 10 minutes twice. The tissue was hydrated in an ascending alcohol series (100 %>70 %>50 %>30 %>H2O) for 5 minutes each. Antigen Retrieval was performed in citrate buffer pH 6.5 for 20 min at 100°C, after which the sections were cooled for 10 min on ice and washed twice in PBS for 5 min. Next, the tissue was incubated in a blocking buffer of 2 % goat serum and 0.01 % Triton X-100 PBS for 30 minutes. Finally, sections were incubated with primary antibody solution 1:100 at 4°C overnight in a humid chamber. The following day, the slides were washed three times in PBS for 5 minutes and then incubated in a secondary Alexa fluorophore-conjugated antibody solution for 45

minutes at RT. The sections were washed three times in PBS, mounted with aqueous mounting medium Antifade Gold + DAPI and stored for imaging.

Table 2.3 List of Antibodies used and their concentration in TBST 1 % Milk

Name	Manufacturer	#	Host	Size[kD]	Dilution
GAPDH	Sigma	MAB374	Mouse	37	1:10000
APG-2	Santa Cruz	Sc-6240	Rabbit	110	1:1000
APG-2 (HSPA4)	Santa Cruz	Sc-365366	Mouse	110	1:1000
LC3B	Cell Signaling	2775s	Rabbit	15/17	1:1000
P62	Cell Signaling	5114s	Rabbit	60	1:1000
Ubiquitin	Dako	20458	Rabbit	Range	1:1000
rabbit-HRP	Cell signaling	7074S	Goat	NA	1:10000
mouse-HRP	Cyvita	NXA931	Sheep	NA	1:10000

Table 2.4 List of Primers used

mm_Hspa4_F GACTGTGTTGTCTCGGTTCC	mm_Hspa4_R TCTAAGGCAGGAAGGTCTTGTT
mm_NppA_F CTGCTTCGGGGGTAGGATTG	mm_NppA_R GCTCAAGCAGAATCGACTGC
mm_NppB_F AAGGACCAAGGCCTCACAAA	mm_NppB_R GCCAGGAGGTCTTCCTACAAC
mm_SQSTM1_F GGCCACCTCTCTGATAGCTTCT	mm_SQSTM1_R GACATTGGGATCTTCTGGTGGA
mm_PINK1_F AGAGTATGGAGCAGTTACTTACAG	mm_PINK1_R GGCAGCATATCAGGATAGTC
mm_PRKN_F CCCGGTGACCATGATAGTGTT	mm_PRKN_R TTCCCGGCAAAAATCACACG

mm_Hspa4_F GACTGTGTTGTCTCGGTTCC	mm_Hspa4_R TCTAAGGCAGGAAGGTCTTGTT
mm_NppA_F CTGCTTCGGGGGTAGGATTG	mm_NppA_R GCTCAAGCAGAATCGACTGC
mm_NppB_F AAGGACCAAGGCCTCACAAA	mm_NppB_R GCCAGGAGGTCTTCCTACAAC
mm_SQSTM1_F GGCCACCTCTCTGATAGCTTCT	mm_SQSTM1_R GACATTGGGATCTTCTGGTGGA
mm_TRIM63_F GGTGCCTACTTGCTCCTTGT	mm_TRIM63_R CCTGGTGGCTATTCTCCTTGG
mm_LC3_F CTTGACCAACTCGCTCATGTTA	mm_LC3_R GACCGCTGTAAGGAGGTGC
msGAPDH_F GAGACGGCCGCATCTTCTT	msGAPDH_R CAATCTCCACTTTGCCACTGC

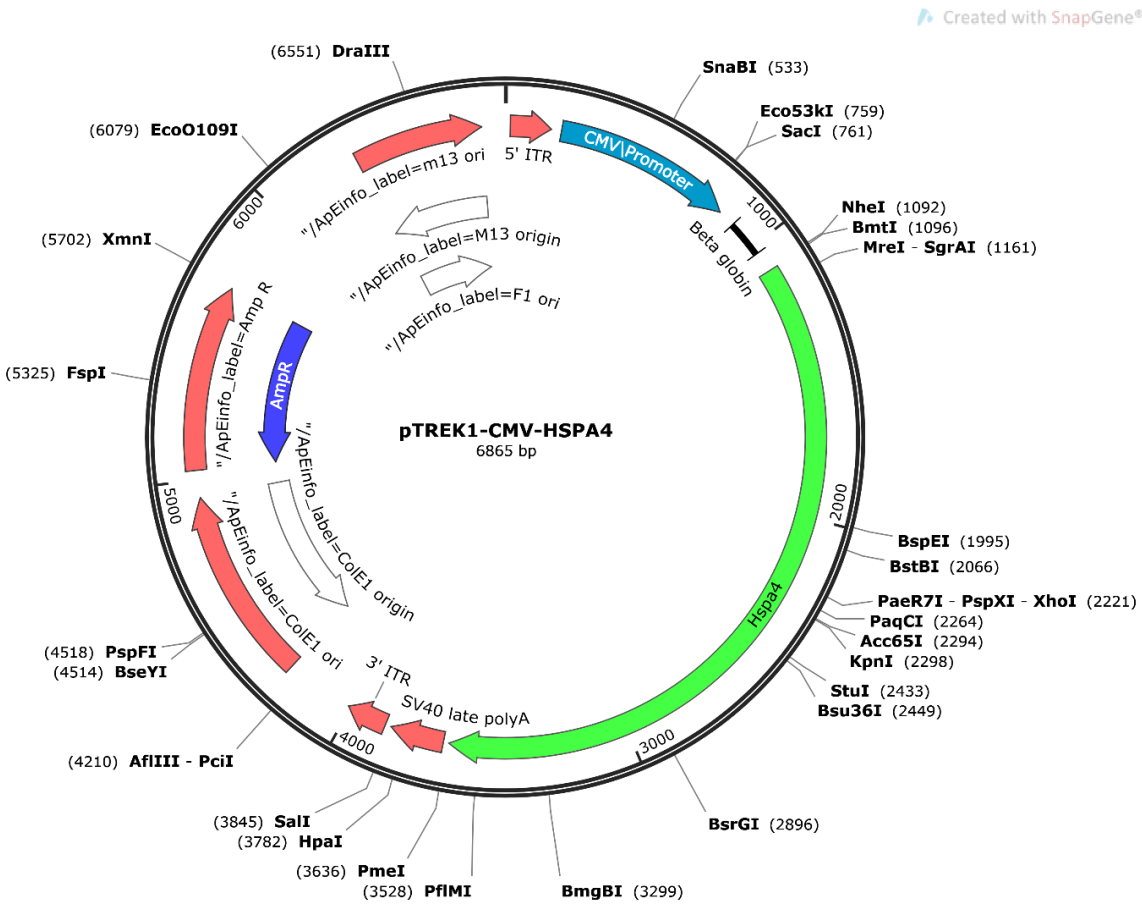

Figure 2.12.1 Schematic representation of the AAV9-Vector containing the full-length gene for Hspa4.

AAV 9 production was kindly provided by Prof. Dr. Stefan Engelhardt (TMU-Pharmacology and Toxicology, Munich). HEK293-T cells were cultivated in DMEM, 10 % fetal bovine serum before transfection. The transgene and helper plasmid pDP9rs was transfected into the HEK293 cells using Polyethyleneimine (Sigma-Aldrich). After 72 hours, the viruses were purified from benzonase-treated cell crude lysates over an iodixanol density gradient (Optiprep, Sigma-Aldrich). AAV titers were determined by a real-time polymerase chain reaction (PCR) on vector genomes using the SYBR Green Master Mix (Roche).

Table 2.5 Calculations used by Vevolab software to determine Echocardiographic parameters (adapted from Vevo instruction manual)

Name	Description	Units	Formula
LV Vol;d	Left ventricle volume diastole	µl	((7.0 / 2.4 + LVID;d)) * LVID;d3

LV Vol;s	Left ventricle volume systole	µl	((7.0 / 2.4 + LVID;s)) * LVID;s3
%EF	LV ejection fraction	%	100 * ((LV Vol;d – LV Vol;s) / LV Vol;d)
%FS	LV Fractional Shortening	%	100 * ((LVID;d – LVID;s) / LVID;d)
LV Mass	LV Mass Uncorrecte	mg	1.053 * ((LVID;d + PWTh;d + AWTh;d)3 – LVID;d3)
LV Mass Cor	LV Mass corrected	mg	LV Mass * 0.8
LV-W/BW	LV weight to bodyweight	mg/g	LV Mass / body weight

2.13. Echocardiographic measurement of Longitudinal Strain

The application VevoLab (version 3.1.0) was used to measure strain. Strain indicates how much the left ventricle of the heart stretches or squeezes compared to its original shape. When different parts of the heart wall move at different speeds during the heartbeat, it causes deformation. Strain rate is a way to measure how quickly this deformation happens. To calculate strain at a specific spot inside the heart, we measure the distance between that spot and another point inside the heart at the starting point of the heartbeat (always the R-Wave). Then this measurement is compared to the distance between the same two points at a different time during the heartbeat. The difference between these distances is shown as a percentage of the original distance.

$$S = \frac{\triangle L}{L_0} = \frac{L - L_0}{L_0} \qquad SR = \frac{S}{\triangle t} = \frac{(\triangle L / L_0)}{\triangle t} = \frac{(\triangle L / \triangle t)}{L_0} = \frac{\triangle V}{L_0}$$

where:

S is the longitudinal strain

$\triangle L$ is the absolute change in length

L_0 is the baseline length (at end diastole/ the R-Wave)

$\triangle V$ is the velocity gradient in the segment.

Figure 2.13.1 Formula for Strain and strain rate (VevoStrain User Guide)

In strain analysis, the natural acoustic markers (called speckles) in the B-Mode cine loop are tracked across the cardiac cycle, and velocity vectors are estimated using special algorithms. The tracing pattern on the B-Mode image is copied during the heart's beating and for all cycles

examined. This kind of strain analysis is seen as not relying on angles and has less differences between different users compared to other ways of measuring heart function using ultrasound.

2.14. Time-to-Peak (maximum opposite wall delay)

Time-to-Peak is the time it takes for each of the six equal parts of the LV wall to reach its highest point after the R-Wave (the starting point). Depending on the measurement, for example velocity or displacement, this value is calculated individually. Each part of the LV wall was divided into nine smaller points and the maximum peak was determined. In the table, "Pk" is the highest point for each part, and "TPC ms" is the time it takes to reach that highest point from the starting point (R-Wave). The table also gives an average value for the highest point and time for all six parts. Lastly, the "maximum Opposing Wall Delay" (MOWD) is calculated by finding the difference between the highest and lowest TPC ms values. This measurement describes if there is a delay between different parts of the LV and indicates how synchronized they are.

3. Results

3.1. HSPA4-knockout was rescued by heart tissue-directed overexpression and prevented cardiac remodeling.

As previously described, HSPA4-KO animals develop concentric left ventricular hypertrophy with preserved ejection fraction alongside cardiac fibrosis and an accumulation of poly-ubiquitinated protein substrates [Mohamed 2012].

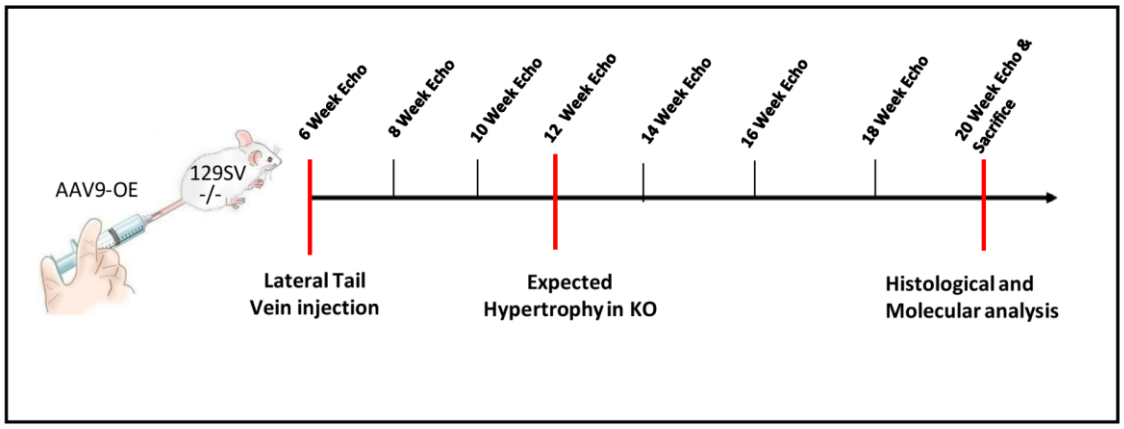

Figure 3.1.1 Experimental setup for rescue of the cardiac phenotype in HSPA4-KO mice

6 weeks old C57BL/6Jx129/Sv double knockout (-/-) mice were injected with 10^12 AAV9-HSPA4 particles via the left lateral tail vein. Heart morphology was monitored via echocardiography every two weeks, where seen hypertrophy of the left ventricular wall was expected in 12-week-old mice. Additionally, mice of the same age expressing the HSPA4 gene (+/+) were monitored as wildtype control and HSPA4 (-/-) and treated with 10^12 AAV9-DsRed control virus as knockout control. Litter mates and both sexes were spread randomly in all groups. After the mice reached the age of 20 weeks, the cardiac phenotype reached a plateau phase, the mice were sacrificed, and the left ventricles were prepared for histological and molecular analysis.

The HSPA4 KO mouse line described in this study has a double knockout in the germ line; therefore, the knockout would be present in all cells of the organism [Held 2011]. The cardiac remodeling observed can be the primary effect of the HSPA4 KO in the heart due to impaired cellular functions, or secondary stressors outside the cardiovascular system could induce it. An AAV9 Vector containing the Hspa4 gene was used to overexpress HSPA4 in the heart to determine if the knockout effects are

a primary cardiac phenotype. We chose this vector as it shows higher cardiac tissue tropism than other AAVs [Inagaki 2006]. For this 6 Weeks old, HSPA4-KO mice were injected via the lateral tail vein and monitored via echocardiography for 14 weeks **(Fig. 3.1.1)**. From the previous study, it became apparent that at this age, the animals would not have developed the cardiac phenotype yet, which made it the ideal time point for intervention by overexpression of HSPA4 in the heart as cardiac hypertrophy started developing about 10-12 weeks after birth [Mohamed 2012]. At the end of the experiment, the hearts were excised and left ventricular tissue samples were stained with anti-HSPA4 to assess the degree of overexpression compared to the wild type. The overexpression was successful with an average of 7 times higher protein expression($p=<0.0001$) than the wildtype in left ventricular tissue samples determined by western blot **(Fig 3.1.2 A-B)**. The wild type and knockout control animals, treated with control virus AAV9-DsRed, showed the expected average and missing expression.

During the basal cardiac remodeling, it would have been expected that the KO hearts develop hypertrophy of the ventricles [Mohamed 2012]. Therefore, the hearts were weighed after excision, and the dry weight was normalized to tibia bone length to minimize biases stemming from the sex of the animals and fluctuations in body weight from the time of day. **(Fig 3.1.2 C)**. Here an increase in normalized heart weight was seen between KO (mean=8.158) and OE (mean=6.870) animals($p=0.0128$) compared to the WT control (mean=6.54 $p=0.0047$). Interestingly the degree of hypertrophy followed a normal distribution that overlapped with the control group and was only detected when analyzed as a population.

Suppose the tensile strength of individual cardiac muscle fibers decreases. In that case, the ventricular wall needs to increase in thickness according to Laplace's Law to exert still the same amount of force [Badeer 1963]. The hypertrophy was also seen in

histological stains of the KO-heart's short axis, where the walls of the left and right ventricles increased compared to the control. Furthermore, this basal hypertrophy in the KO was reduced in the OE group at the point of sacrifice **(Fig 3.1.2 D)**. Since its invention, ultrasound cardiography (UCQ) has been a staple method in assessing cardiac function non-invasively [Singh 2007]. In this experiment, the short axis of the left ventricle was measured in anatomical motion mode using Vevo-Lab imaging software every two weeks. Here the left ventricular anterior wall thickness relative to the left ventricular diameter in the diastole was used to assess the degree of hypertrophy. At the beginning of the experiment, the ventricular wall thickness was still comparable in all groups, which did not change for four more weeks. Between weeks 10 and 12, the hypertrophy developed rapidly in the KO group but not in the OE group. Over the remaining eight weeks, the LVAW of the KO group plateaued while the OE group stayed close to the WT control. At 20 weeks of age, prevention of concentric hypertrophy was determined by measuring relative wall thickness(unitless) with a difference of 0.4236 in KO to 0.2385 ($p=0.0013$) in OE at the endpoint **(Fig 3.1.2 E)**. Even though the KO group shows highly hypertrophic hearts, the heart function assessed by ejection fraction (EF) was ultimately unaffected in all groups during the experiment **(Fig 3.1.2 F)**. Therefore, the hypertrophic response seen in KO animals at 12 weeks of age was prevented by overexpressing HSPA4 in the heart

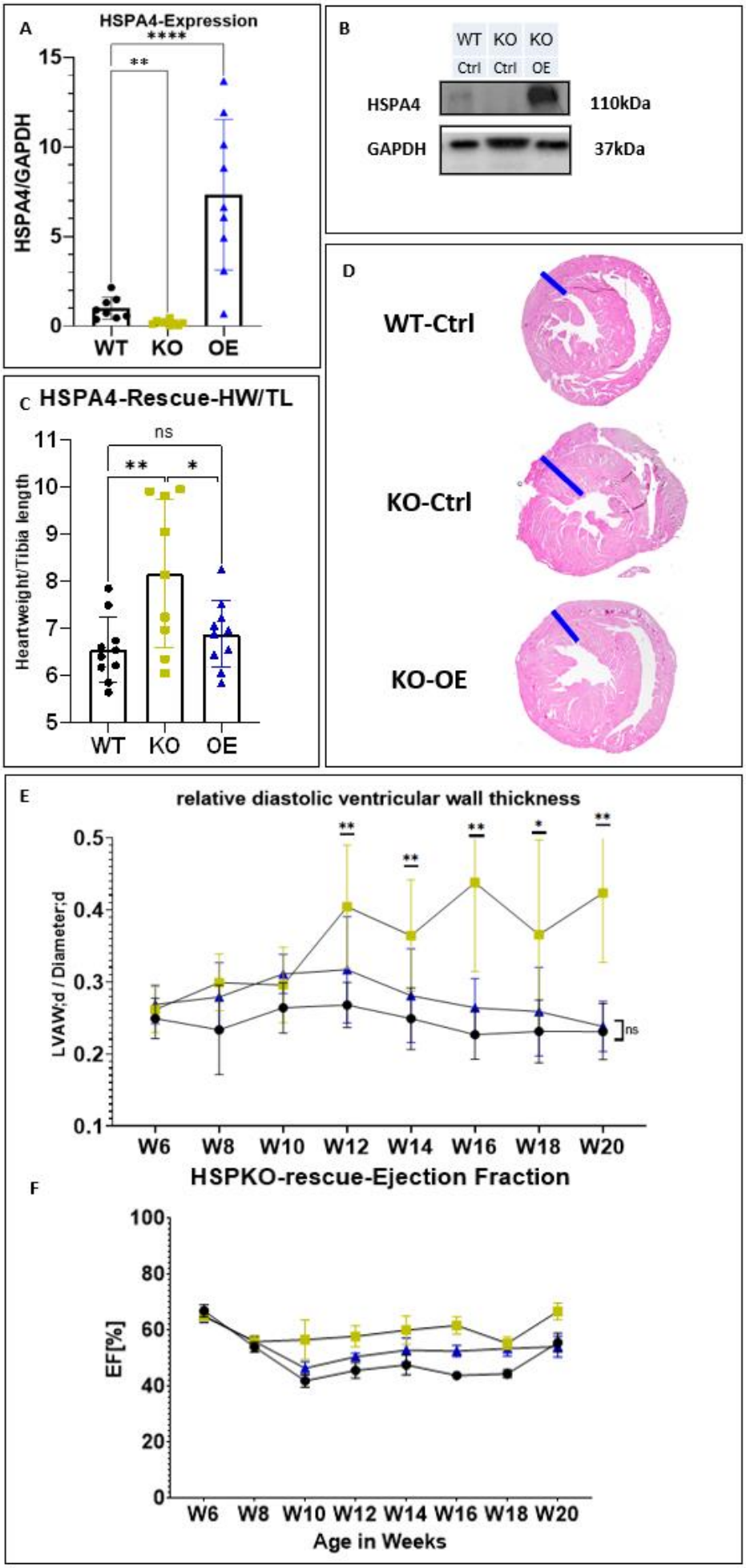
A
HSPA4-Expression
****
**
HSPA4/GAPDH
15
10
5
0
WT
KO
OE
B
WT
KO
KO
Ctrl
Ctrl
OE
HSPA4
110kDa
GAPDH
37kDa
C
HSPA4-Rescue-HW/TL
ns
**
*
Heartweight/Tibia length
11
10
9
8
7
6
5
WT
KO
OE
D
WT-Ctrl
KO-Ctrl
KO-OE
E
relative diastolic ventricular wall thickness
LVAW;d / Diameter;d
0.5
0.4
0.3
0.2
0.1
**
**
**
*
**
ns
W6
W8
W10
W12
W14
W16
W18
W20
HSPKO-rescue-Ejection Fraction
F
EF[%]
100
80
60
40
20
0
W6
W8
W10
W12
W14
W16
W18
W20
Age in Weeks

Figure 3.1.2 Cardiomyocyte-specific overexpression of HSPA4 rescued the phenotype in the heart in systemic HSPA4 KO

A-B) Relative HSPA4 protein expression determined via immunoblotting from isolated left ventricular heart tissue of AAV9-DsRed treated mice expressing wildtype HSPA4 (+/+, WT) and double knockout (-/-; KO) in comparison to AAV9-HSPA4 overexpressing vector (-/-; OE) C) Dry Heart weight in relation to tibia bone length at point of sacrifice [mg/mm] D) Histological sections of the short axis of wildtype, knockout, and rescued animals ventricles stained with haematoxylin-eosin. Blue bar was placed tangentially to the papillary muscles and indicates the axis measured [mm] E) Echocardiographic data of left ventricular anterior wall thickness concerning left ventricular diameter during diastole monitored after injection of AAV9-HSPA4[mm/mm]. F) Echocardiographic measurement of the left ventricular ejection fraction throughout the experiment [%] (WT-Control black N= 8; KO-control yellow N=9; KO-OE blue N=9) Statistical analysis performed as 1-way ANOVA in A&B and 2-way ANOVA in time-dependent graph E&F) expression normalized to GAPDH

As shown in the previous dissertation work of Barakat 2010. cardiac remodeling in HSPA4-KO animals might start as early as 15 days after birth, demonstrated by the increased expression pro hypertrophic marker ANP [Barakat 2010]. However, cardiac fibrosis was also found as early as two months old in animals. Indeed, sections were stained in this experiment for excess collagen in the ECM with Picrosirius red. The relative fibrotic area was determined as 0.82 % in the WT compared to 6.463 % in KO and 2,053 % (p=0.0015) in the rescued animals **(Fig 3.1.3 A-B)**. Therefore, cardiac fibrosis was ameliorated by overexpressing HSPA4 in the heart of KO animals.

Furthermore, the total mRNA from left ventricular tissue was isolated, and the expression of COL1A1 and the associated cross-linking enzyme LOX2 was determined via quantitative real-time PCR. Here a relative mRNA expression reduction from 5.155 in KO to 1.415 (p=0.0014) in OE and 7.610 to 1.059 (p=0.002) was found, respectively **(Fig 3.1.3 C-D)**, showing that expressing HSPA4 prevented cardiac fibroblasts from producing excess ECM material. This data suggests that cardiac fibrosis was prevented by overexpressing HSPA4 in the heart of KO animals.

During pathological cardiac remodeling, cardiomyocytes increase their size to exert the additional force needed to compensate for damaged functions by increasing their

length in dilated cardiomyopathies or their width in hypertrophic cardiomyopathies [Toischer 2010]. Since concentric hypertrophy was seen in echocardiography and histology, next, the extracellular matrix of the myocardium was stained via wheat germ agglutinin conjugated to an alexa555 fluorophore. Here the cellular margins of the cardiomyocytes were outlined, and about 200 cells per sample were measured utilizing a semi-automatic approach **[Appendix FIJI]** for their minimal ferret's diameter **(Fig 3.1.3 F).** In this experiment, the average cardiomyocyte size of 9.109 µm in KO was reduced to 8.482 µm (p=0.0427) in the OE group in comparison to WT 8.01 µm (p=0.1477) **(Fig 3.1.3 F)**. The wall thickness was ameliorated in the OE group, and cardiomyocyte size was reduced compared to the KO group. Cardiomyocytes excrete the natriuretic peptides ANP and BNP in response to increased load, which ultimately reduces blood pressure by increased natriuresis and are commonly used as biomarkers determining cardiac hypertrophy [Vuolteenaho 2005]. The accompanying results support this claim that the relative mRNA expression of the cardiac stress marker NppA and NppB compared to WT control were reduced from 28.29 in KO to 5.301 (p=0.0046) in OE and 6.694 in KO to 1.436 (p=0.0014) in OE respectively **(Fig 3.1.3 G-H)** These commonly used biomarkers indicate that the volumetric burden of the heart is significantly reduced after overexpression of HSPA4.

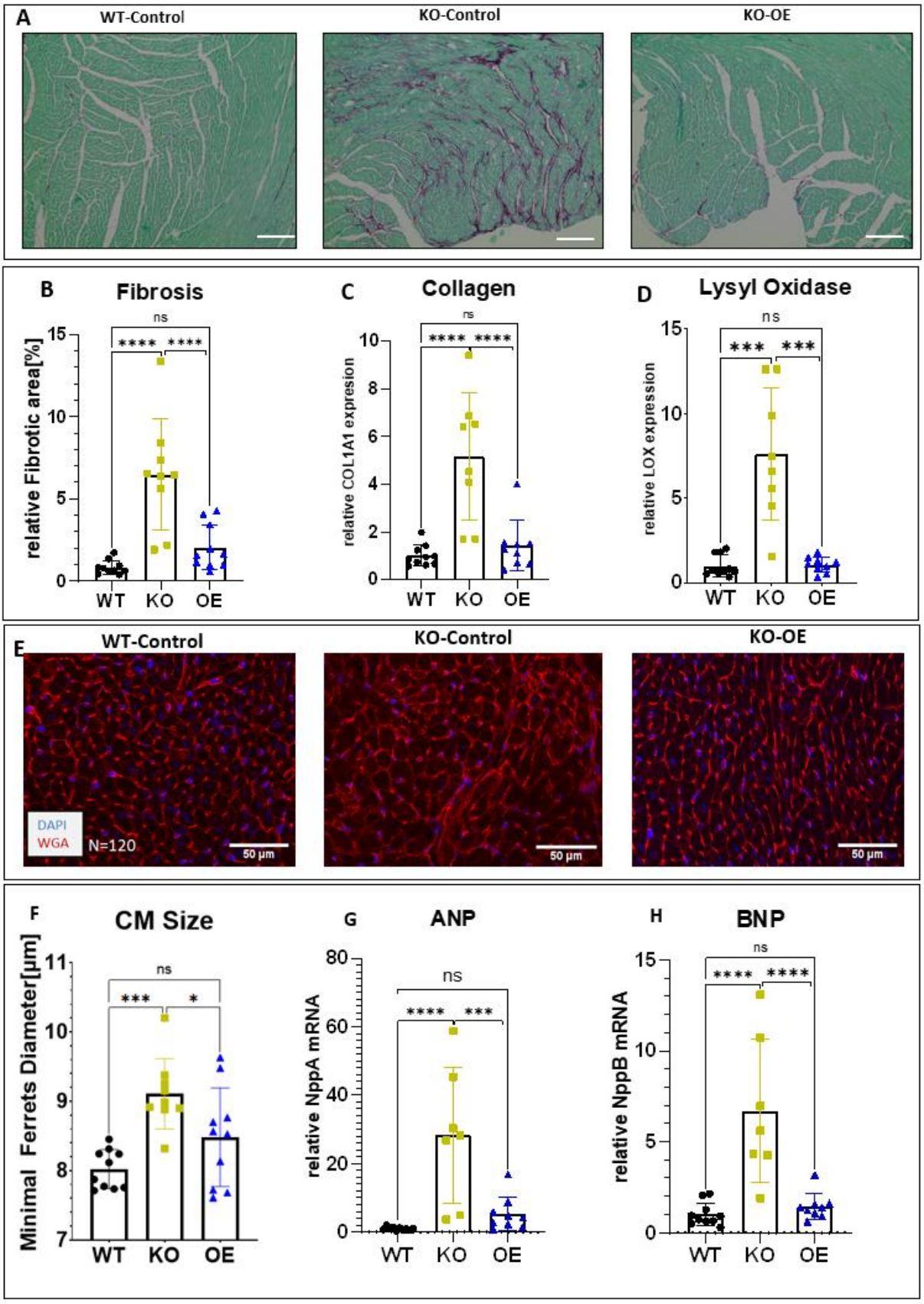

Figure 3.1.3 Overexpression of HSPA4 in Cardiomyocytes rescued the fibrotic phenotype in the left ventricle in HSPA4 knockout mice.

A) Histological sections of left ventricular tissue of Wildtype (WT); HSPA4 knockout (KO) and rescued knockout (KO-OE) animals stained with Sirius red (collagen) as fibrosis marker and

fast green (cytosolic proteins) for contrast. B) Relative fibrotic area was determined by measuring the area of stained collagen in the whole left ventricle via ImageJ software macro-FIBROSIS(Appendix), showing a marked decrease in the interstitial fibrotic area after overexpression. In addition, C-D) relative mRNA expression of collagen1a1 and lysyl oxidase determined via quantitative real-time PCR showing a significant decrease of these fibrotic markers after overexpression E)Histological sections of left ventricular tissue extracellular matrix stained via fluorescently labeled WGA red and nuclei with DAPI imaged with CY3(555nm) and DAPI(359nm) filter at 20x magnification F) The minimal ferret's diameter of 120 cells per animal was measured via ImageJ software WGA-Macro (appendix) showing the rescue of cardiomyocyte size after overexpression G-H) relative mRNA expression measured via qPCR of cardiac stress markers diuretic peptides NppA and NppB showing a significant decrease after overexpression. (WT-Control black N= 10; KO-control yellow N=10; KO-OE blue N=8) Statistical analysis performed as 1-way ANOVA expression normalized to GAPDH

Since the left ventricular ejection fraction was unchanged even though the myocardial compliance was expected to be reduced with a high degree of hypertrophy and fibrotic tissue, the global longitudinal strain (GLS) as a more sensitive parameter was used to assess heart function. During systole, the ventricle undergoes circumferential thickening and longitudinal shortening, which can be measured over a certain period. This strain in this context refers to a unitless parameter of the length of LaGrange speckle tracking in 2D echocardiographic images with a high temporal resolution before and after contraction averaged over multiple measurement points. [Potter 2018]. Here a substantial difference in strain was found 16 weeks after birth in the KO group, with a differential GLS of the left ventricle from -13.71 % in the WT to -9.428 % in the KO ($p=0.0009$), which was not significant in the OE group compared to WT control **(Fig3.1.4. A-B)**. Additionally, the time until the peak of contraction in opposing quadrants of the left ventricle was measured and increased to 69.89ms in KO and 33.40ms ($p= 0.0043$) in the HSPA4 overexpression group compared to 17.8 in WT control **(Fig3.1.4 C-D)**.

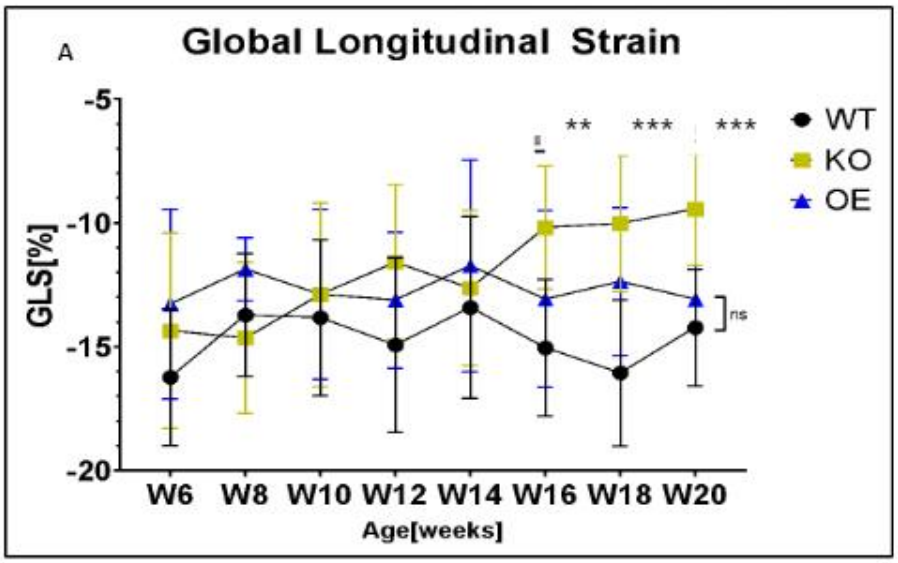
A
Global Longitudinal Strain
GLS[%]
-5
-10
-15
-20
W6 W8 W10 W12 W14 W16 W18 W20
Age[weeks]
**
***
***
ns
WT
KO
OE

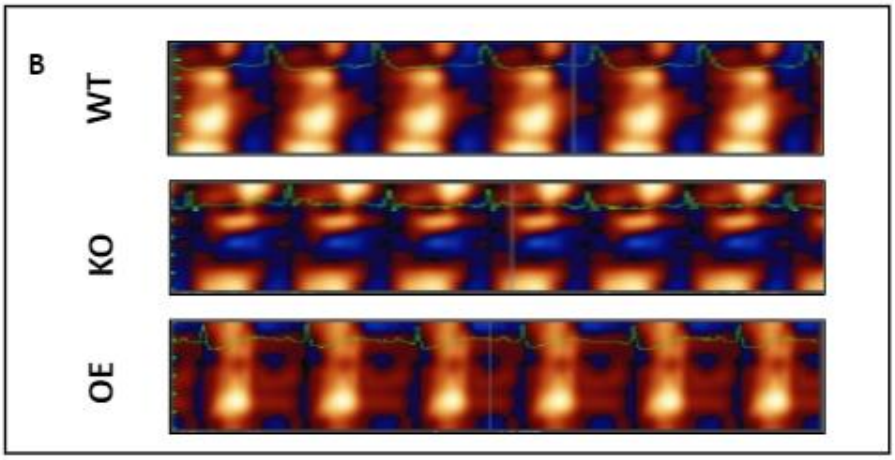
B
WT
KO
OE

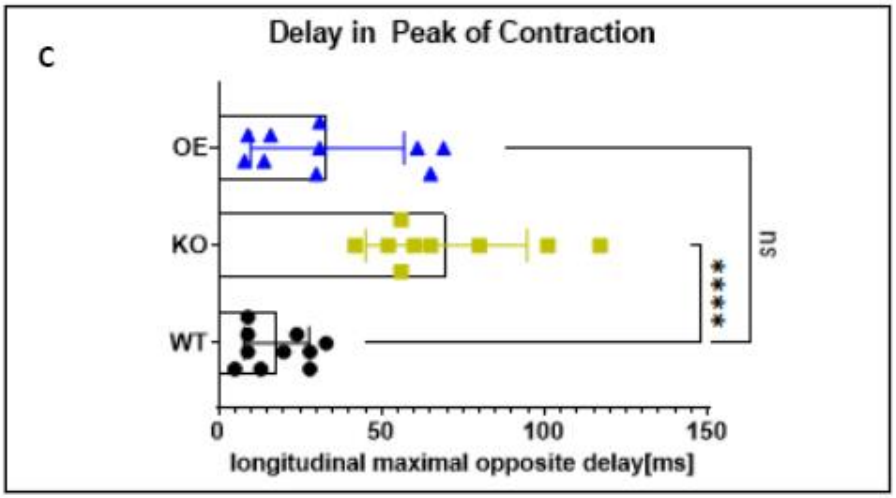
C
Delay in Peak of Contraction
OE
KO
WT
ns
****
0
50
100
150
longitudinal maximal opposite delay[ms]

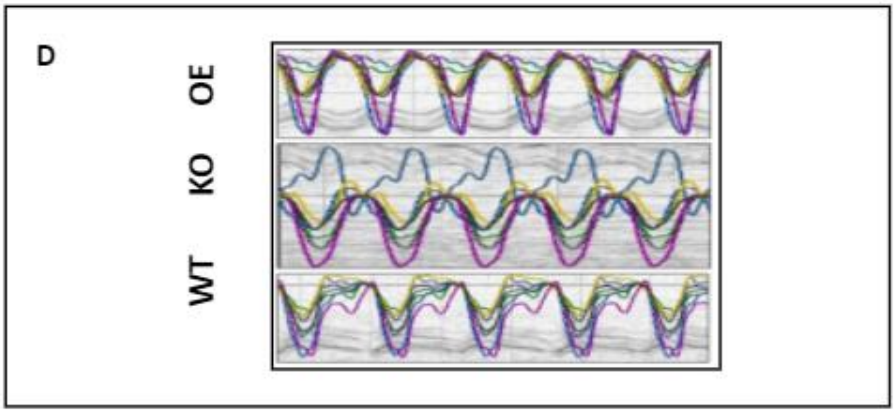
D
OE
KO
WT

Figure 3.1.4 Echocardiographic assessment of cardiac remodeling in the HSPA4-KO rescue experiment

A) Global longitudinal strain measured via echocardiographic VevoStrain Software version (3100), showing a decrease in the left ventricle strain in KO animals at 16weeks of age but not in rescued OE group. B) Heat map representation of the Global longitudinal strain depicted in A. over six cardiac cycles (Yellow-Red high, Blue low). A uniform strain color in each cycle depicts physiological function. In contrast, uneven strain indicates dysfunction as seen in the KO C) Delay of the contraction between the opposing walls of the left ventricle in longitudinal echocardiography during systole. In the KO, an increased opposite wall delay can be seen, indicating uneven contraction of the left ventricle. This was ameliorated in the OE group D) Histogram of longitudinal strain divided into six sections: posterior base(green); posterior mid(white); posterior apex(teal); anterior base(blue); anterior mid(yellow); and anterior apex(purple) in 20-week-old animals analyzed in C. In the KO sample, peak contraction of the posterior apex occurs during the other segments' relaxation, indicating a possible hindrance in signal transduction. (WT-Control Black N=10; KO-control Yellow N=9; OE-rescue blue N=10) Statistical analysis performed as and 2-way ANOVA in time-dependent graph A and as 1-way ANOVA in C)

To summarize, the knockout of HSPA in the heart leads to cardiac remodeling in the form of concentric hypertrophy and interstitial fibrosis, possibly as a compensatory mechanism as the ejection fraction is still preserved. Nonetheless, ventricular elasticity was lowered, and abnormalities in contractions occurred, which might have been the reason for lowered mortality in the old animals. Overexpression of HSPA4 in the heart prevented cardiac remodeling and demonstrated that the observed phenotype was primarily from impairments in cardiomyocyte function and not from increased load in other organs.

3.2. HSPA4 is needed for proteostasis and autophagy in the heart

As Mohamed *et al.* previously described, HSPA4 KO animals accumulate poly-ubiquitylated proteins in the heart. Ubiquitin was named after its ubiquitous expression in all types of tissue, as it is a vital post-translational modification of proteins to mark them for degradation. If the conformation of a protein in the cell changes due to a myriad of stressors (e.g., oxidative stress or kinetic stress), an inner hydrophobic KFERQ motif is exposed, which is recognized by a system of ubiquitin-transferring

ligases. The fate of the protein is decided by which lysine residue it was modified as well as how many ubiquitin molecules were attached. Single misfolded proteins are mostly monoubiquitylated on their K14 residue and either degraded by the UPS or CMA. If the misfolded proteins aggregate, the surface is poly-ubiquitylated and degraded via macro-autophagy (MA). Since the total amount of ubiquitinylated proteins was increased in HSPA4-KO animals, a dysregulation of the protein quality control was suspected [Arndt 2010].

The tissue was stained against aggregated proteins via an open β-sheet intercalating dye to visualize an accumulation of misfolded proteins in left ventricular tissue sections. Aggresomes are a few nanometers wide vesicles that form inside the cell when autophagic processes are impaired and autophagosomes fuse [Li 2020]. Following visual analysis of fluorescent images in HSPA4-KO, left ventricular tissue sections showed a marked increase of these vesicles in knockout animals. Furthermore, aggresome-dye positive vesicles were lower in the OE group compared to KO **(Fig 3.2.1 A&B)**. These results suggested that without HSPA4, physiological protein quality control and autophagic processes were impaired, which led to the accumulation of cytotoxic aggresomes. P62/Sequestosome-1 is a ubiquitin-like protein that acts as an adaptor between the ubiquitylated cargo and the transmembrane protein LC3B-II in the autophagosomal vesicle. Under physiological conditions, P62 is engulfed in the autophagosome and degraded alongside the cargo after fusion with the lysosome. [Gottlieb 2010] It acts as a marker in protein degradation as its accumulation indicates dysregulated PQC. In the KO samples, a co-localization of ubiquitin and P62 was seen, indicating heightened protein degradation compared to the WT control. The OE group showed fewer positive cells than the KO group and was more similar to the WT control **[Fig 3.2.1 C&D].**

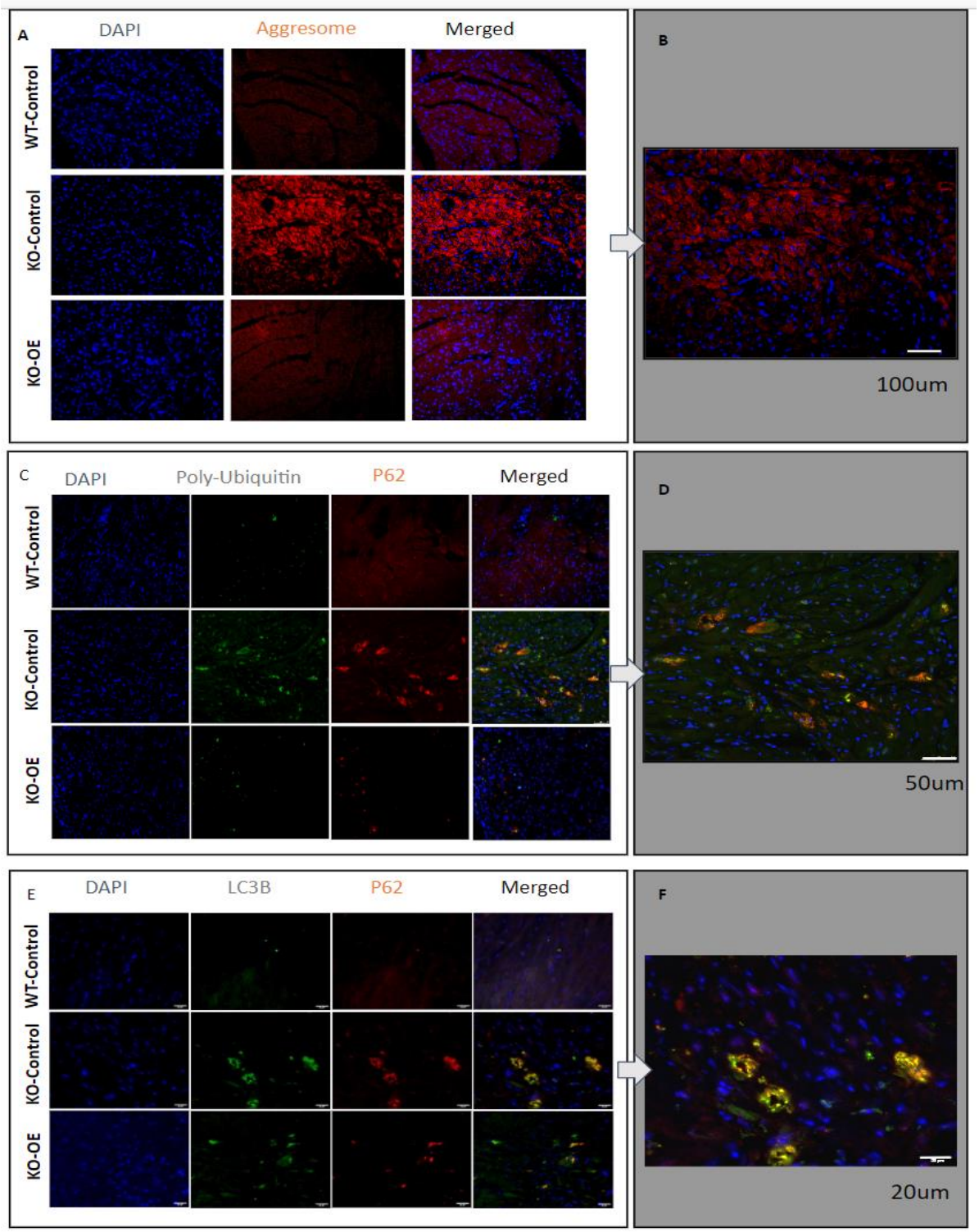

Figure 3.2.1: Aggresome formation alongside autophagic markers P62 and LC3B were normalized after HSPA4 OE in the heart

A) Histological sections of wildtype-control (WT-Ctrl); HSPA4 knockout (KO-Ctrl), and rescued HSPA4 knockout (KO-OE) were stained with an exposed beta-sheet intercalating dye as well as DAPI. B) Zoomed image of the KO control showing a high amount of positive vesicles,10x magnification C) Co-Immunofluorescence of WT-ctrl; KO-Ctrl and KO-OE against poly-ubiquitylated proteins and P62/Sequestosome-1 D) Zoomed image of KO control showing co-localization indicating high protein degradation, 20x magnification E) Co-immunofluorescence of WT-ctrl; KO-ctrl and KO-OE histological sections against

P62/sequestosome-1 and LC3B. F) Zoomed image of KO control showing a co-localization of autophagosomal markers P62 and LC3B, indicating a high amount or blockage of autophagic protein degradation, 63x magnification)

Furthermore, the autophagosomal sequestration protein LC3B-II was markedly increased and co-localized with P62/SQSTM1 in the KO group, which may indicate blocked autophagic degradation **(Fig3.2.1 E&F)**.

Alongside the immunofluorescence, an immunoblot against poly-ubiquitinylated proteins was performed and showed a difference from 2.613-fold in KO to 1.051-fold(p=0.0001) in OE compared to the WT control **(Fig3.2.2 A)**. The P62/SQSTM1 protein expression showed an upregulation of 4-fold (p=0.0142) in the KO group, which was reduced to 0.8873 in the OE group (p=0.0073) compared to the WT control **(Fig 3.2.2 B).** To quantify autophagosomal vesicle formation, immunoblots against LC3B showed one band for the cytosolic form at 17kDa and the lipidated transmembrane isoform LC3B-II at 15 kDa. This data shows that an increase of 2.6-fold (p=0.0446) was seen in LC3B-I and 3.5-fold (p=0.0066) in LC3B-II, respectively, in the KO group compared to the WT control **(Fig 3.2.2 C)**. In the OE group, the expression level of LC3B-I was reduced from 2.59 in KO to 0.95 in OE (p=0.0275), and LC3B-II levels from 2.577 in KO to 1.168 in OE(p=0.0142) respectively compared to the WT expression**.**

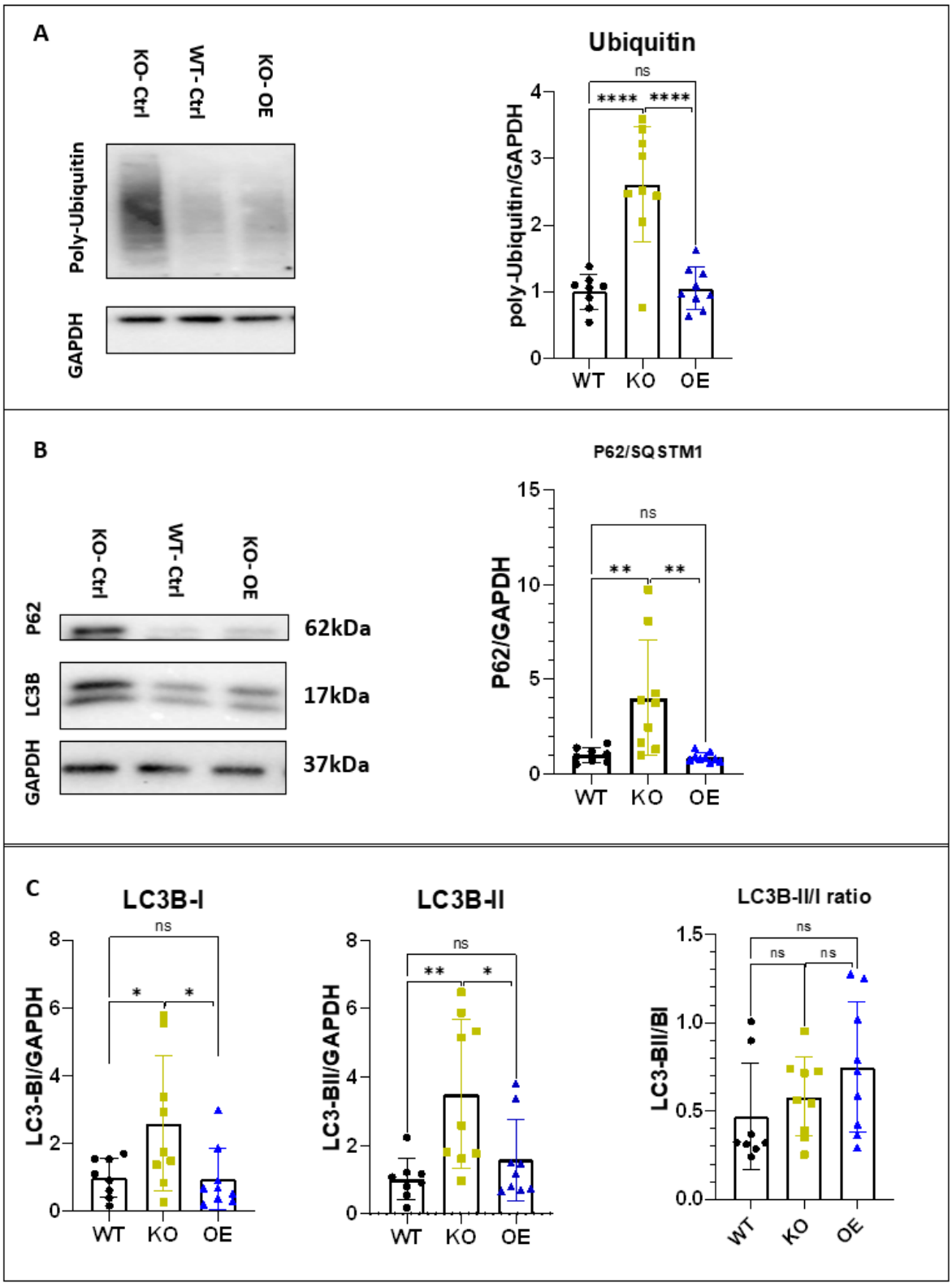

Figure 3.2.2 Aggregated proteins and autophagic markers P62 and LC3B were lower than in KO after HSPA4 OE in the heart

A) Immunoblots of left ventricular heart tissue against poly-ubiquitin B) Analysis of band intensity of poly ubiquitylated proteins showing an increased amount of poly-ubiquitylated proteins in the KO samples but not the rescued animals. B) Immunoblot of P62/SQSTM1 and LC3B. P62/SQSTM1 was significantly higher expressed in the KO group but not the OE

group. C) Analysis of band intensity of LC3B I (upper band) and LC3B II (lower band) and the ratio of LC3BI to LC3BII conversion. LC3BI and LC3BII levels increased in the KO but not in the OE group. (WT-Control Black N=8; KO-control Yellow N=9; OE-rescue blue N=8) Statistical analysis performed as 1-way ANOVA, expression normalized to GAPDH

3.3. HSPA4 overexpression in pressure-overloaded hearts

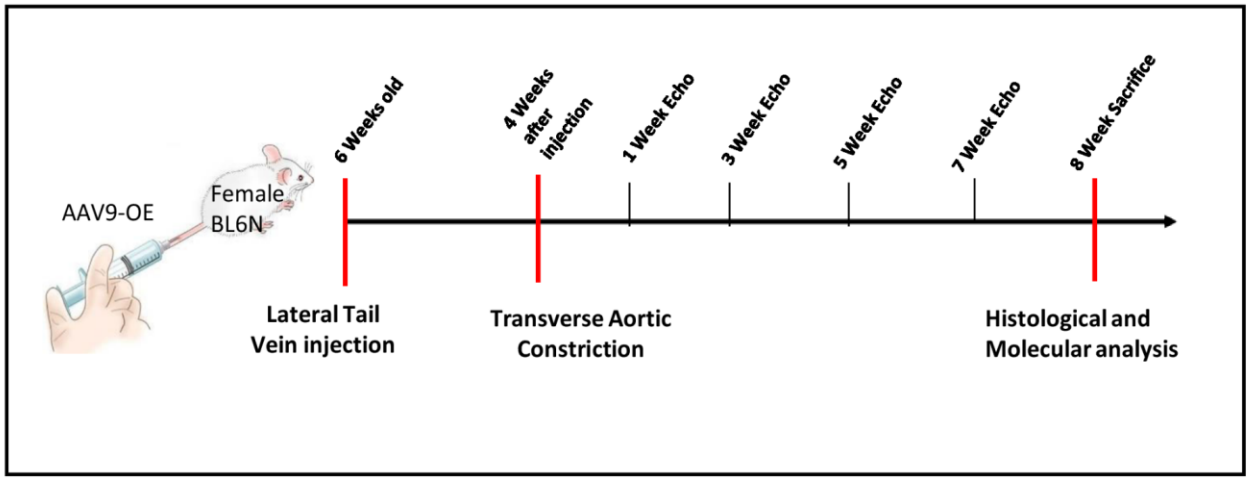

Figure 3.3.1 Experimental Setup of HSPA4 overexpression in Pressure Overload model

Six weeks old female WT Bl6/N mice were injected with 10^12 AAV9-HSPA4 or AAV9-DsRed control particles via the left lateral tail vein. At ten weeks of age, pressure overload was induced via transverse aortic constriction. Heart morphology was monitored via echocardiography one week, three weeks, five weeks, and seven weeks after TAC. At eight weeks, the mice were sacrificed, and the left ventricles were prepared for histological and molecular analysis.

As previously published in our lab, the expression of HSPA4 is elevated in pressure overload of the heart [Mohamed 2012]. To investigate if HSPA4 overexpression has a protective effect on the heart in the pressure overload model 6 weeks old female BL6N mice were injected with AAV9-HSPA4, and transverse aortic constriction (TAC) operation was performed four weeks after and monitored for eight weeks **(Fig 3.3.1)**.

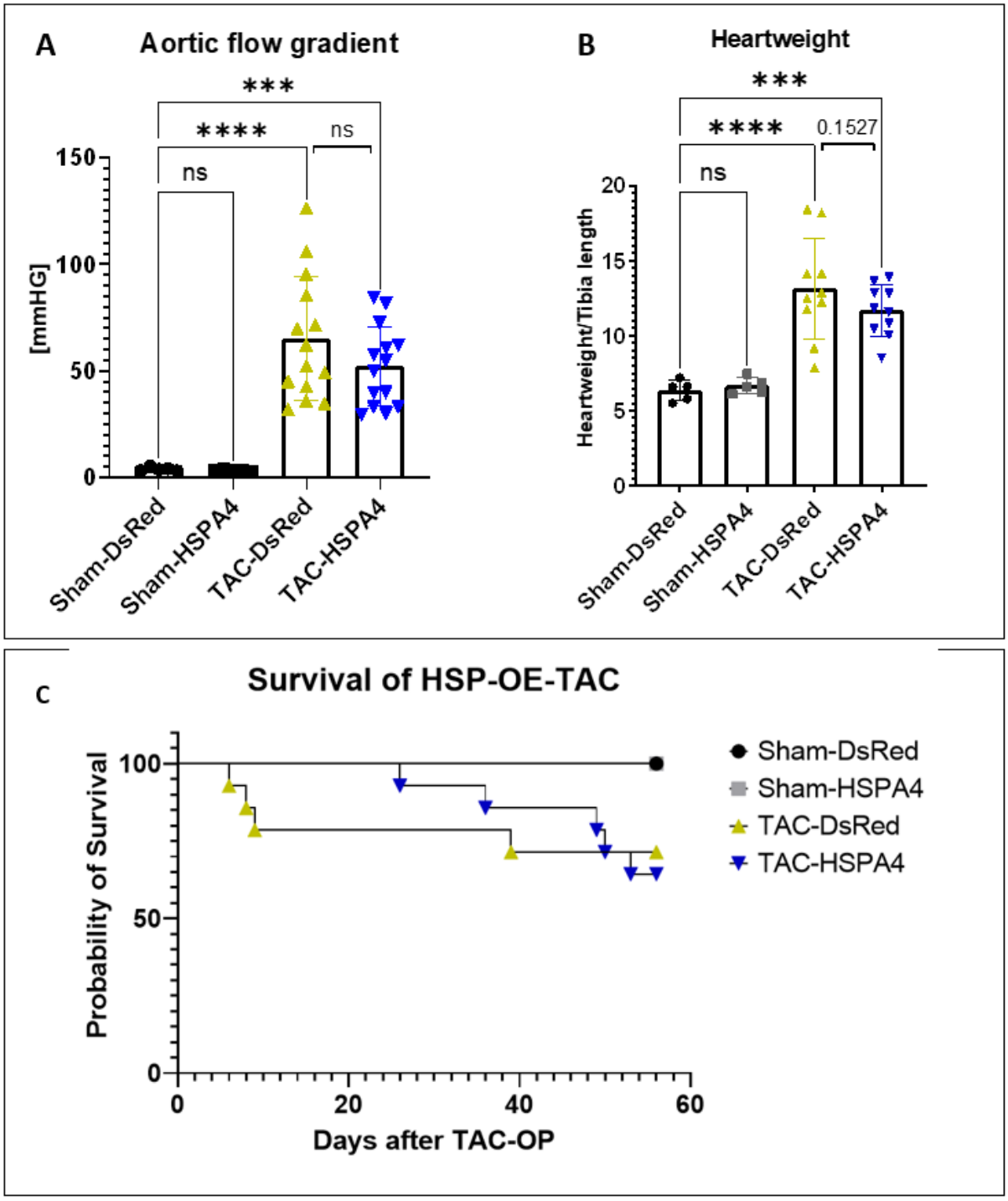

Figure 3.3.2 Progression of hypertrophy to heart failure after TAC

A) Difference in blood flow velocity before and after the transverse aortic constriction showing increased pressure in TAC groups demonstrating a successful operation B) dry heart weight relative to tibia bone at the point of sacrifice C) Kaplan Meyer Survival graph of Transverse Aortic constriction (TAC) operated animals with sham operation as control as well as AAV9-HSPA4 overexpression (blue) with AAV-9 DsRed (yellow) as control. Statistical analysis was performed as 1-way ANOVA.

The increase in blood pressure was verified by measuring the blood flow velocity in the aorta in front of the constriction and after the constriction via doppler echocardiography,

formulating a mean transaortic gradient in mmHG [Baumgartner 2009]. Here an increase in pressure from the mean of 3-5 mmHg in Sham-operated animals to a mean of 50-60 mmHG in TAC-operated animals was determined **(Fig 3.3.2 A)**. Alongside these findings, the heart weight normalized to tibia bone length at the point of sacrifice was increased significantly in both groups. However, it showed no significant difference with 13.13 mg/mm in TAC-DsRed and 11.65 mg/mm in TAC-HSPA4 **(Fig 3.3.2 B)**. Survival after the TAC operation was monitored in the groups of Sham-DsRed control, Sham-HSPA4 control, TAC-DsRed, and TAC-HSPA4 for 60 days after the operation. Even though lower mortality was seen in the OE group, the final survival percentage was non-significant, with 71 % in TAC-DsRed and 64 % in TAC-HSPA4. **(Fig 3.3.2 C)**

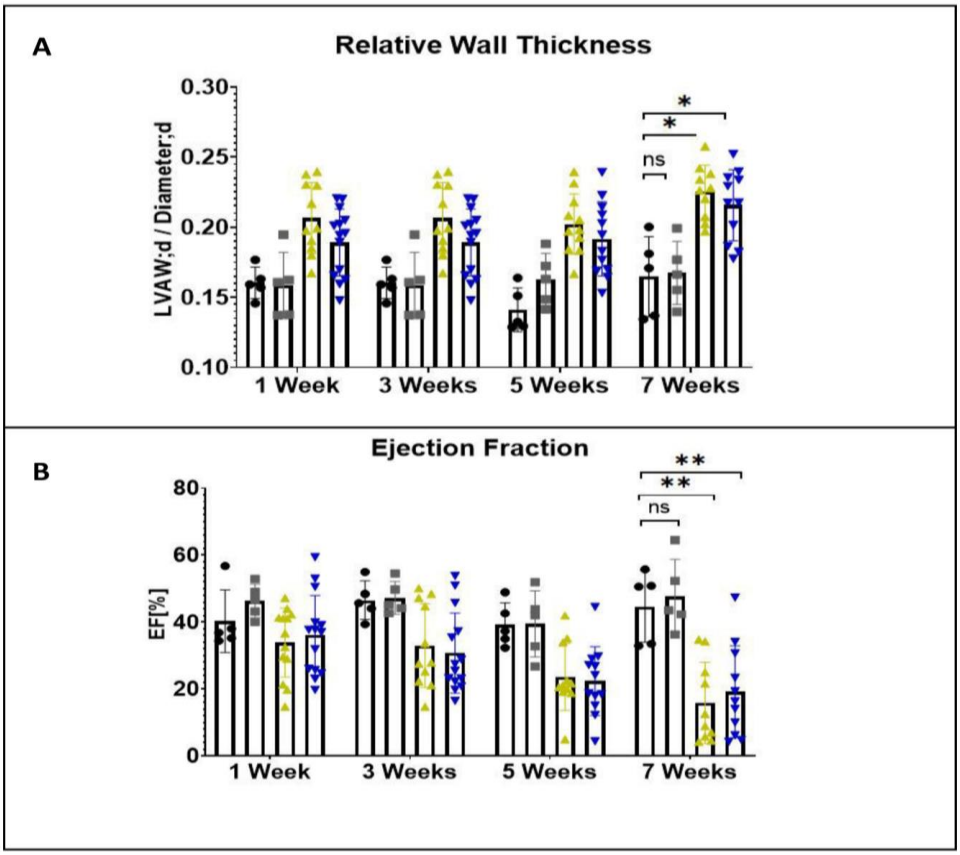

Figure 3.3.3 Echocardiographic progression after TAC

Echocardiographic measurements were taken every two weeks, beginning with the first week after TAC. A) The left ventricular anterior wall thickness in diastole normalized to the ventricular diameter during diastole as an indicator for hypertrophy. Both TAC groups show a marked increase in wall thickness compared to Sham-DsRed. B) Determination of ejection fraction compared to Sham. The EF decreased gradually until the 7th week when the

Experiment was closed due to ethical concerns. (Sham-DsRed black N=5, Sham-HSPA4 grey N=5, TAC-DsRed N=15, TAC-HSPA4 N=15) statistical analysis as 2-way ANOVA.

The left ventricular wall thickness was normalized to the ventricular diameter (mm/mm) and showed a thicker wall in TAC-DsRed and TAC-HSPA4 5 weeks after TAC **(Fig 3.3.3 A).** At 7 weeks, the relative wall thickness of Sham-DsRed is 0.1647 and not significantly different from Sham-HSPA4 with 0.1675 (p=0.9941). TAC-DsRed and TAC-HSPA4 are significantly increased with 0.2252 and 0.2157, respectively(p=<0.0001). There was no significant difference between the TAC groups (p= 0.9045).

The ejection fraction was calculated from echocardiographic doppler imaging of the short axis of the left ventricle, in which a gradual decrease would be expected after TAC, ultimately leading to heart failure **(Fig 3.3.3 B)**. Three weeks after TAC, a significant difference from 46 % in sham groups to 33 % in both TAC groups is seen, deteriorating to 15 % at week 7. In the 7th week, Sham-DsRed showed a mean EF of 44.71 % and was not significantly different from Sham-HSPA4 with 47.81 % (p=0.9371). The mean EF of TAC-DsRed and TAC-HSPA4 was lowered to 15.86 % and 19.14 %, respectively (p=<0.0001). Both TAC-DsRed and TAC-HSPA4 showed an almost identical progression compared to each other(p=0.9961).

In summary, the overexpression of HSPA4 overexpression did not influence mortality, left ventricular hypertrophy, or Ejection Fraction in the pressure overload mouse model.

As expected in the pressure overload model, the cardiac stress markers ANP and BNP were elevated in the TAC animals as measured by relative mRNA expression **(Fig 3.3.4)**. In this experiment, the expression was not different in Sham-DsRed and Sham-HSPA4 (p=0.9997,0.9742) for ANP and BNP. TAC-DsRed showed a mean differential expression of 23.03-fold for ANP and 5.685 for BNP compared to Sham-DsRed

(p=0.0039, p=0.0053). Interestingly, the ANP expression in TAC-HSPA4 was ameliorated to 10.63-fold, making it non-significantly different from Sham-DsRed (p=0.2684). Similarly, the expression of BNP was non-significantly different, with 3.386-fold compared to Sham-DsRed (p=0.1932). Directly comparing TAC-DsRed with TAC-HSPA4 shows a significant difference in ANP expression (p=0.0339) but not in BNP expression (p=0.0702).

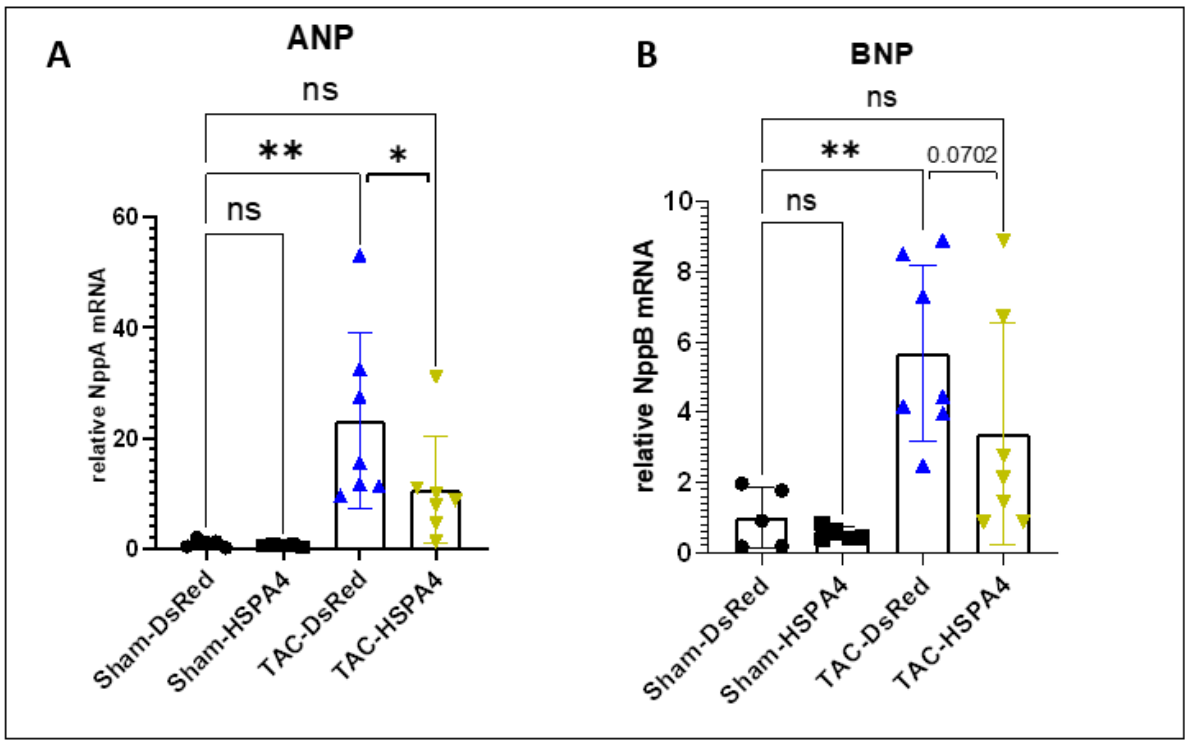

Figure 3.3.4 Cardiac Stress markers in quantitative real-time PCR

The mRNA expression of the cardiac stress markers ANP and BNP were measured from a subset of left ventricular tissue RNA isolates. The expression was not significantly changed from Sham-DsRed to Sham-HSPA4 but markedly increased in TAC-DsRed. The expression of both markers is still elevated in TAC-HSPA4 but non-significantly so. (Sham-DsRed black N=5, Sham-HSPA4 grey N=5, TAC-DsRed N=8, TAC-HSPA4 N=8) Expression was normalized against GAPDH Statistical analysis as 1-way ANOVA.

On the protein level, autophagic markers and ubiquitinylated proteins were analyzed via immunoblot to investigate the molecular effects of HSPA4 overexpression in the pressure overload model **(Fig 3.3.5 A-B)**. Poly-ubiquitylated proteins were not accumulated in either TAC group, indicating that physiological UPS degradation was

intact in these mice eight weeks after TAC **(Fig 3.3.5 C)**. Beclin-1 is a protein involved in the nucleation of the autophagosomal membrane and is activated by post-translational phosphorylation. A lowered but non-significant expression of Beclin was seen in the TAC-DsRED group (p=0.0617) but not in TAC-HSPA4 (p=0.4456)**(Fig 3.3.5 D)**. No significant change was observed in autophagic marker protein P62/SQSTM1 in Sham-HSPA4 compared to Sham-DsRed (p=0.8780). A non-significant trend for upregulation was observed in TAC-DsRed (2.058-fold p=0.0649) but not TAC-HSPA4 group (1.149-fold p=0.9084) **(Fig3.3.3 E)**. Furthermore, even though an increase in both TAC groups of cytosolic LC3B-I of 2.204-fold (p=0.0155) and 2.191-fold(p=0.0193) was found, there was no change in the active autophagosomal bound isoform LC3B-II, indicating that autophagy was not blocked in this experimental setup **(Fig3.3.5 F)**. Interestingly the LC3BII to LC3BI ratio, indicating turnover from cytosolic to membrane-bound isoform, was significantly lower in TAC-DsRed (p=0.0368) but not in TAC-HSPA4 (p=0.3726).

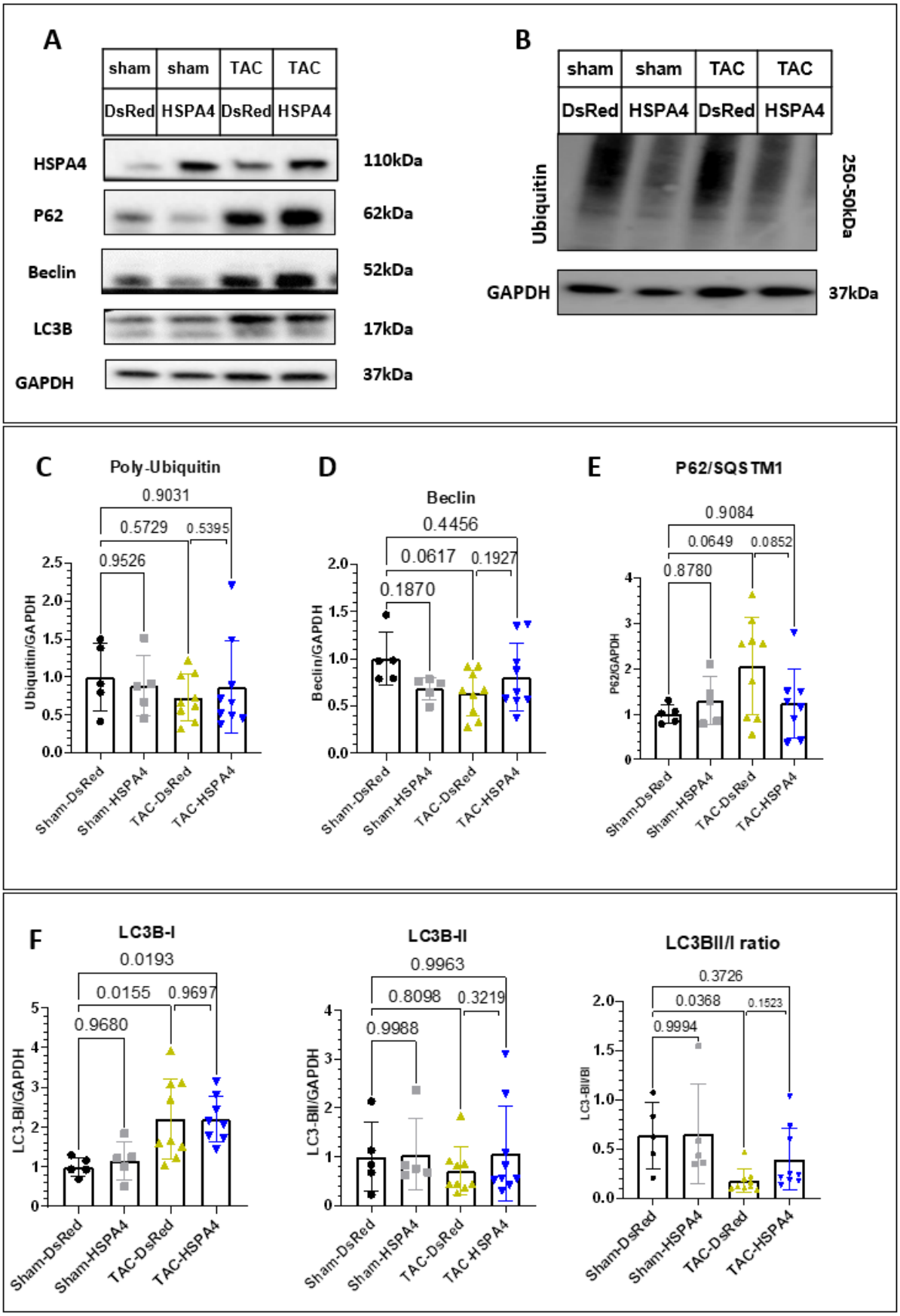

Figure 3.3.5 Protein Expression levels of targets involved in UPS and autophagic degradation

A) Immunoblot of left ventricular heart tissue against HSPA4, P62/SQSTM1, Beclin, and LC3B B) Immunoblot against poly-ubiquitin C) Analysis of band intensity of the Blot depicted in B with no change between the groups. D) Analysis of band intensity of Beclin 1 showing a non-significant trend for downregulation in TAC-DsRed. E) Analysis of band intensity of P62/SQSTM1 showing a non-significant trend for upregulation in TAC-DsRed. F) Analysis of band intensity of LC3BI (upper band) and LC3BII (lower band) showing a significant increase in LC3BI in both TAC-DsRed and TAC-HSPA4. There was no significant change in LC3BII, but LC3BII by LC3BI ratio was significantly lower in TAC-DsRed (Sham-DsRed black N=5, Sham-HSPA4 grey N=5, TAC-DsRed N=9, TAC-HSPA4 N=9) Expression was normalized against GAPDH Statistical analysis as 1-way ANOVA.

3.4. HSPA4 overexpression in the context of Doxorubicin-induced cardiotoxicity

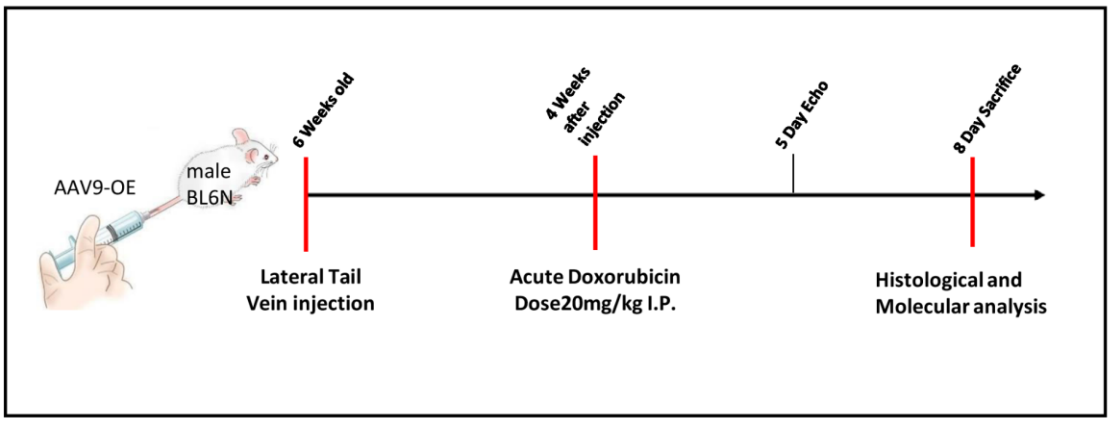

Figure 3.4.1 Experimental Setup of HSPA4 overexpression in the Doxorubicin cardiotoxicity model

Six weeks old male WT Bl6/N mice were injected with 10^12 AAV9-HSPA4 or AAV9-DsRed control particles via the left lateral tail vein. At ten weeks of age, Doxorubicin was administered at 20 mg/kg i.p alongside the Saline Control group. Heart morphology was monitored via echocardiography five days after the DOX intervention. At eight days, the mice were sacrificed, and the left ventricles were prepared for histological and molecular analysis.

The treatment with Doxorubicin can lead to acute, chronic, and even gradually progressive side effects during treatment and may cause permanent damage to the heart [Sheibani 2022]. Commonly used ranges in animal models are an acute dose of 20 mg/kg and the more clinically focused chronic dose of 3-5 mg/kg once per week over a month. To assess which treatment regimen would show the most promising prospects in HSPA4-overexpression intervention, a preliminary group of mice was

tested for treatment efficiency and effect on protein quality control. (Fig DOX 4 & DOX 6 Appendix)

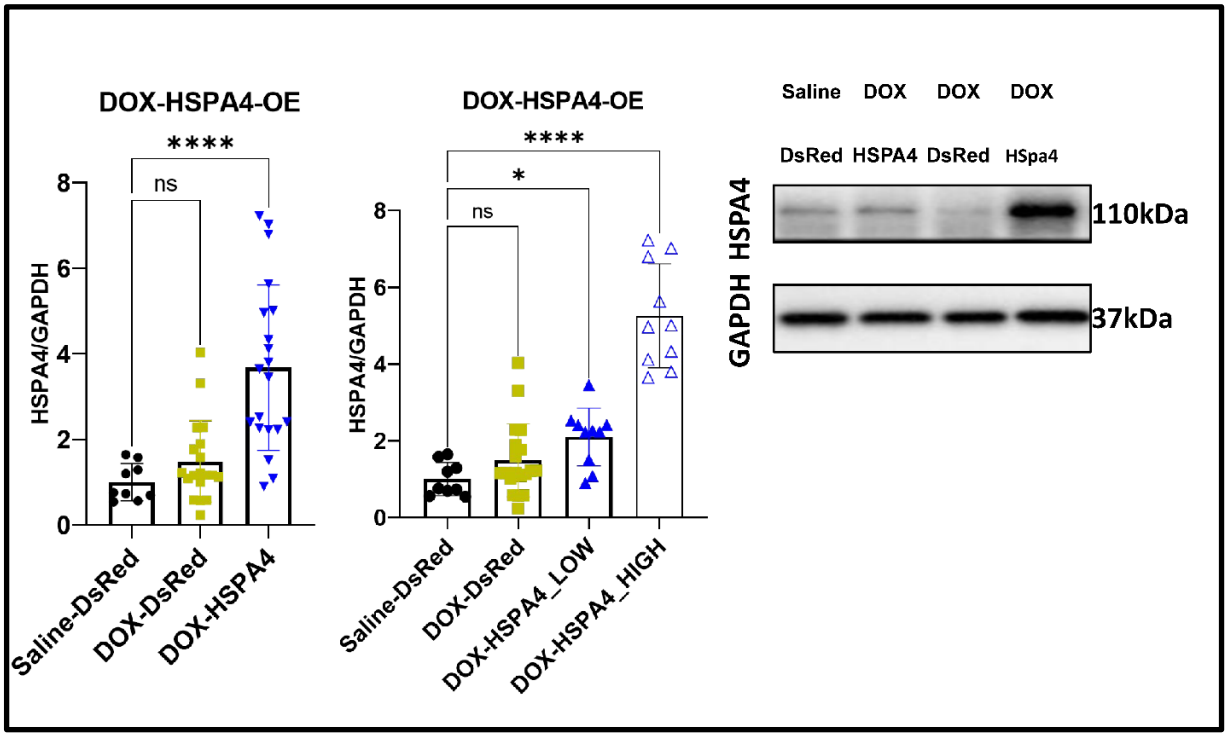

Figure 3.4.2 HSPA4 overexpression in left ventricular heart tissue

HSPA4 Protein levels determined via immunoblotting of Saline Control; Doxorubicin treated AAV9-DsRed; Doxorubicin treated AAV9-HSPA4 low expression, and Doxorubicin treated AAV9-HSPA4 high expression (Median of all Samples in OE group was used as cutoff) (Saline-DsRed N=9, DOX-DsRed N= 19, DOX-HSPA4 N=20. Low N=10. High N=10) Expression was normalized against GAPDH, 1-way ANOVA was used for statistical analysis

Since improved protein quality control in HSPA4-KO mice was seen, a protective effect against doxorubicin cardiotoxicity was hypothesized. The expression level of HSPA4 was determined via immunoblot. and the overexpression groups were divided into low-efficiency (LE; 2.101-fold p=0.0381) and high-efficiency overexpression (HE; 5.256-fold p=<0.0001) **(Fig 3.4.2 A)**. The OE mice were grouped and divided by the median, as a pattern of expression-dependent response appeared throughout the data sets, but both Data sets will be shown.

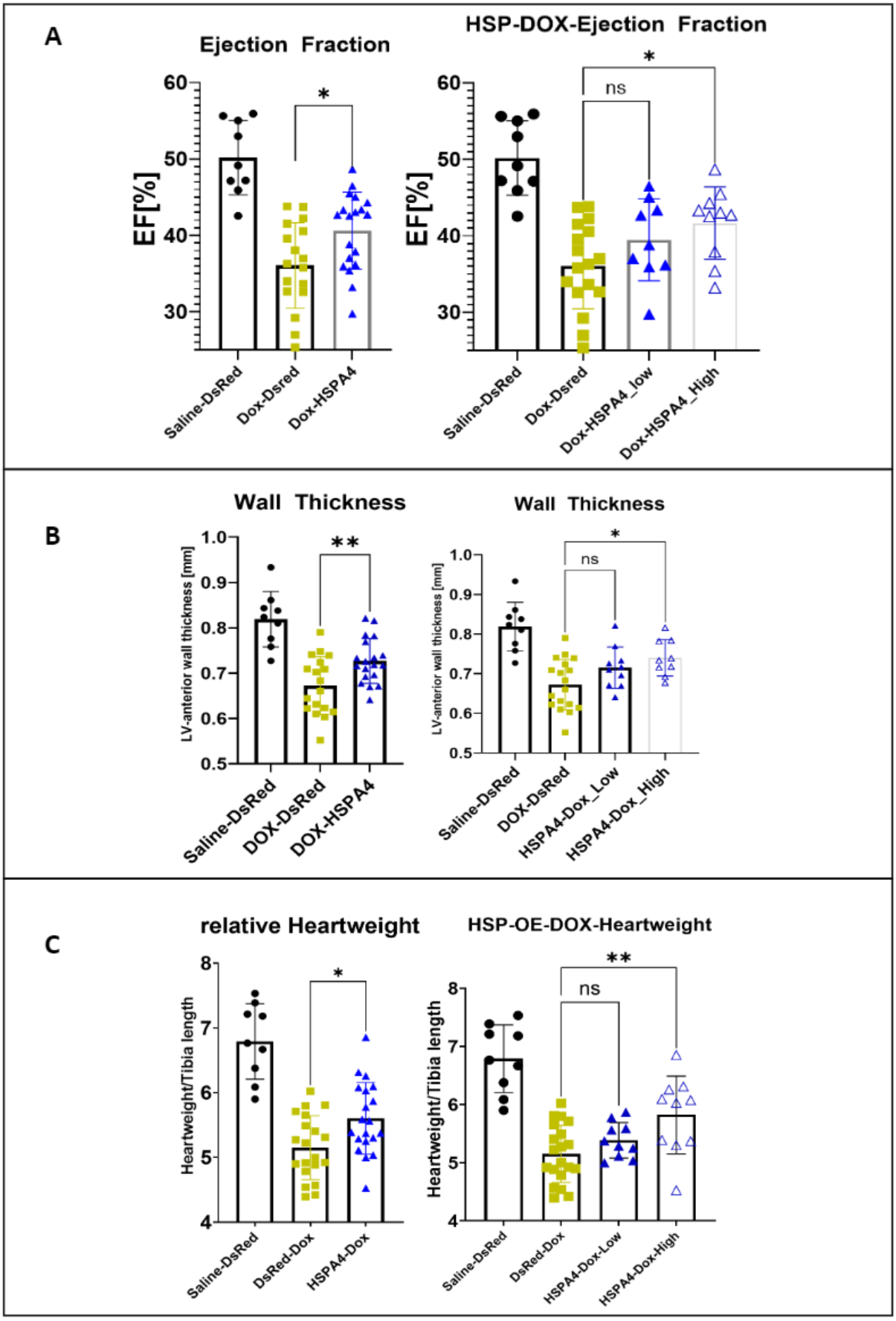

Figure 3.4.3 Echocardiographic assessment of DOX-induced cardiac atrophy

An echocardiographic measurement was performed five days after the DOX injection. A) The ejection fraction, DOX-DsRed and DOX-HSPA4, were markedly lowered compared to the Saline-DsRed control. Comparing DOX-DsRed and DOX-HSPA4 shows a significantly higher EF in the overexpression group. IF the HSPA4 group is split into low and high expression, only the high expression group retains the difference. B) Left ventricular wall thickness determined via echocardiography. Both Dox-treated groups show a marked thinning of the ventricular wall compared to the Saline-DsRed control. Comparing DOX-DsRed with DOX-HSPA4 shows a significantly thicker wall in the overexpression group. C) The relative dry heart weight was determined after the sacrifice of the mice. Both DOX-treated groups showed a marked reduction in heart weight compared to the Saline-DsRed control. Comparing Dox-DsRed with Dox-HSPA4 shows that the hearts are significantly heavier in the overexpression group. The significance is retained only in the high expression group after splitting the group into high and low. These findings indicate a expression-dependent effect. (Saline-DsRed black N= 9, DOX-DsRed yellow N=18, DOX-HSPA4_low, blue-filled N= 10. DOX-HSPA4_high blue-hollow N=10) Statistical analysis performed as 1-Way ANOVA

Anthracycline treatment can lead to dilated cardiomyopathy as late as 15 years after treatment in patients [McGowan 2017]. In contrast, treating mice with 20 mg/Kg Doxorubicin leads to immediate effects in cardiac atrophy alongside reduced function resulting in rapid weight loss and increased mortality [Willis 2019]. In this experimental setup, the effect of acute doxorubicin treatment was evaluated via echocardiography just five days after treatment. Here a reduction in ejection fraction from the Saline-DsRed control of 50.16 % was present in all groups. However, an ameliorated effect from the DOX-DsRed of 36,05 % to DOX-HSPA4_high 41.66 % was determined(p=0.0206), while the DOX-HSPA4 low group only showed a non-significant improvement to 39.47 %(p=0.2249) **(Fig 3.4.3 A)**. This finding correlates with the left ventricular anterior wall thickness, where a marked decrease from 0.8181 mm in Saline-DsRed control to 0.6724 mm (p=<0.0001) was seen in DOX-DsRed. Comparing DOX-DsRed with DOX-HSPA4_low with 0.7153 mm showed a non-significant difference in wall thickness (p=0.1294), but compared to the DOX-HSPA4_high group with 0.7398 mm, the wall was significantly thicker (p=0.132) **(Fig 3.4.3 B)**. The heart weight at the point of sacrifice was determined and normalized to tibia bone length. Here an overall reduction in the normalized heart weight of the DOX-treated groups compared to the Saline-DsRed control was observed. However,

comparing the heart weight from the DOX-DsRed group 5.150 mg/mm to the DOX-HSPA4_high group with 5.821 mg/mm showed significantly heavier hearts in the overexpression group (p=0.0035). An insignificant trend could be seen in the heart weight of the HSPA4_low group with 5.385 mg/mm compared to DOX-DsRed **(Fig 3.4.3 C)**.

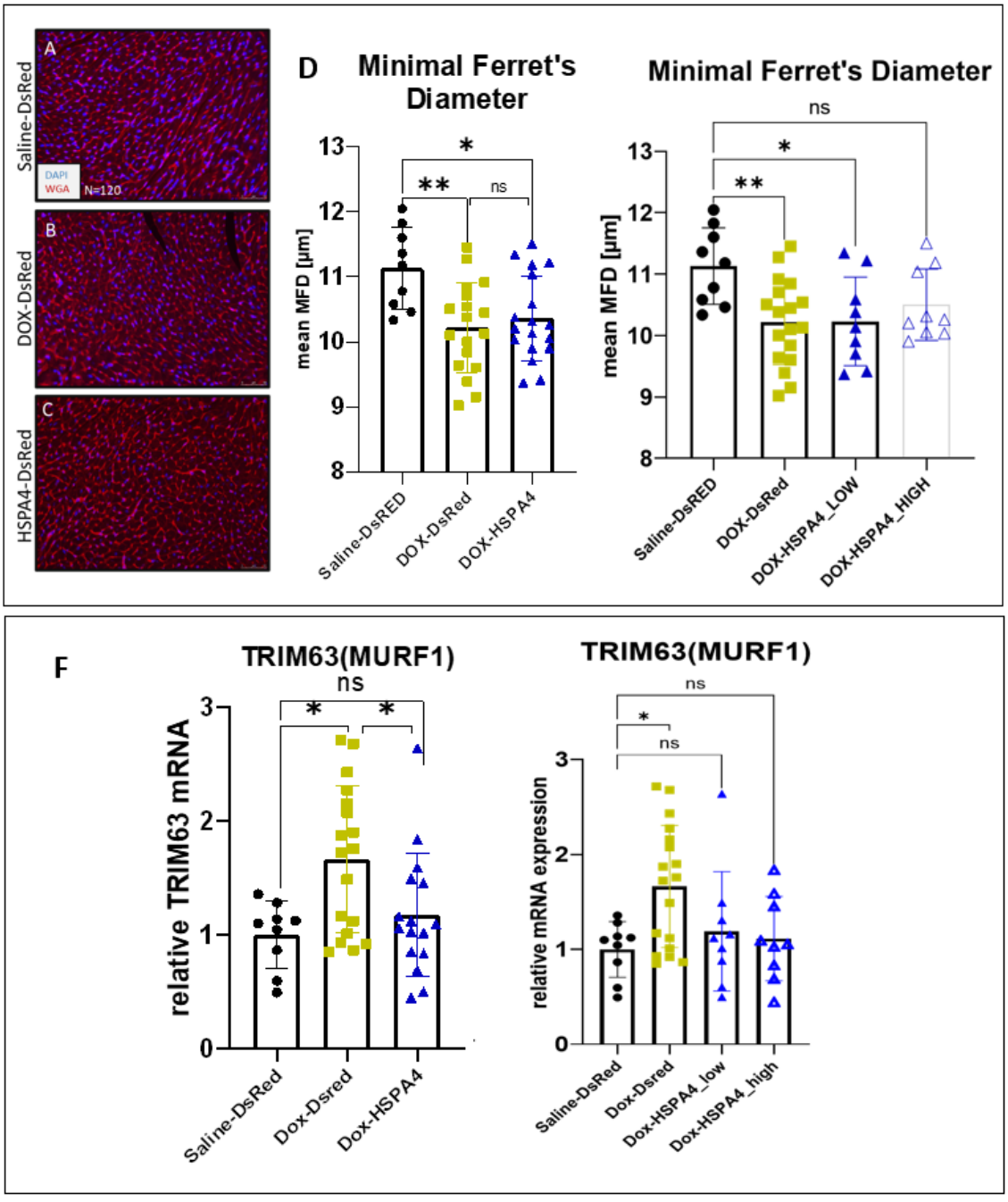

Figure 3.4.4 HSPA4 overexpression in the heart reduces doxorubicin-induced atrophy

A-C) WGA stain in saline control, Doxorubicin treated control, and Doxorubicin treated with HSPA4 overexpression. D) The minimal fiber diameter has been determined in all groups

showing a significant difference in Saline-DsRed against DOX-DsRed treated group and in the DOX-HSPA4_low overexpressing group. In the DOX-HSPA4_high, the cardiomyocyte size was not-significantly smaller than the Saline-DsRed control. F) Additionally, the mRNA expression of the atrophic transcription factor TRIM63 shows a marked increase in DOX-DsRed treated group but not in either DOX-HSPA4_low or DOX-HSPA4_high overexpressed groups. (Saline-DsRed black N= 9, DOX-DsRed yellow N=18, DOX-HSPA4_low, blue-filled N= 10. DOX-HSPA4_high blue-hollow N=10) Statistical analysis performed as 1-Way ANOVA

Further investigating if heart weight loss stems from the reduction in cardiac fiber size, the cardiomyocyte diameter was determined histologically. Similarly, a reduction of cell size from 11.13 µm in the Saline-DsRed control to 10.22 (p=0.0048) in the DOX-DsRed group was ameliorated to 10.50 (p=0.1235) in the DOX-HSPA4_high group **(Fig 3.4.3 D)**. Additionally, the atrophic transcription factor trim63 was elevated only in the DOX-DsRed group(p=0.0140) but not in the DOX-HSPA4_low or DOX-HSPA4_high overexpression groups **(Fig 3.4.2 C)**. Overall, the anthracycline treatment-induced cardiac atrophy in the left ventricle was ameliorated by HSPA4 overexpression in the heart in a expression-dependent manner.

As experiments from overexpressing HSPA4 in the HSPA4 KO animals showed improvements in protein quality control with HSPA4 overexpression, immunoblots of the previously tested autophagic markers and ubiquitylation pattern were performed **(Fig 3.4.5 A)**. In the immunoblots of the Saline-DsRed, DOX-DsRed, DOX-HSPA4_low, and DOX-HSPA4_high groups, no apparent change was observed in poly-ubiquitinated substrates. **(Fig 3.4.6)**.

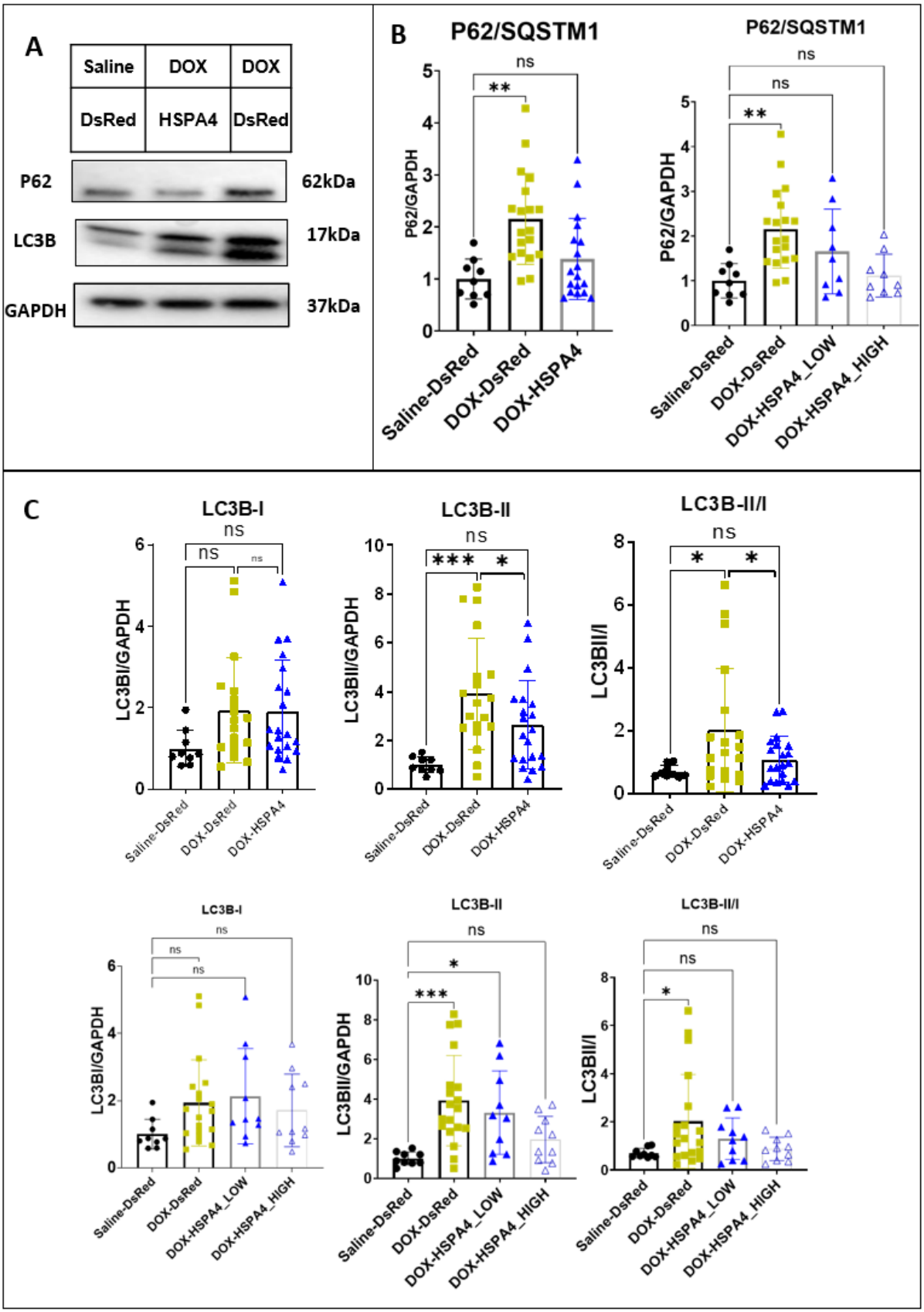

Figure 3.4.5 HSPA4 overexpression in the heart ameliorates doxorubicin-induced blockage of Autophagy

A) Immunoblot of left ventricular heart tissue against P62/SQSTM1 and LC3B with GAPDH

as loading control B) analysis of band intensity of P62/SQSTM1 showing a significant increase in DOX-DsRed group compared to Saline-DsRed. Comparing Saline-DsRed with the DOX-HSPA4 overexpression group shows no significant increase in the P62 protein level. Splitting the overexpression group shows no significant upregulation of P62 in both HSPA4_low and HSPA4_high groups but a lower expression in HSPA4_high. C) Analysis of LC3B-I (upper band) and LC3B-II(lower band) intensity shows a significantly upregulated expression of LC3B in the DOX-DsRed group but not in the DOX-HSPA4 overexpression group compared to the Saline-DsRed control. Splitting the overexpression group shows a significantly higher protein level of LC3B-II compared to Salien-DsRed in DOX-HSPA4_low but not in DOX-HSPA4_high. The LC3BII to LC3B-I ratio depicts an elevated turnover of LC3BI to LC3B-II in DOX-DsRed but not the overexpression group. This is still the case after splitting the group into HSPA4_low and HSPA4_high. (Saline-DsRed black N= 9, DOX-DsRed yellow N=18, DOX-HSPA4_low, blue-filled N= 10. DOX-HSPA4_high blue-hollow N=10) Statistical analysis performed as 1-Way ANOVA

On the other hand, a marked increase in autophagosomal markers P62/SQSTM1 by 2.154-fold (p=0.0014) in DOX-DsRed with a reduction to 1.655-fold(p=0.1689) in DOX-HSPA4_low and 1.114-fold (p=0.9757) in DOX-HSPA4_high groups was detected compared to Saline-DsRed control **(Fig 3.4.5 B)**. Concurrently, autophagosome bound LC3B-II showed a marked increase in DOX-DsRed treated group compared to the Saline-DsRed control by 3.915-fold (p=0.0008) with a reduced effect on the DOX-HSPA4_low group to 3.310-fold(p=0.0220) and an ameliorated effect to 1.951-fold(p=0.5164) in the DOX-HSPA4_high group **(Fig3.4.5 C)**.

The increase is in line with our current understanding that anthracycline treatment blocks autophagic degradation in the cell by deacidifying lysosomes and therefore stopping the degradation of cargo-P62-LC3B complexes. These findings suggest that HSPA4 overexpression is protective against ROS-induced proteomic stress induced by Doxorubicin.

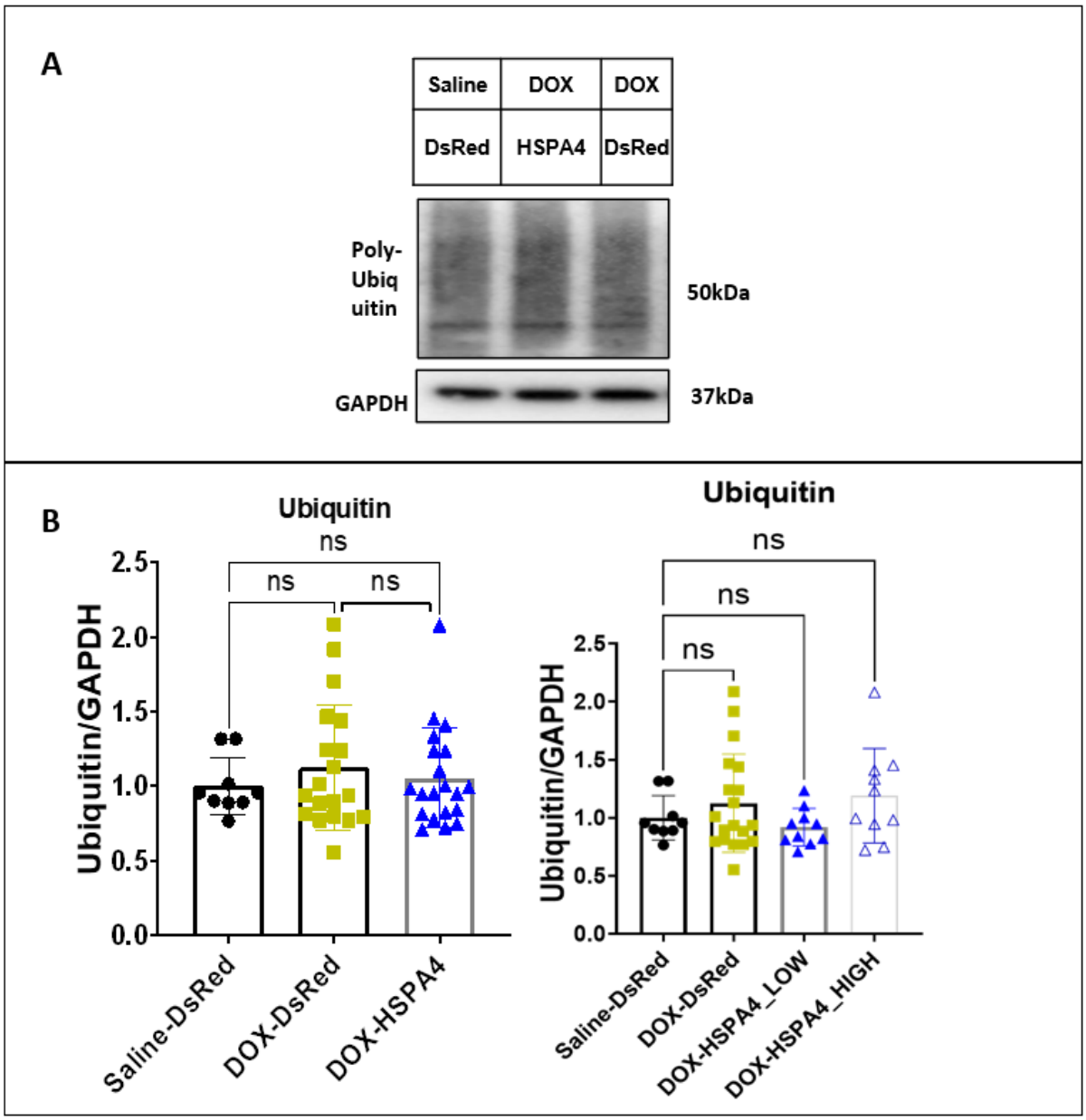

Figure 3.4.6 Ubiquitinylated proteins were not strongly accumulated and unaffected by HSPA4 overexpression

A) Immunoblot of left ventricular heart tissue against poly-ubiquitin with GAPDH as loading control B) analysis of band intensity of poly-ubiquitin showing no significant differences after DOX administration or HSPA4 treatment. (Saline-DsRed black N= 9, DOX-DsRed yellow N=18, DOX-HSPA4_low blue-filled N= 10. DOX-HSPA4_high blue-hollow N=10) Statistical analysis performed as 1-Way ANOVA

4. Discussion

4.1. The phenotype of HSPA4 knockout mice could originate from reduced cardiac compliance

It was previously described that HSPA4 knockout mice suffer from muscular dystrophy, juvenile lethality and growth retardation, the development of kyphosis after three-quarters of a year, and concentric cardiac hypertrophy [Held 2011]. Interestingly, in a different study, the knockout of BAG3 showed a very similar phenotype with growth retardation, early mortality, and muscular dystrophy. [Homma 2006]. BAG3 belongs to a co-chaperone family with six members of Hsc70 that replaces BAG1 on the chaperone complex leading to a shift from proteasomal degradation to chaperone-assisted macroautophagy and is associated with the accumulation of the increased amount of protein aggregates **(Fig. 1.2.2)** [Gamerdinger 2009]. Furthermore, BAG3 was shown to interact with CapZ, an actin-capping protein specific for Z-discs, leading to cytoskeletal disarray and cardiac hypertrophy [Hishiya 2010]. In a more recent study, a heart-specific knockout of BAG3 showed early lethality alongside eccentric cardiac hypertrophy and systolic dysfunction, along with the downregulation of small HSPs like HSPB5, also known as CryAB [Fang 2017]. Dysfunctional CryAB is known to be the main contributor to desmin-related cardiomyopathy and will lead to the formation of aggresomes and upregulation of autophagic degradation [Tannous 2008].

This led to the hypothesis if HSPA4 could hold a similar structural support role in the cell. Compared to these studies, the hearts missing HSPA4 showed concentric hypertrophic growth of cardiomyocytes and the left ventricle **(Fig 3.1.2 - Fig 3.1.3)**, similar to BAG3 knockouts and dysfunctional HSPB5. Possible biases may arise from selecting parameters for image analysis alongside the varying infection rate of individual cardiomyocytes with the AAV9 vector. Nonetheless, it can be assumed that

overexpression preserved physiological function in most of the cardiomyocytes and prevented hypertrophic growth of the left ventricle.

Furthermore, cardiac fibrosis developed in the BAG3 knockout hearts, possibly due to increased apoptosis. In this study, a slightly higher apoptosis rate has been observed, but not whether the positive cells were non-cardiomyocytes **(FIG. APO APPENDIX)**. To test this a co-staining with cardiomyocyte markers would have needed to be established. This discrepancy could be explained by the fact that even though HSPA4-KO showed a similar phenotype to BAG3-KO mice, most BAG3-KO mice did not survive more than a month, and the mortality in the long-time study of Feng et al. was about 90 %.

On the other hand, the HSPA4-KO mice in this study showed an early lethality of 1/3rd (32 %) of neonates carrying the knockout. They survived for at least ten months without mortality, demonstrating a less severe phenotypic progression. Recently it was shown that the pattern of ventricular fibrosis could be correlated with the integrity of the gap junctions in the heart [Handa 2021]. Interestingly, the histological pattern of fibrosis **(Fig. 3.1.3)** in HSPA4 knockout hearts being patchy rather than compact hints at interruptions of electrophysiological signal transduction, possibly due to disconnection of gap junctions [Ngyuen 2014; Verheule 2021].

It was hypothesized that HSPA4 co-localizes with the tight junction protein ZO-1 in MDCK cells under stressful conditions [Tsapara 2006]. This protein is involved in arrhythmogenic cardiomyopathy in the physiological distribution of the area composita **(FIG 1.3.3)** by interaction with connexin43 and Cadherin-2 and can influence the size, number, and distribution of the junctions [De Bortoli 2018; Borrmann 2006; Straub 2003]. Furthermore, small HSPs have been shown to prevent tachycardia-induced remodeling by co-localizing and stabilizing cytoskeletal structures [Ke 2011]. Therefore, it is possible that the chaperoning of HSPA4 is needed to support the

physiological anchoring to cytoskeletal networks and formation or re-distribution of junction proteins in the *area composita* of the heart, making it a crucial element in the physiological exertion of the force of cardiomyocytes.

With reduced structural integrity of the left ventricle, the cardiac function would be expected to be influenced. Nonetheless, the ejection fraction was preserved in the HSPA4KO animals studied in this work **(Fig. 3.1.2 F)**. The echocardiographic speckle vector tracking assessed early signs of dysfunction to determine the global longitudinal strain **(Fig. 3.1.4 A-B)**. This parameter describes the mean extent of deformation that the left ventricular wall undergoes during the cardiac cycle and can be a good indication of the loss of elasticity of the heart [Potter 2018]. From this data, it can be inferred that the ventricles of animals in the HSPA4-KO group are generally stiffer than expected and need to exert higher forces to maintain normal ejection fraction ranges. An additional indicator for the early signs of arrhythmia was the increase in longitudinal opposite wall delay **(Fig. 3.1.4 C-D)** in 20 weeks old mice. The observed delay in the contraction of different ventricle segments might stem from the increased interstitial fibrosis leading to inefficient ectopic electrophysiological signal transduction [Verheule 2021].

Moreover, in the preceding study on HSPA4-KO mice, ion channel signaling and hypertrophy genes were already differentially regulated in 4-week-old mice, indicating disrupted electrophysiological signaling [Bakarat 2010]. Interestingly, while the activation of these pathways seemed to be initiated early on in development, the hypertrophic phenotype is not apparent until 12 weeks of age **(Fig. 3.1.2 E)**, and the progression of cardiac hypertrophy and fibrosis was prevented by overexpressing HSPA4 in 6-week-old mice. Could a more time-dependent effect be the cause of the development of pathology, not unlike the desmin-related cardiomyopathy from mutated HSPB5? It would be interesting to overexpress HSPA4 at different time points of

phenotype progression to see if morphological changes can be reverted with expression at 12 or 16 weeks of age in a therapeutic approach. Finally, intraventricular pressure-volume loop measurement would give more insights into how much cardiac compliance is compromised in hearts missing HSPA4.

4.2. HSPA4 has a non-redundant chaperoning role in the heart.

Aggresome formation was found in 20-week-old KO mice but not in the rescued hearts **(Figure 3.2.1 A)**. The accumulation of poly-ubiquitylated substrates was prevented by HSPA4 overexpression **(Figure 3.2.2 A)**. Furthermore, the autophagic markers P62/SQSTM1 **(Figure 3.2.2 B)** and LC3B **(Figure 3.2.2 C)** were markedly increased in KO animals but not in the OE-rescued group. This data shows that the overexpression of HSPA4 could have prevented the accumulation of poly-ubiquitylated proteins in cardiomyocytes or increased autophagic degradation measured by P62 and LC3B levels. Therefore, in the heart, it can be assumed that HSPA4 is necessary for preventing the aggregation of proteins and promoting degradation by the autophagic system.

In the heart, HSPA4 has yet to be studied extensively, even though recently, it was shown that the knockdown of HSPA4 accentuates mitochondrial damage and apoptosis in isolated cardiomyocytes from a mouse LPS sepsis model [Han 2020]. These protective properties of the chaperone could either be achieved by the intrinsic properties of stabilizing cytosolic proteins as a holdase, preventing an interaction partner like TJP-1 from losing conformation under stress conditions, or, on the other hand, it could be a rate-limiting function as a nucleotide exchange factor of the much better studied HSP70 [Oh 1997].

The HSP70 complex acts as an adaptor between the known pathways in protein quality control and co-chaperones, dictating the fate of the non-native cargo **(Fig 1.2.2)**. Since HSPA4 as a member of the HSP110 family, acts as a heterodimer with HSP70 and dramatically increases the chaperoning function, any of these chaperone-mediated processes could have been disrupted. The disruption of physiological folding and mediated proteasomal degradation would explain the accumulation of poly-ubiquitylated substrates found in the left ventricular tissue samples. The non-native proteins were more prone to aggregation with diminished HSP70 complex chaperoning function, forming perinuclear aggresomes similar to the HSPA4 knockout mice. These aggregates are enclosed in endosomal structures to prevent cytotoxicity and will be temporarily stored until more chaperone molecules are available [Vitiello 2022].

Interestingly, disaggregation is also performed by the HSP70 complex, and the diminished function in HSPA4-KO hearts would explain the increased aggresomes found [Rampelt 2012; Doyle 2013]. If the aggresomes cannot be disaggregated, they must be degraded via the autophagic pathway, as their size overwhelms the proteasome. Therefore, the ubiquitin adaptor P62/SQSTM1 would accumulate on the aggregates initially recognized by LC3B on the autophagosome, fuse with lysosomes, and be degraded. The increased amounts of P62/SQSTM1 and cytosolic LC3B-I and transmembrane LC3B-II indicated an increased activation of autophagic degradation, which was eventually overwhelmed. Interestingly, the immunofluorescence of these autophagic markers showed high co-localization around a ring-like rupture in many of the cardiomyocytes investigated in HSPA4-KO histological slides **(Figure 3.2.1 E-F)**.

Therefore, the proposed lowered efficiency of HSP70 complex chaperoning functions could lead to the observed phenotype, as a lack of HSPA4 would lead to diminished

chaperone recruitment, disaggregation, and stabilization/refolding of non-native protein substrates **(Fig 4.2.1).**

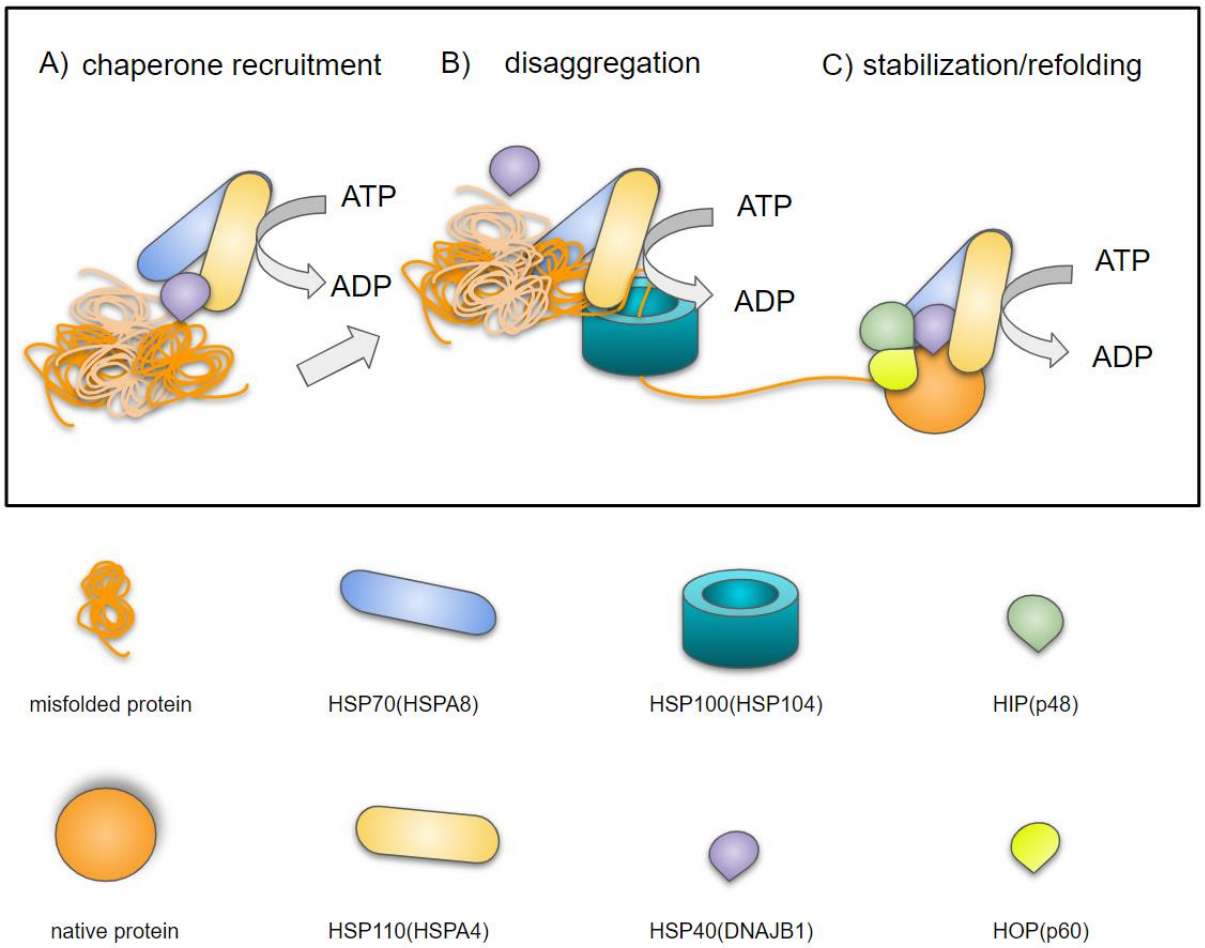

Figure 4.2.1 Rate limiting nucleotide exchange in protein disaggregation

The cardioprotective effects of HSPA4 overexpression shown in this work could be assigned to the nucleotide exchange function being the bottleneck in protein quality control. (A) Hydrophobic regions are exposed if proteins aggregate from increased stress, which recruits HSP40 family proteins and HSP70 to build a chaperoning complex. HSPA4 exchanges ADP with ATP on the nucleotide-binding cleft of HSP70. facilitating closed conformation and partially stabilizing the aggregated protein while HSP40 is released. (B) The chaperone complex recruits the hexameric HSP100 co-chaperone complex, where another nucleotide exchange takes place to unravel the aggregated protein by channeling it through the HSP100 pore. (C) The separated protein then regains its native conformation spontaneously or with the help of the HSP70:HSP110:HIP: HOP chaperone complex, where the cargo protein is released after nucleotide exchange. Therefore, a high HSPA4 expression would lead to an increased rate in all these processes and improve protein stability. (based on Schuermann 2008 & Doyle 2013)

Therapeutic insights of this experiment are that the overexpression performed in this study could have improved chaperoning function of the HSP70 complex as it is a concentration-dependent process [OH 1997, Dragovic 2006, Schuermann 2008]. With an increased pool of HSPA4, the disaggregation function of the complex could have worked at higher efficiency, clearing the already aggregated proteins from the cells and preventing further damage [Rampelt 2012]. Hypothetically, increased chaperone-mediated autophagy and proteasomal degradation could remove non-natively folded proteins faster and prevent further aggregation. Finally, the restored folding capabilities of the HSP70 complex could have normalized protein quality control and signal transduction in the heart.

Since HSPA4 is not the only member of the HSP110 subfamily, the question arises why protein quality control was disrupted even though the homologous HSPA4L and HPSH1 were still functional. Interestingly, earlier studies on this model showed that HSPA4L and HSPH1 were not upregulated upon the knockout of HSPA4 [Bakarat 2010. Held 2011. Mohamed 2012]. These findings could indicate a non-redundant function of the homologs in the cell. Further indications in this direction are structural studies of the HSP110 members **(Fig. 4.1.2)**. Here, it can be inferred that even though HSP110 proteins are very similar and bind to HSP70 in nucleotide exchange and co-chaperoning functions, the substrate binding domains of these proteins show differences. This raised the hypothesis if each member of the HSP110 protein family has its own target substrate. It would certainly explain why only the knockout of one of its members led to the disruption of protein quality control and why the other members could not replace the function. Here, co-immunoprecipitation of HSPA4 followed by mass spectrometry could identify more specific targets of the HSP70 complex and further elucidate the targets like TJP-1 that HSPA4 binds to. This would offer an

increased understanding of how chaperones maintain physiological protein quality control in aggregation-prone diseases like desmin-related cardiomyopathy.

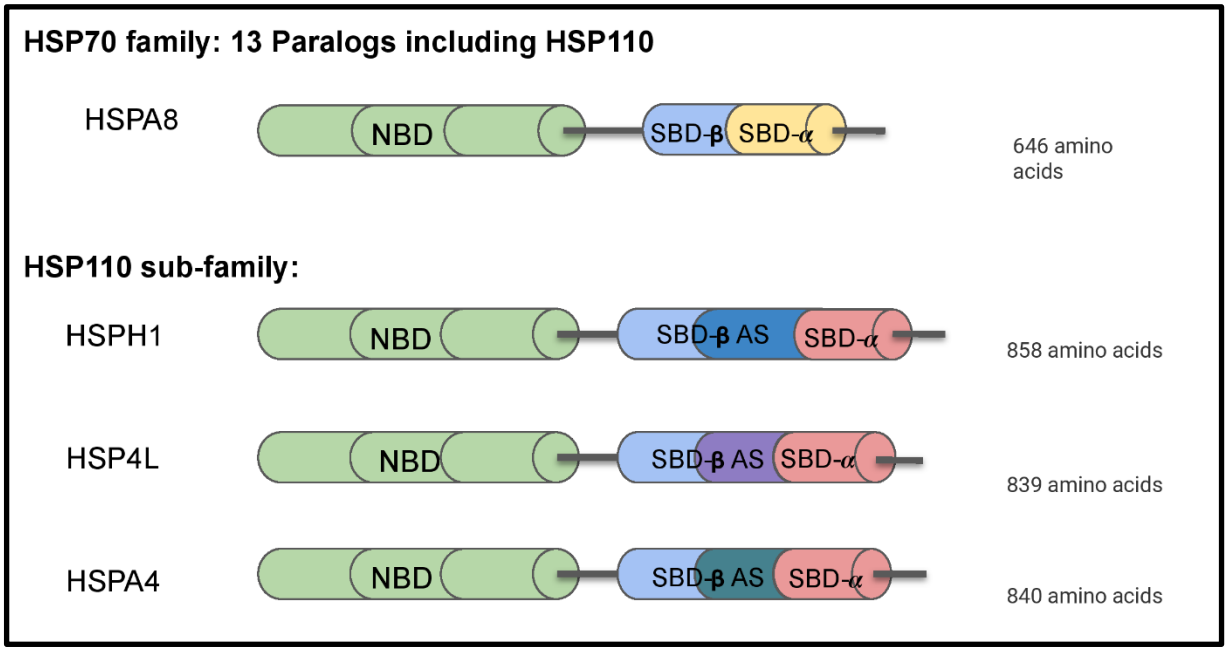

Figure 4.2.2 Structural comparison of HSP70 family proteins

The HSP110 subfamily consists of three members in mammals, namely HSPH1, HSP4L, and HSPA4, and was derived from paralogous events in the HSP70 gene family. The translated proteins are highly homologous in their nucleotide-binding domain (NBD), which can bind ATP and has an ATPase function. The NBD is connected with a hydrophobic linker to the chaperone's substrate binding domain (SBD). The SBD consists of a beta-sheet region, which binds tightly to the substrate, and an alpha-helix region which acts as a molecular lid, preventing the complex from dissociating without nucleotide exchange. The HSP110 proteins have been classified as nucleotide exchange factors and form a heterodimer with HSP70 proteins. It is suspected that the structurally different SBD-alpha of HSP110 binds to the NBD of HSP70 and encourages nucleotide exchange, opening the molecular lid and releasing the substrate. The three members of the HSP110 subfamily mainly differ in their amino acid sequence in the acidic region of SDB-beta, possibly giving them different substrate binding affinities. (based on Lee-Yoon 1995; Easton 2000; Gotoh 2004; Dragovic 2006; Schuermann 2008; Bracher 2015 Cabrera 2019)

4.3. HSPA4 buffered the proteotoxic side effects of doxorubicin-induced cardiotoxicity

A study from the last decade revealed that the reactive oxygen species of Fe2+DOX derivates lead to damaged and misfolded proteins after treatment. An increase in the expression of HSP proteins was reported, and that an HSP70 transgenic overexpression model showed to be effective in ameliorating cardiotoxicity [Naka 2014]. Considering the function of HSPA4 as a nucleotide exchange factor and rate-limiting sister chaperone of HSP70. similar protective properties were expected. An AAV9-vector gene therapy approach overexpressing HSPA4 in the heart was used, after which mice were stressed with an acute lethal dose of doxorubicin **(Fig 3.4.1)**. The first observations were that the rapid weight loss that the subjects experienced, as well as sudden death, were not different in groups treated with the HSPA4-OE virus and the control virus, and most animals reached the maximal weight loss criteria, which was set as an ethical endpoint. **(Fig. 3.4.3 B, FIG weight appendix)**. Therefore, HSPA4 overexpression was insufficient to affect the cohort's survival. The extent of overexpression was determined via immunoblotting and interestingly showed a range of high overexpression levels and lower expression levels of HSPA4 in left ventricular heart tissue. This is explained by the efficiency of infection that is difficult to control for in AAV9-based transmission **(Fig. 3.4.2 A)** [Inagaki 2006]. To better determine the infection efficiency, a fluorescent reporter could be co-expressed with the gene of interest.

With an acute doxorubicin dose of 20 mg/kg, a reduction in heart function and cardiac atrophy would have been expected in a mouse model [Willis 2019].

The heart function was determined via echocardiography five days after injection and showed a marked decrease in ejection fraction in all DOX-treated groups. Interestingly,

a HSPA4 expression-dependent protective effect was seen with higher EF in the DOX-HSPA4_high group **(Fig 3.4.3 A)**. From the echocardiographic data, the left ventricular wall thickness was measured and showed the same trend with ameliorated thinning in the DOX-HSPA4_high group **(Fig 3.4.3 B)**. After the animals were sacrificed, the dry heart weight was determined, showing a reduction in weight in all DOX-treated groups but again less in the DOX-HSPA4_high group **(Fig 3.4.3 C)**. Similarly, the cardiomyocyte size was determined and showed a higher mean minimal ferret's diameter in the DOX-HSPA4_high group **(Fig 3.4.4 D)**. Therefore, high levels of HSPA4 overexpression significantly lessened the effect of atrophy in the DOX-HPSA4_high group.

Furthermore, the abundance of apoptotic cells was not significantly higher in DOX-treated groups, alongside a marginal increase in fibrosis. These findings support the hypothesis that cardiac atrophy is induced by individual cardiomyocyte volume reduction instead of cell death. **(FIG DOX APOP)** Overall, a cardioprotective effect was seen in highly overexpressing HSPA4 in the heart, similar to HSP70 overexpression, ameliorating the doxorubicin-induced cardiac atrophy.

That the overexpression of HSPA4 did not rescue the increased mortality and weight loss in animals could have multiple reasons. Naka et al. utilized a chronic disease model similar to ours in figure **(DOX 6)**. Indeed, they found a decrease in heart function just as this study did, further analyzed the HSP70 expression, and found a significant increase. In contrast to the HSP70 study, the acute group appeared to be the more promising target for HSPA4 overexpression and intervention. In our hands, the autophagic markers were not increased by the chronic treatment.

Willis et al. showed that the atrophic transcription factor and ubiquitin ligase

TRIM63/MURF1 **(Fig. 1.5.2)** were differentially expressed after acute 20 mg/Kg DOX treatment. In the DOX-treated mice in this experiment, an upregulation of MURF1 mRNA was measured in left ventricular heart tissue, which was ameliorated by overexpressing HSPA4 **(Fig 3.4.4 F).** The pathways most likely leading to MuRF1 expression in acute doxorubicin treatment could be the increased ROS production, which builds the inflammatory transcription factor NFkB [Schakman 2012]. Furthermore, the Fe2+-DOX derivates would damage mitochondrial membranes and transmembrane proteins, inducing the activation of AMPK and FoxO, a family of atrophy-associated genes [Kang 2017].

Interestingly, FoxO was also shown to increase the expression of the autophagy-related genes BNIP3 and LC3 [Mammucari 2007; Zhao 2007]. Additionally, doxorubicin is known to inhibit the master regulator of autophagy, mTORC1 [Heras-Sandoval 2014]. This inhibition indicates that the damaged proteins and organelles would be degraded by the autophagic pathway rather than the ubiquitin-proteasome system. Moreover, the animals treated in this dissertation showed a non-significant rate of poly-ubiquitinylated proteins, which is expected because doxorubicin inhibits topoisomerase-2-beta in a UPS-dependent manner. It is not leading to the degradation of large amounts of protein, blocking the UPS. [Li 2016]. So rather than overburdening the UPS, doxorubicin downregulates overall protein expression.

There are three types of autophagy in the cell: macroautophagy, microautophagy, and chaperone-mediated autophagy. Only macroautophagy can degrade larger aggregates and damaged organelles [Johansen 2011]. The proteins or organelles marked for degradation are targeted by p62/SQSTM1 leading to the segregation of the cargo by binding LC3B [Lim 2015]. LC3B-I is lipidated by phosphatidylethanolamine (PE) to LC3B-II and functions in autophagosomal membrane elongation and maturation [Pankiv 2007]

Autophagic markers P62/SQSTM1 and autophagosomal transmembrane protein LC3B-II were significantly increased **(Fig. 3.4.5)**. Interestingly, HSPA4 overexpression in the heart showed a expression-dependent reduction of these autophagic markers. Here the ROS-damaged proteins could be stabilized by increased HSP70:HSPA4 chaperoning efficiency. Furthermore, HSPA4 was reported to have an HSP70 and ATP-independent holdase function, therefore buffering the proteotoxic side effects of doxorubicin treatment [Dragovic 2006]. This raises the hypothesis if the exerted effect of ameliorated autophagy of HSPA4 overexpression is indirect by stabilizing damaged proteins, or if this chaperone directly affects autophagic degradation.

DOX leads to pathological over-activation of macroautophagy by inhibiting the anti-apoptotic protein BCL-2, a regulator of Beclin-1 that is responsible for increased LC3B-I to LC3-BII conversion and, therefore, autophagosome maturation [Kobayashi 2010]. Therefore, an accumulation of P62/SQSTM1 and LC3B-II would be expected after DOX treatment, which was found in the DOX control group and ameliorated after HSPA4 overexpression **(Fig 3.4.4)**.

The LC3B-II to LC3B-I ratio is used to assess the autophagic function of the cell, even though this does not determine whether these were from decreased or increased macroautophagy. This ambiguity means that the reduction of accumulation of P62/SQSTM1 and LC3B-II with HSPA4 overexpression could be either from lowered autophagosomal generation (decreased macroautophagy) or a more efficient clearing of autophagosomes by increasing lysosomal function and autophagosome-lysosome fusion [Klionsky 2017].

Chaperone-mediated autophagy is an HSP70 and, therefore, also HSPA4 dependent process that encompasses lysosomal membrane integrity, acidification, and autophagic flux [Saftig 2008]. It is a highly selective ATP-dependent process in reducing the proteotoxic load critical for maintaining protein quality control and

organelle homeostasis [Singh2012; Li2011; Orenstein2010]. Here, the KFERQ motiv on non-native proteins is directly recognized by the HSP70 chaperone complex and translocated to the lysosomal surface binding LAMP-2 and traverses the lysosomal membrane into the matrix [Cuervo 2000; Dice 1990; Macri 2015]. HSPA4, similarly to HSP110. could play a role in chaperone-mediated autophagy as a nucleotide exchange factor of HSP70 in chaperone recruitment. Here the nucleotide exchange would be the rate-limiting factor closing the molecular lid of HSP70 and securing the cargo for translocation to LAMP2A for degradation through the lysosome. As indicated in **(FIG 4.1.2)**, HSPA4 could have a role in identifying specific substrates in tandem with HSP70. This specificity could also play a role in recruiting unknown co-chaperones in the CMA translocation, where ADP is exchanged for ATP, opening the molecular lid of HSP70 and releasing the cargo. GFAP is phosphorylated and recruited to the LAMP2 complex to form the lysosomal pore. If this process requires different nucleotide exchange and if HSP70:HSPA4 is involved has yet to be discovered. To summarize, the observed clearance of autophagosomal markers could be explained by the increased efficiency of chaperone-mediated autophagy after HSPA4 overexpression. Therefore, proteotoxic stress on cardiomyocytes would be reduced, and cardiac function would be improved **(Fig 4.2.1)**.

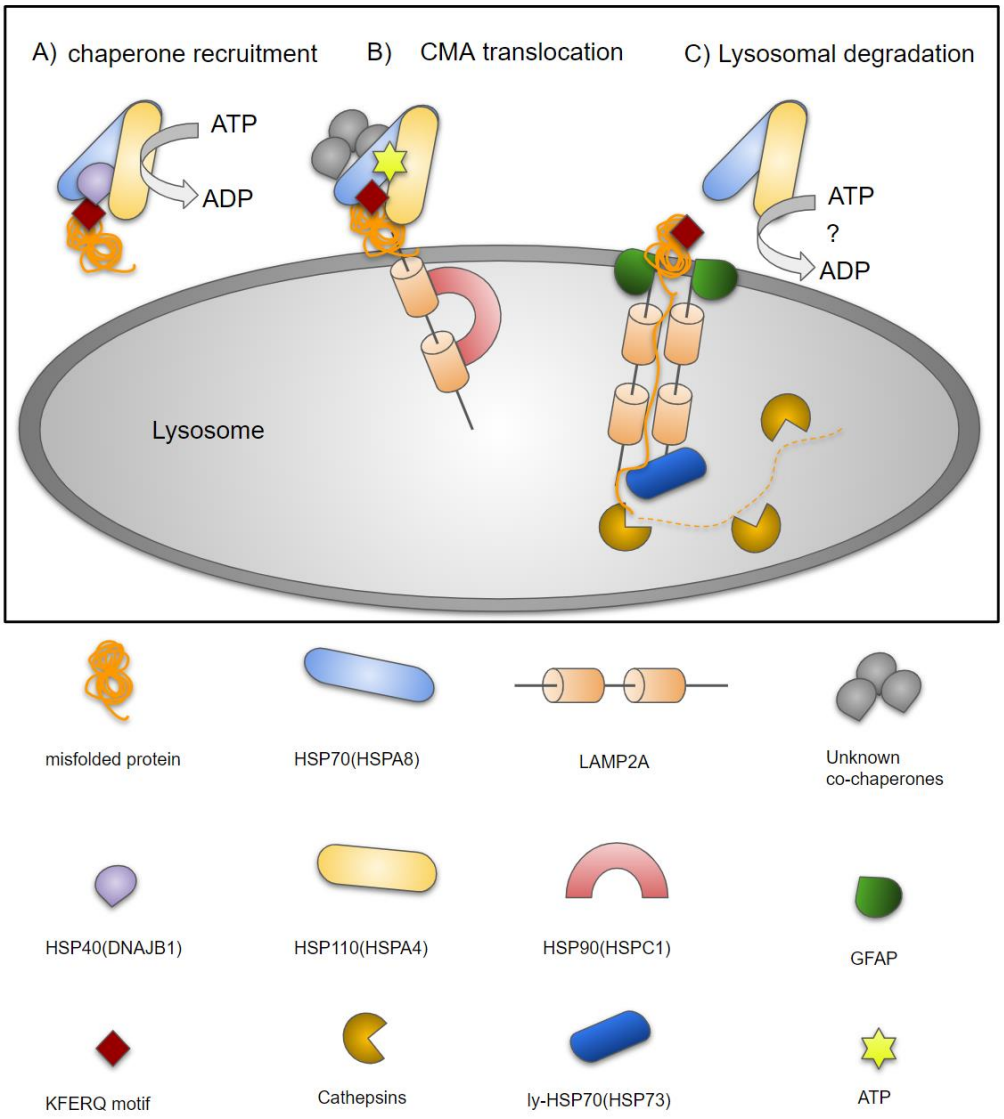

Figure 4.3.1 HSPA4 could be rate limiting in chaperone-mediated autophagy.

Non-native target proteins are recognized by their KFERQ motive by the HSP70:HSP110:HSP40 chaperone complex. A) The cargo is stabilized in the molecular lid of HSP70 by exchanging ATP to ADP by HSP110. B) The HSP70 chaperone complex translocates the cargo towards the lysosomal membrane bound LAMP2A, which HSP90 stabilizes. Here the ATP is exchanged by unknown co-chaperones of HSP70. which releases the cargo. C) LAMP2A is recruited alongside glial fibrillary acidic protein (GFAP), forming a molecular pore for the cargo to traverse into the lysosome facilitated by lysosomal HSP70. Here Cathepsins degrade the cargo, and the HSP70 complex is free to locate another target. It is still being determined if the translocation through the molecular pore needs energy in the form of ATP and if HSP110 plays a role here.

The DOX-induced mitochondrial damage and disrupted autophagic processes could lead to a metabolic imbalance in the cardiomyocytes, promoting a more fetal gene program initiating atrophic pathways that lead to cardiomyocyte “hibernation” [Taegtmeyer 2010]. The ATP-independent holdase abilities of HSPA4 could stabilize ROS-damaged mitochondrial proteins, while an increased autophagic clearance would provide an increased pool of amino acids that could be catabolized.

4.4. HSPA4 did not prevent cardiac remodeling in the TAC model but might have a role in reverse remodeling after de-loading of the heart.

In this work, HSPA4 was overexpressed in the heart, after which a TAC operation was performed, drastically increasing pressure on the left ventricle **(Fig 3.3.2 A)**. As a result, the animals developed cardiac hypertrophy, reduced systolic function, and increased mortality **(Fig3.3.2 B-C)**. Unexpectedly, autophagy regulatory protein Beclin 1 was not increased after eight weeks of TAC **(FIG 3.3.5)**. The post-translational phosphorylation of Beclin-1 leads to the initiation of autophagic nucleation [Kang 2011]. Therefore Beclin 1 expression levels would not need to change to increase autophagic activity. The phosphorylation status of Beclin-1 was not tested for in this work but would be an interesting future approach to studying the effect of HSPA4 overexpression in autophagic initiation.

Additionally, Autophagic markers P62/SQSTM1 and LC3B were only increased in some animals but not significantly as a group **(FIG 3.3.5 E-F)**, and poly-ubiquitylated proteins were not increased after TAC **(FIG 3.3.5 C)**. These results were unexpected, as autophagic degradation was reported to be upregulated as early as four weeks after

TAC [Nishida 2009]. Differences in experimental setup could have affected the readout. The mouse strain used by Nishida *et al.* was of mixed 129SV/BL6J background, and the samples were collected one week and four weeks after TAC. In this work, Bl6N background was used as the standard TAC on 129SV was insufficient to induce a hypertrophic response (Fig 129SVTAC Appendix). Additionally, mice were sacrificed eight weeks after TAC which might have affected the expression differentially from the reported four-week time point. Finally, the detection method and choice of antibodies could have masked an effect in this cohort.

Because of the before-mentioned reasons, there was not an apparent blockage of autophagy detectable in this experimental setup, and HSPA4 overexpression was insufficient in inducing an increased turnover in PQC. Interestingly the HSPA4 overexpression that reduced poly-ubiquitylated substrates in the knockout model and that improved autophagic clearance in the doxorubicin model would not downregulate these markers beyond the base level in either sham or TAC animals. These results suggest that excess in the HSPA4 protein pool is generally beneficial and does not lead to hyperactivation of protein degradation by either UPS or autophagic clearance.

The inhibition of mTOR signaling is known to positively affect hypertrophic development by enhancing autophagy, as drugs like Rapamycin are commonly used as treatment [Yamaguchi 2019]. The mentioned findings raise the question if HSPA4 overexpression could be used to reverse remodeling processes in cardiac unloading.

During cardiac hypertrophy, the cell's energy demands increase significantly with its volume, leading to ROS-damaged mitochondrial proteins and lipids accumulation. In prolonged hypertrophic response, like in the severe TAC model, an increase in autophagic response was reported around four weeks after surgery [Nakai 2007, Nishida 2009] Atg5 deficient mice were shown to develop cardiac dysfunction within one week after TAC, but not in sham, demonstrating the initially protective modus of

autophagy that later turns maladaptive [Zhu 2007]. On the other hand, cardiac-specific Beclin-1 transgenic KO mice showed cardiac dilatation and dysfunction as early as three weeks after the operation, indicating a detrimental effect of hyperactivated autophagy in the transition from cardiac hypertrophy to heart failure [Rifki 2012]. Alternatively, Beclin-1 was shown to affect a negative feedback loop by inhibiting autophagosome-lysosome function [Matsunaga 2009]. This raises the hypothesis if the HSP70:HSPA4 chaperone-mediated autophagy be beneficial in this context. Certainly, it would be interesting to investigate further the time-dependent proteostatic effect that autophagic degradation seems to have.

It has been reported that cardiac hypertrophy can regress during unloading, for example, with LVAD support. It is clinically treated with b-adrenergic receptor blockers and renin-angiotensin-aldosterone system antagonists [Koitabashi 2012, Cohn 2000. Cohn 2001]. However, these procedures are inadequate and need further research to procure novel and effective therapeutics. It was shown that autophagic initiation complex protein Atg5 deficient mice showed less recovery from LV hypertrophy after the removal of angiotensin II pumps, indicating a vital role in regaining balanced protein degradation and synthesis [Oyabu 2013].

Furthermore, it was shown that reverse remodeling was prevented in Beclin-1 deficient mice, and FoxO1 as well as FoxO3 are induced one week after unloading, as they lead to the induction of autophagy and catabolic pathways [Cao 2013]. Therefore, recovery from mild hypertrophic stimulus could be accentuated by affecting the FoxO transcription factor or the well-studied and exercise-induced upstream regulator PGC-1alpha [Rowe 2010]. From this the hypothesis can be formed if HSPA4 would have similar beneficial effects on reverse remodeling in the catabolic pathways.

4.5. Potential therapeutic relevance

The AAV9-mediated overexpression of BAG3 in mice with LV dysfunction after previously suffering from coronary artery ligation serves as an excellent example of gene replacement therapy [Knezevic 2016]. It is one of the first gene therapies that, rather than targeting a direct calcium signaling influencing gene, e.g., SERCA2, replenishes the pool of an HSP70 co-chaperone and autophagy-associated protein [Jake 2019]. Further similarities to HSPA4 are that BAG3 overexpression did not lead to an increase in contractility in Sham controls, which was also seen in Sham-HSPA4 groups, making it safe for long-term therapy in patients (Figure 3.3.3 B). BAG3 is downregulated in patients with ischemic and non-ischemic dilated cardiomyopathy, and haploinsufficiency was shown in familiar idiopathic dilated cardiomyopathy [Feldman 2014]. On the other hand, HSPA4 was shown to be up-regulated in pressure-overloaded hearts of mice and patient samples [Mohamed 2012]. It is, therefore, not as simple as replacing the insufficient protein pool with overexpression to improve cardiac function. Certainly, HSPA4 overexpression could be beneficial in enhancing chaperoning and autophagy in the recovery of the heart during reverse remodeling. Still, if this holds, faithful would need to be tested in further experiments before drawing a conclusion. Strengthening protein stability and autophagy, as is already being done in case of BAG3, could be advantageous as an adjuvant therapy to cardiotoxic chemotherapeutics like doxorubicin. Cardiovascular complications can occur as late as 10 years after DOX treatment has ceased, and it is hypothesized that the acute cardiotoxic effects linger and lead to the chronic phenotype [Wenningmann 2019]. Strengthening chaperoning and autophagy by HSPA4 overexpression before DOX treatment could buffer the cardiotoxic effects and prevent long-term complications.

Challenges in gene replacement therapy are the method for gene delivery. It was shown that direct injection into the hearts of both small and large animals only showed

an effect in cells close to the injection site and along the needle's path [Rengo 2009, McTiernan 2007]. The efficacy of infection was improved in mice and rats by injecting into the aortic root proximal to the placement of a transaortic clamp, which would be too big of surgery in larger animals like humans [Roth 2004, Pleger 2007]. Gene delivery was achieved with minimal intervention by injecting intravenously in this work and before in other groups and would be the preferred mode of action [Pacak 2006]. The AAV9 serotype was the most effective for cardiac gene delivery alongside low immunogenic response [DiMattia 2012]. Despite these characteristics, AAV vectors still demonstrate a certain level of immune response that can lead to decreased transcription of the gene of interest, limited biologic effects, and even the development of myocarditis [Jaski 2009]. A probable explanation is that 30 % to 50 % of the population already holds AAV-neutralizing antibodies [Mingozzi 2013]. Omitting the immune response asks for alternative methods for gene transduction, like the recently popularized administration of synthetic modified mRNA, and could open the door for novel therapeutic approaches [Tusup 2019, Evers 2022].

5. CONCLUSION

The overexpression of HSPA4 in the heart has rescued the hypertrophic phenotype in HSPA4-KO mice. Interestingly, an accumulation of poly-ubiquitinylated proteins and an excessive activation of autophagic degradation was found in HSPA4-KO animals, while the closely related genes HSP110 and HSPA4L were still functional. By this, a non-redundant chaperone and disaggregation function of HSPA4 can be inferred, where differential targets are bound to the substrate binding domain. The interaction with tight junction receptor ZO1 could reduce electrophysiological signal transduction through the area composita. If this interaction were preserved after replenishing the HSPA4 chaperoning pool would be an exciting approach for further functional studies. Likewise, collagen production was normalized, and fibrosis was prevented. Therefore, the heart muscle was not impaired in its plasticity, as shown by the global longitudinal strain reduction. If the lowered fibrosis was achieved by improved cardiomyocyte function or improved protein quality control in cardiac fibroblasts stands to be determined by identifying interaction partners in cardiac cellular subtypes, for example, through single-cell sequencing.

The administration of an acute dose of Doxorubicin led to the blockage of autophagic processes in left ventricular tissue and cardiac atrophy response. By overexpressing HSPA4 in the heart, chaperoning of ROS-stressed proteins might have been improved, which ameliorated the cardiotoxic side effects of the drug. The extent of mitochondrial damage would need to be determined in further experiments by measuring mitochondrial stress markers or performing a structural analysis of the mitochondrial lamina. Another hypothesis for buffering the cardiotoxic response is that the blockage of autophagic degradation could have been mitigated by enhanced chaperone-assisted autophagy. In this case, lysosomal tracking dyes and co-staining with

lysosome-associated proteins LAMP2-A could further elucidate the involvement of HSPA4 in this process.

The maladaptive hypertrophic response of pressure-overloaded hearts was not prevented by overexpression of HSPA4. It was reported that increased autophagic response is maladaptive in prolonged pressure overload. Nonetheless, similar studies in autophagic-related proteins show that enhanced autophagy can be beneficial in returning to physiological protein quality control after de-loading the heart. Suppose similar responses can be expected by overexpressing HSPA4 needs to be determined in future studies. In this case, it is fascinating if the overexpression can revert hypertrophic remodeling after de-loading the heart, possibly by disaggregating sarcomeric proteins.

This dissertation shows that the directed manipulation of protein quality control through a deeper understanding of HSP70 binding chaperone proteins could be a therapeutic approach in treating or preventing maladaptive responses in cardiac remodeling. Furthermore, by focusing on more cell type-specific approaches in understanding the role of HSPA4, the function of this co-chaperone could be further elucidated. Hopefully, future findings will lead to additional discoveries in how the intricate parts of protein quality control can be utilized to reveal future therapies.

APPENDIX

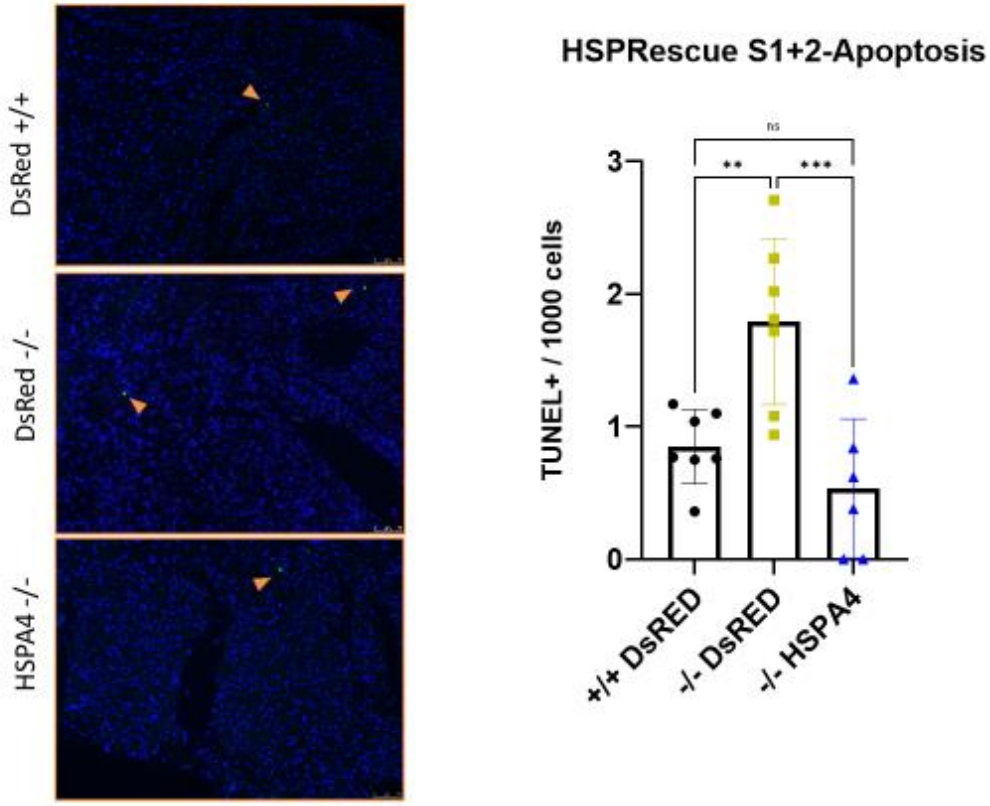

FIG HSP-Rescue Apoptosis: Histological slides of left ventricular tissue were treated with in situ cell death detection kit (Sigma-Aldrich) according to manufacturer protocol. The left ventricle was fully imaged, and positive nuclei were counted against the total cell number by FIJI particle detection. The data was plotted as TUNEL positive cells per 1000 cells counted in WT(+/+), KO (-/-), and OE (-/- HSPA4) and showed an increase of positive counts in the knockout hearts but not after overexpression.

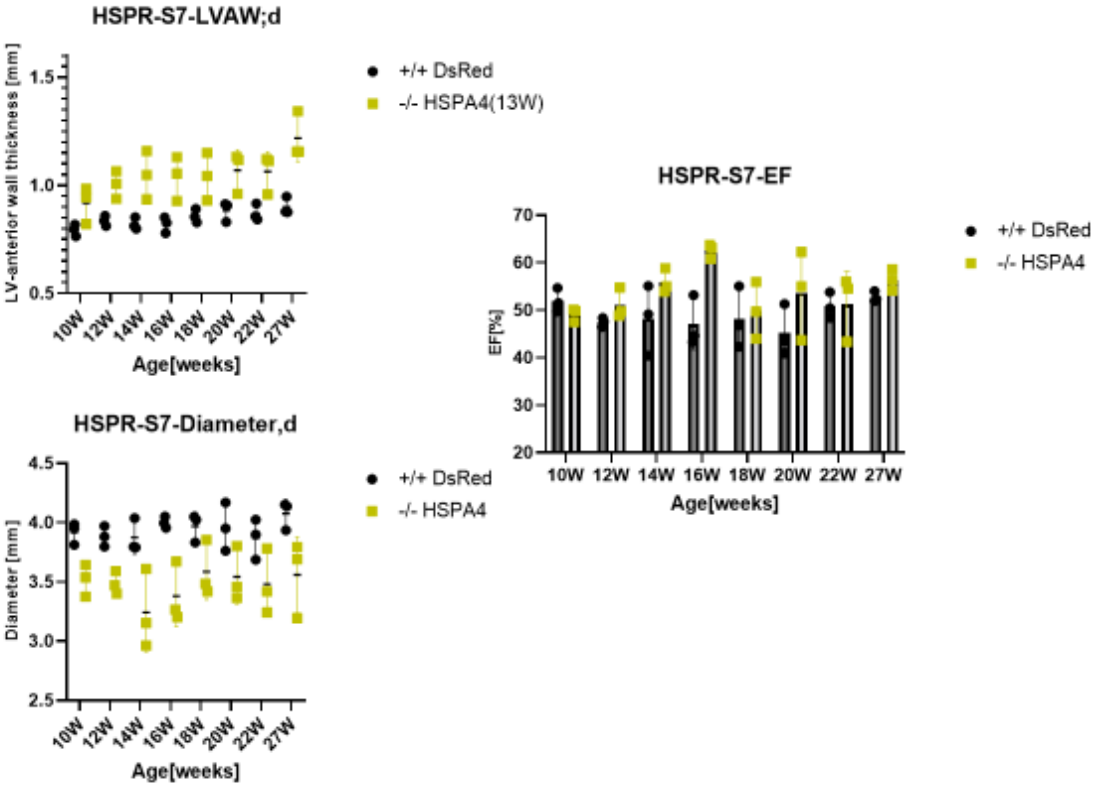

FIG HSPRS7. HSP-Rescue Series 7: Echocardiographic observations of HSPA4 knockout and wildtype animals over 27 Weeks. LVAW'd - left ventricular anterior wall thickness during diastole, EF - Ejection Fraction, left ventricular diameter during diastole

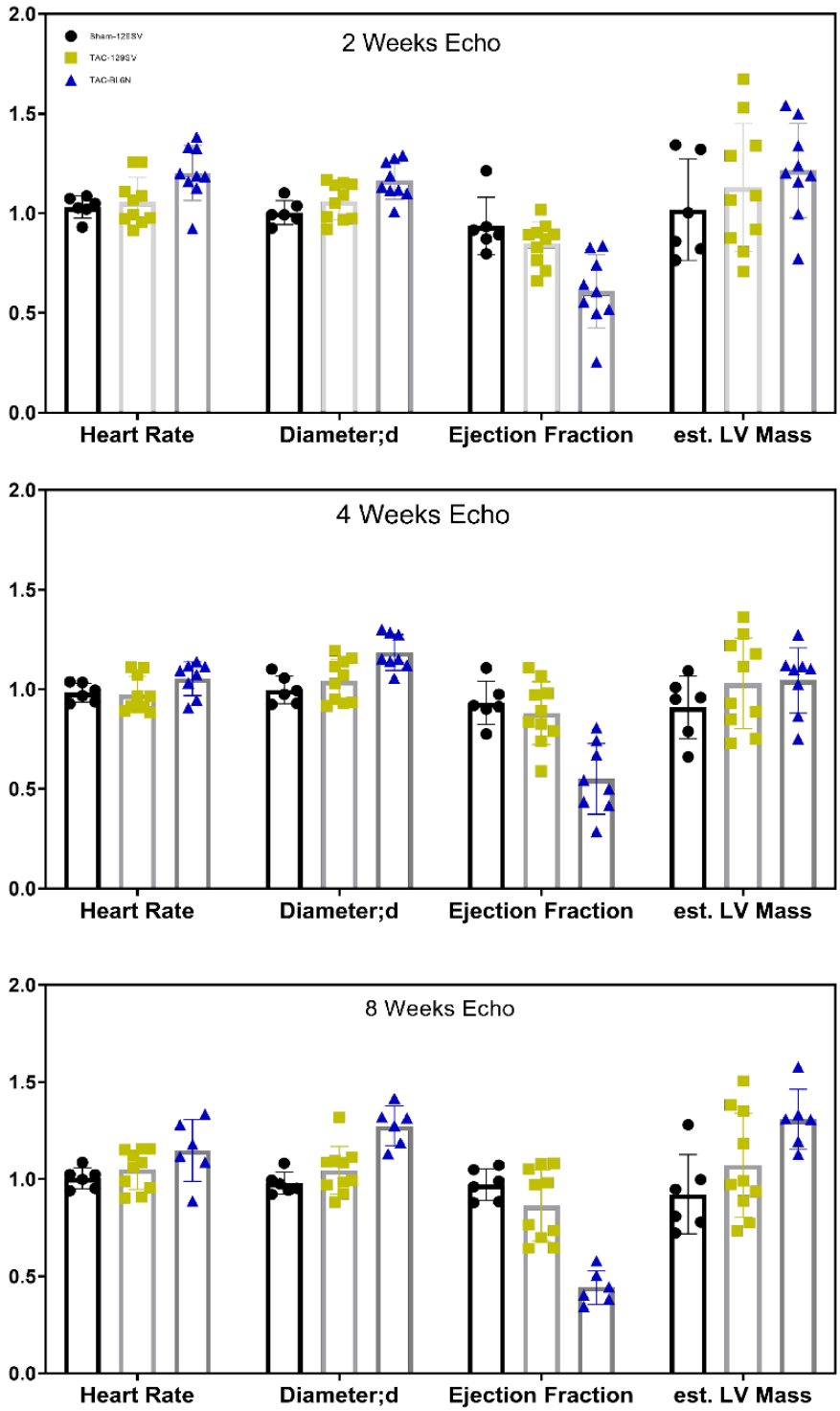

FIG: effect of TAC operation on SV129 and BL6N mouse strain
Mice with the 129SV and BL6N background were operated on with transverse aortic constriction and monitored at weeks 2, 4, and 8 after the operation. Only the already established BL6N background showed the desired effect of reduced ejection fraction. It increased LV Mass at the end of the experiment, concluding that SV129 might be resistant to TAC.

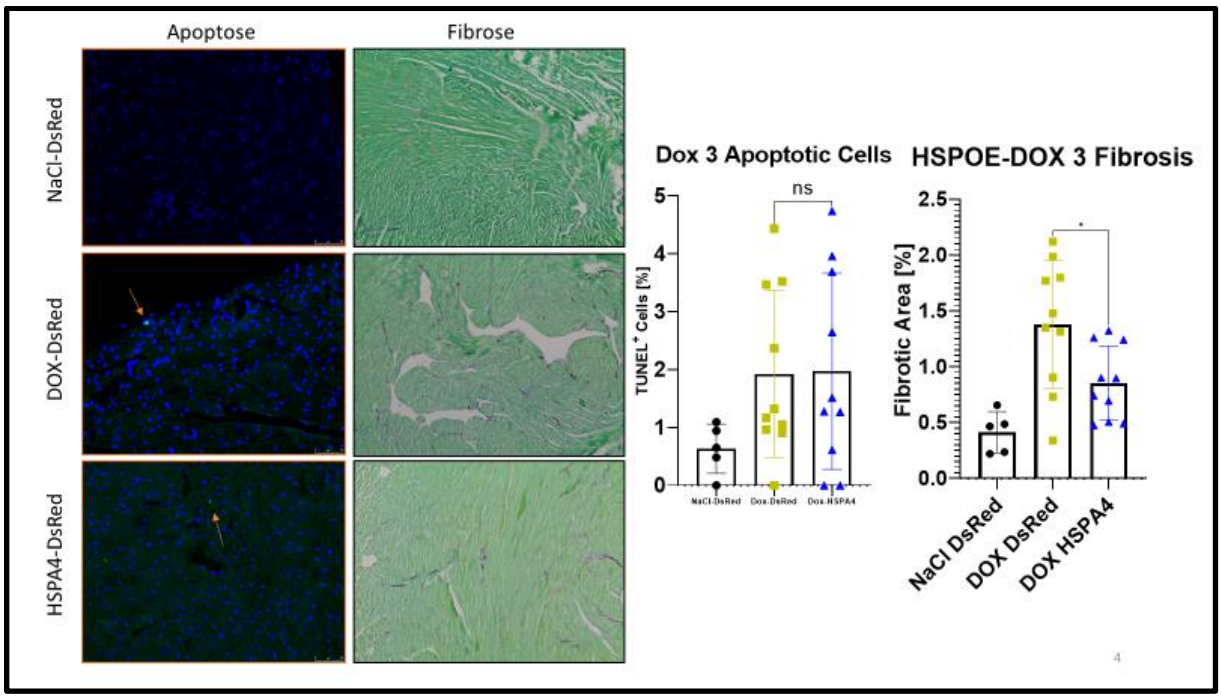

FIG DOX 3: Histological assessment of left ventricular tissue sections of DOX treated groups with and without HSPA4 overexpression: Apoptotic cells were determined with TUNNEL stain showing a non-significant increase in both groups. Cardiac fibrosis was slightly increased in DOX treated group, which was ameliorated by HSPA4 overexpression.

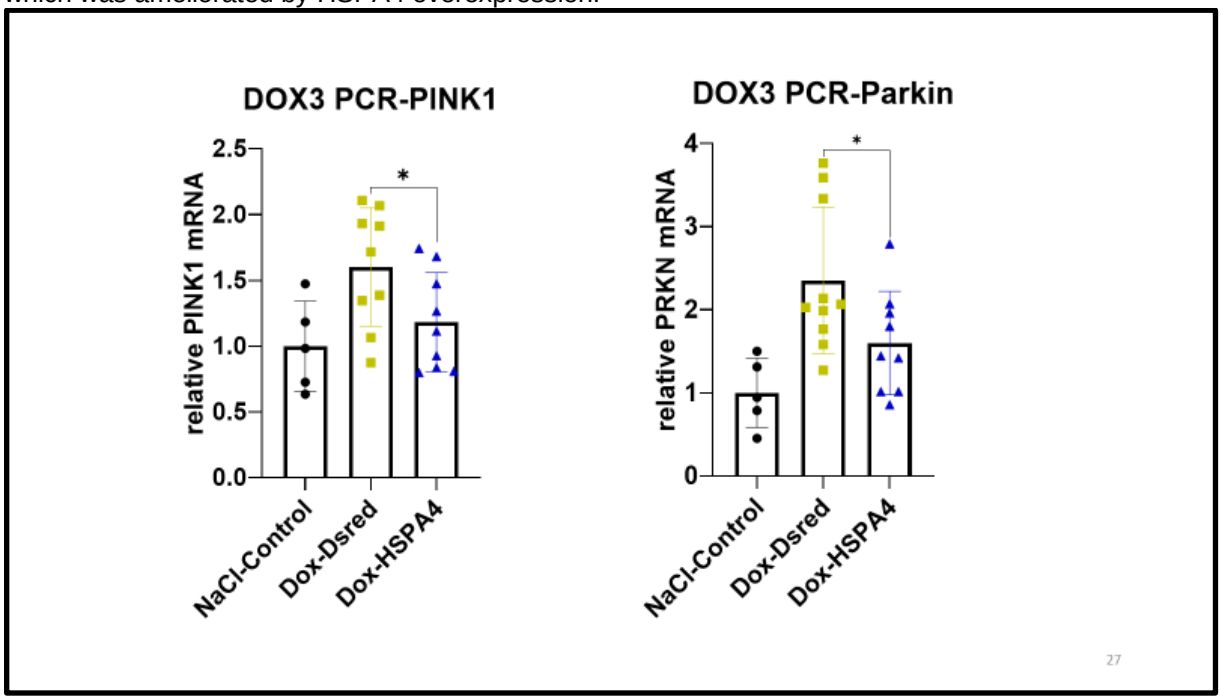

Fig Dox3: mRNA expression of mitophagy markers PINK1 and Parkin: The mRNA levels of Saline control, DOX treated control, and DOX treated overexpression were measured in qPCR with the mitochondrial damage associated with Parkin and the ubiquitin ligase PINK1; both genes involved in mitophagy.

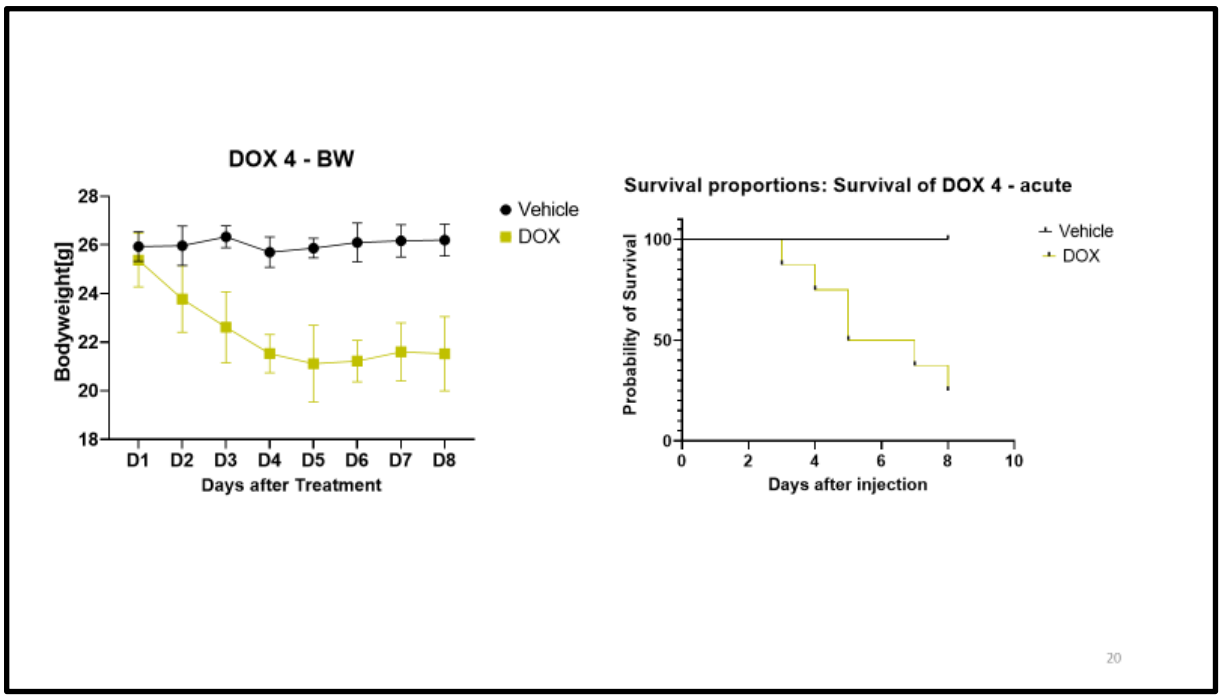

FIG DOX 4: Acute dose Doxorubicin treatment: A group of five male BL6/N mice at 8-10 weeks old were injected with 20 mg/kg Doxorubicine and monitored for one week. The treated group lost weight rapidly, and individual animals were censored if they lost more than 20 % of body weight at the end of the experiment. Only 2/5 of treated animals survived.

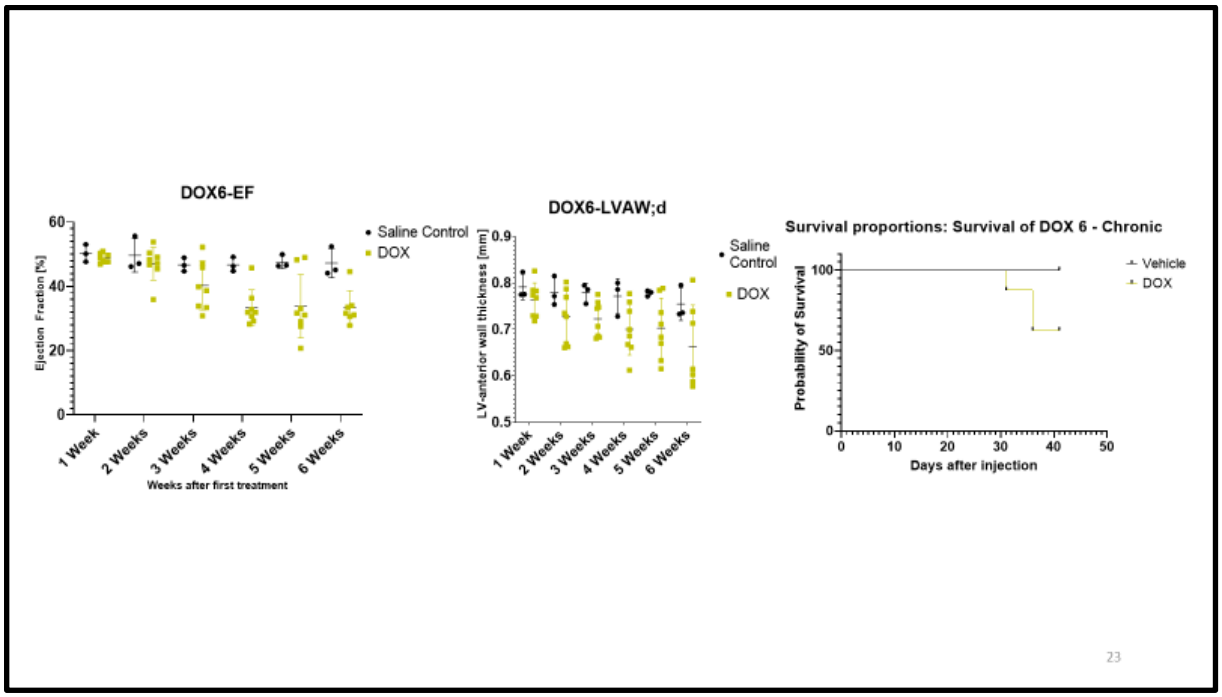

FIG DOX 6: Chronic doxorubicin treatment group: Eight male BL6/N mice were injected i.P with Doxorubicin 5 mg/kg once a week for four weeks. Echocardiographic monitoring of the EF showed a marked decrease in function after four weeks of the first injection. Alongside this, the echocardiographs showed deterioration of the left anterior wall thickness around the same time. Six weeks after the first injection, the overall well-being of the animals decreased, and 3/8 animals had to be euthanized, which ended the experiment.

WGA-Analysis.ijm

```
dir = getDirectory("image");
original = getTitle();
//name without file extension
name = getTitle();
dotIndex = indexOf(name, ".tif");
imageName = substring(name, 0, dotIndex);
//run("Brightness/Contrast...");
//run("Enhance Contrast", "saturated=0.35");
//run("RGB Color");
run("8-bit")
run("Apply LUT");
//run("Set Scale...", "distance=0 known=0 pixel=1 unit=pixel");
//run("Invert");
run("Gaussian Blur...", "sigma=1");
run("Auto Threshold", "method=Percentile");
//run("Sharpen");
//run("Auto Local Threshold", "method=Niblack radius=10 parameter_1=0 parameter_2=0 white");
run("Analyze Particles...", "size=100.00-500.00 circularity=0.60-1.00 show=Outlines display exclude include summarize")

  title = "Minimal Fiber Diameter";
  var _RESULTS_TABLE = "Minimal Fiber Diameter";
    handle = "["+_RESULTS_TABLE+"]";
  if (!isOpen(_RESULTS_TABLE)) {
          run("Table...", "name="+handle+" width=600 height=400");
        print(handle, "\\Headings:title\tMinFeret\tMinFeretScaled");
  }
  //for Schleife notwendig um alle REsults zu erfassen
  for(i=0; i<nResults(); i++){
  MFDpx1 = getResult("MinFeret",  i);
  MFDscaled = (MFDpx1/1.2);
  print(handle, imageName + "\t" + MFDpx1 + "\t" + MFDscaled);
  }


//for Schleife zur Berechnung des Mittelwertes
//Number of results in "Area" Column
//Some variables
N=0;
MFD=0;
mean_MFD=0;
total_variance=0;
variance_MFD=0;
SD_MFD=0;
SE_MFD=0;
max_MFD=0;
min_MFD=0;


N = nResults;

//Mean "MFD"column
for (a=0; a<nResults(); a++) {
    MFD=MFD+getResult("MinFeret",a);
    }
    mean_MFD=(MFD/nResults/1.2);

//Max value in "MinFeret" column
for (a=0; a<nResults(); a++) {
    if (getResult("MinFeret",a)>max_MFD)
    {
     max_MFD = getResult("MinFeret",a);
      }
      else{};
}

//Min value in "Area" column (note: requires max value)
min_MFD=max_MFD;
for (a=0; a<nResults(); a++) {
    if (getResult("MinFeret",a)<min_MFD)
    {
     min_MFD = getResult("MinFeret",a);
      }
      else{};
}
max_MFD=max_MFD/1.2;
min_MFD=min_MFD/1.2;

//Variance of "Area" column
for (a=0; a<nResults(); a++) {
    total_variance=total_variance+(getResult("MinFeret",a)/1-(mean_MFD))*(getResult("MinFeret",a)/1-(mean_MFD));
    variance_MFD=total_variance/(nResults-1);
}

//SD of "Area" column (note: requires variance)
SD_MFD=sqrt(variance_MFD);

//SE of "Area" column (note: requires SD)
SE_MFD = (SD_MFD/(sqrt(N)));

title = "Stat Results MFD";
  var _SUMMARY_TABLE = "Stat Results MFD";
    handle = "["+_SUMMARY_TABLE+"]";
  if (!isOpen(_SUMMARY_TABLE)) {
          run("Table...", "name="+handle+" width=600 height=400");
        print(handle, "\\Headings:title\tN\tMean\tVar\tSD\tSE\tMax\tMin");
        }
print(handle, imageName + "\t" + N + "\t" + mean_MFD + "\t" + variance_MFD + "\t" + SD_MFD + "\t" + SE_MFD + "\t" + max_MFD + "\t" + min_MFD);

run("Clear Results");
//close("*");
```

FIJI macro for determination of cardiomyocyte size of WGA fluorescent histological slides

DR_MeasureFibroticArea_SiriusRed+FC.ijm

```
dir = getDirectory("image");
original = getTitle();

//name without file extension
name = getTitle();
dotIndex = indexOf(name, ".tif");
imageName = substring(name, 0, dotIndex);
//original2 = name + "_2.png";
run("RGB Stack");
run("Gaussian Blur...", "sigma=5 slice");
run("Auto Threshold", "method=Minimum");
run("Create Selection");
run("Measure");
setSlice(2);
run("Select None");
run("Auto Threshold", "method=MaxEntropy");
run("Create Selection");
run("Measure");

imageTitle = "test";
    title = "Fibrosis area";
    var _RESULTS_TABLE = "Fibrosis area";
    handle = "["+_RESULTS_TABLE+"]";
    if (!isOpen(_RESULTS_TABLE)) {
            run("Table...", "name="+handle+" width=600 height=400");
         print(handle, "\\Headings:title\ttotal area\tfibrosis area\trelative fibrosis area");
    }
    totalArea = getResult("Area",  nResults-2);
    fibrosisArea = getResult("Area",  nResults-1);
    relativeFibrosisArea = fibrosisArea / totalArea;
    print(handle, imageName + "\t" + totalArea + "\t" + fibrosisArea + "\t" + relativeFibrosisArea);

```

FIJI macro for determination of relative fibrotic area of picrosirius red + fast green stained histological slides

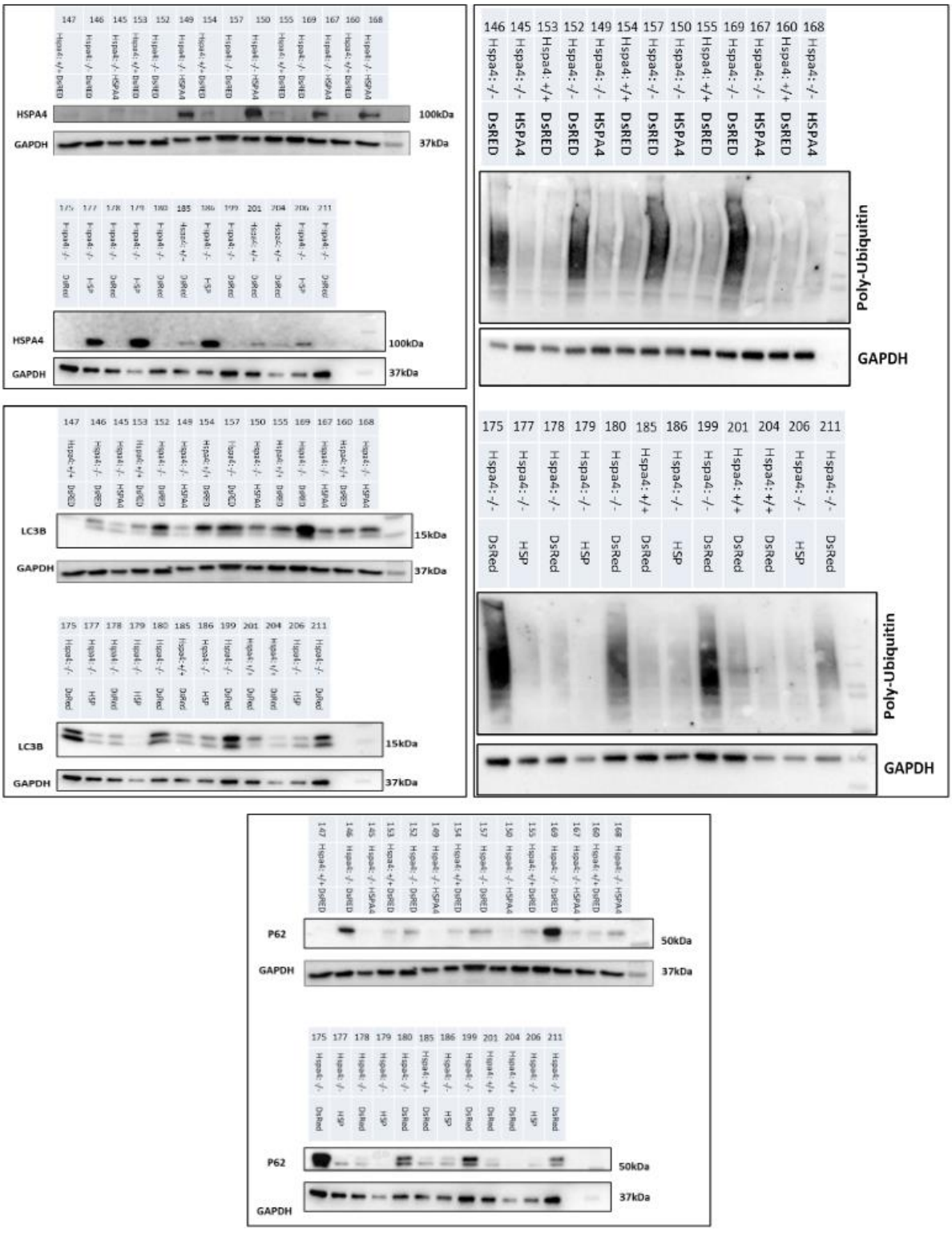

Full Sized Blots of HSPA4 AAV9 overexpression rescue in HSPA4-KO mice

In Figure 0.1

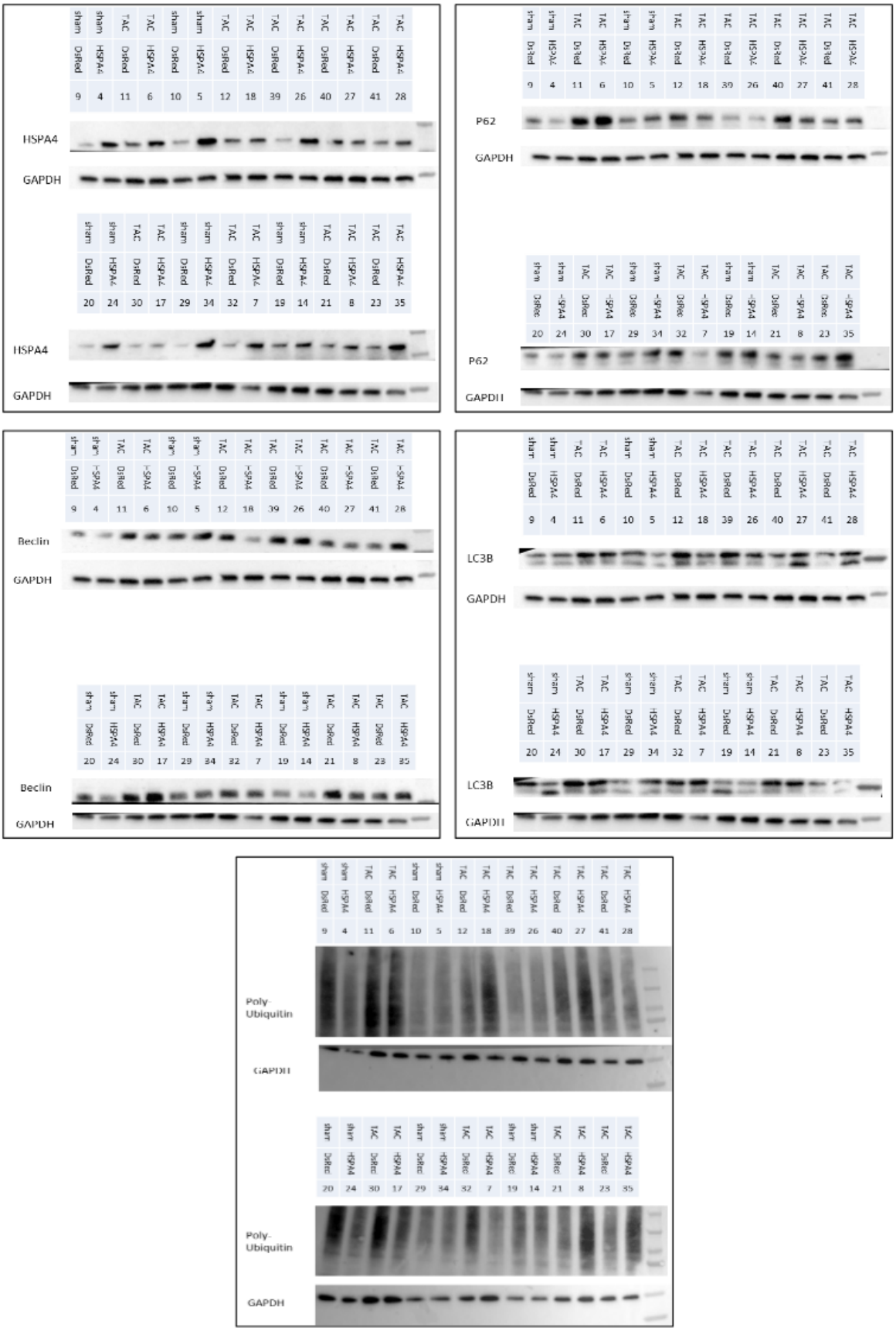

Full Sized Blots of HSPA4-AAV9 overexpression rescue in TAC-PO model

In Figure 0.2

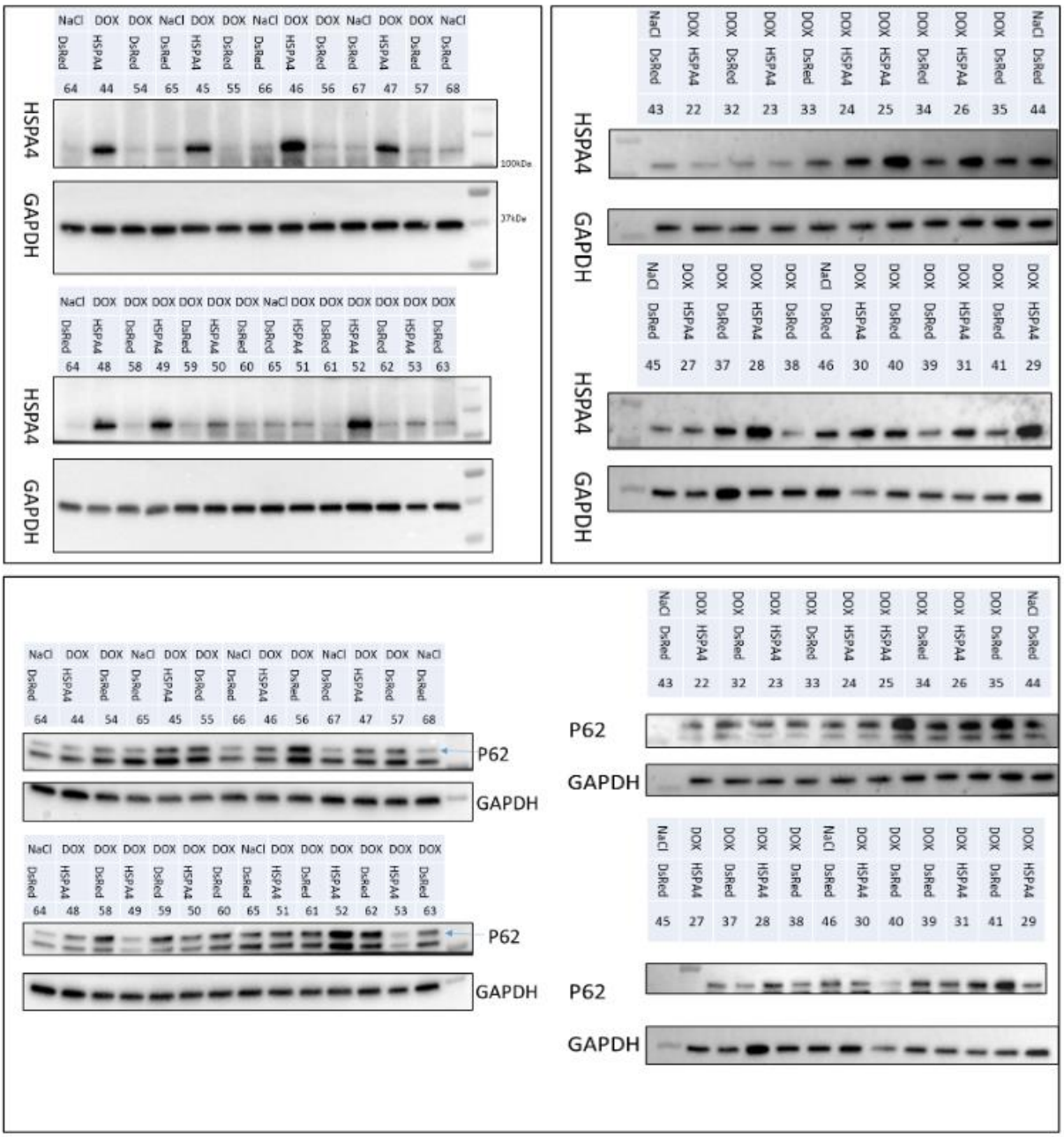

Full Sized Blots of HSPA4-AAV9 overexpression rescue in DOX model (A)
Figure 0.3 and Figure 0.6

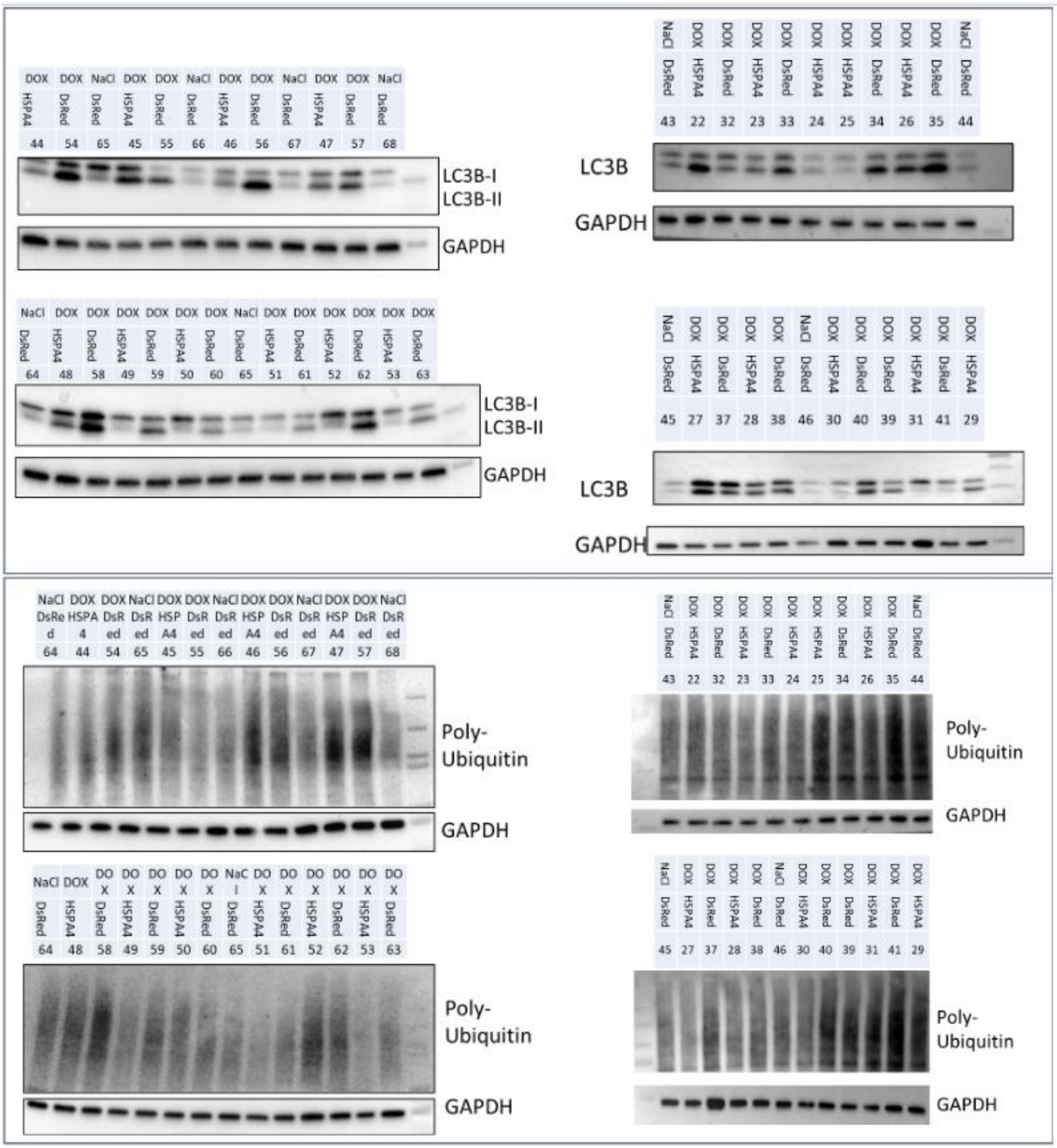

Full Sized Blots of HSPA4-AAV9 overexpression rescue in DOX model (B)

Figure 0.4 and Figure 0.6

References

[Ada+15] Teppei Adachi et al. “Involvement of heat shock protein A4/Apg-2 in refractory inflammatory bowel disease”. In: *Inflammatory Bowel Diseases* 21 (1 Jan. 2015). HSPA4 in inflammation, pp. 31–39. issn: 15364844. doi: 10.1097/MIB.0000000000000244.

[Aij+07] Saima Aijaz et al. “Regulation of tight junction assembly and epithelial morphogenesis by the heat shock protein Apg-2”. In: *BMC Cell Biology* 8 (Nov. 2007). issn: 14712121. doi: 10.1186/1471- 2121-8-49.

[Aim+22] Alberto Aimo et al. *Cardiac remodelling – Part 2: Clinical, imaging and laboratory findings. A review from the Study Group on Biomarkers of the Heart Failure Association of the European Society of Cardiology*. June 2022. doi: 10.1002/ejhf.2522.

[Alv+14] Sara Alvira et al. “Structural characterization of the substrate transfer mechanism in Hsp70/Hsp90 folding machinery mediated by Hop”. In: *Nature Communications* 5 (2014). issn: 20411723. doi: 10.1038/ncomms6484.

[Ank+21] Markus S. Anker et al. *Advanced cancer is also a heart failure syndrome: a hypothesis*. Jan. 2021.doi: 10.1002/ejhf.2071.

[AR11] Rudi Kenneth Allan and Thomas Ratajczak. *Versatile TPR domains accommodate different modes of target protein recognition and function*. July 2011. doi: 10.1007/s12192-010-0248-0.

[Arn+10] Verena Arndt et al. “Chaperone-Assisted Selective Autophagy Is Essential for Muscle Mainte- nance”. In: *Current Biology* 20 (2 Jan. 2010), pp. 143–148. issn: 09609822. doi: 10.1016/j.cub.
2009.11.022.

[Ay+01] J Ay et al. A RANDOMIZED TRIAL OF THE ANGIOTENSIN-RECEPTOR BLOCKER VAL- SARTAN IN CHRONIC HEART FAILURE. 2001. url: www.nejm.org.

[Aze+13] Paula S. Azevedo et al. *Energy Metabolism in Cardiac Remodeling and Heart Failure*. May 2013.doi: 10.1097/CRD.0b013e318274956d.

[Bal+99] Carol A Ballinger et al. *Identification of CHIP, a Novel Tetratricopeptide Repeat-Containing Pro- tein That Interacts with Heat Shock Proteins and Negatively Regulates Chaperone Functions*. 1999, pp. 4535–4545. url: https://journals.asm.org/journal/mcb.

[Bal22] Elizabeth Rosado Balmayor. *Synthetic mRNA – emerging new class of drug for tissue regeneration*.Apr. 2022. doi: 10.1016/j.copbio.2021.10.015.

[Ban+08] Urmi Bandyopadhyay et al. “The Chaperone-Mediated Autophagy Receptor Organizes in Dynamic Protein Complexes at the Lysosomal Membrane”. In: *Molecular and Cellular Biology* 28 (18 Sept. 2008), pp. 5747–5763. issn: 0270-7306. doi: 10.1128/mcb.02070-07.

[BDB21] Pieter Van Der Bijl, Victoria Delgado, and Jeroen J. Bax. *Characterization of the left ventricular response to hypertension: Beyond global longitudinal strain*. July 2021. doi: 10.1093/ehjci/jeab046.

[Boo+20] Eva M. Boorsma et al. *Congestion in heart failure: a contemporary look at physiology, diagnosis and treatment*. Oct. 2020. doi: 10.1038/s41569-020-0379-7.

[Bor+06] Carola M. Borrmann et al. “The area composita of adhering junctions connecting heart muscle cells of vertebrates. II. Colocalizations of desmosomal and fascia adhaerens molecules in the intercalated disk”. In: *European Journal of Cell Biology* 85 (6 June 2006), pp. 469–485. issn: 01719335. doi: 10.1016/j.ejcb.2006.02.009.

[Bor+18] Marzia De Bortoli et al. “Whole-Exome Sequencing Identifies Pathogenic Variants in TJP1 Gene Associated With Arrhythmogenic Cardiomyopathy”. In: *Circulation. Genomic*

and precision medicine 11 (10 Oct. 2018), e002123. issn: 25748300. doi: 10.1161/CIRCGEN.118.002123.

[Boz+16] Luiz H.M. Bozi et al. “Aerobic exercise training rescues cardiac protein quality control and blunts endoplasmic reticulum stress in heart failure rats”. In: *Journal of Cellular and Molecular Medicine* 20 (11 Nov. 2016), pp. 2208–2212. issn: 15821838. doi: 10.1111/jcmm.12894.

[BPV03] RUDOLF A. DE BOER, YIGAL M. PINTO, and DIRK J. VAN VELDHUISEN. “The Imbalance
Between Oxygen Demand and Supply as a Potential Mechanism in the Pathophysiology of Heart Failure: The Role of Microvascular Growth and Abnormalities”. In: *Microcirculation* 10 (2 Jan. 2003), pp. 113–126. issn: 1073-9688. doi: 10.1080/mic.10.2.113.126.

[Bri+01] Klára Briknarová et al. *letters Structural analysis of BAG1 cochaperone and its interactions with Hsc70 heat shock protein*. 2001. url: http://structbio.nature.com.

[Bru+06a] Bianca J.J.M. Brundel et al. “Heat shock protein upregulation protects against pacing-induced myolysis in HL-1 atrial myocytes and in human atrial fibrillation”. In: *Journal of Molecular and Cellular Cardiology* 41 (3 Sept. 2006), pp. 555–562. issn: 00222828. doi: 10.1016/j.yjmcc.2006.
06.068.

[Bru+06b] Bianca J.J.M. Brundel et al. “Induction of heat shock response protects the heart against atrial fibrillation”. In: *Circulation Research* 99 (12 2006), pp. 1394–1402. issn: 00097330. doi: 10.1161/ 01.RES.0000252323.83137.fe.

[BTP17] Jordan J. Bartlett, Purvi C. Trivedi, and Thomas Pulinilkunnil. *Autophagic dysregulation in dox- orubicin cardiomyopathy*. Mar. 2017. doi: 10.1016/j.yjmcc.2017.01.007.

[Buc+15] Gerald D. Buckberg et al. “Ventricular structure-function relations in health and disease: Part I. The normal heart”. In: *European Journal of Cardio-thoracic Surgery* 47 (4 Apr. 2015), pp. 587–601. issn: 1873734X. doi: 10.1093/ejcts/ezu278.

[BV15] Andreas Bracher and Jacob Verghese. *The nucleotide exchange factors of Hsp70 molecular chap- erones*. Apr. 2015. doi: 10.3389/fmolb.2015.00010.

[Cab+19] Yovana Cabrera et al. “Regulation of Human Hsc70 ATPase and Chaperone Activities by Apg2: Role of the Acidic Subdomain”. In: *Journal of Molecular Biology* 431 (2 Jan. 2019), pp. 444–461. issn: 10898638. doi: 10.1016/j.jmb.2018.11.026.

[Cam+20] Paolo G. Camici et al. *Coronary microvascular dysfunction in hypertrophy and heart failure*. Mar.2020. doi: 10.1093/cvr/cvaa023.

[Cao+11] Dian J. Cao et al. “Histone deacetylase (HDAC) inhibitors attenuate cardiac hypertrophy by suppressing autophagy”. In: *Proceedings of the National Academy of Sciences of the United States of America* 108 (10 Mar. 2011), pp. 4123–4128. issn: 00278424. doi: 10.1073/pnas.1015081108.

[Cao+13] Dian J. Cao et al. “Mechanical unloading activates FoxO3 to trigger Bnip3-dependent cardiomy- ocyte atrophy.” In: *Journal of the American Heart Association* 2 (2 2013). issn: 20479980. doi: 10.1161/JAHA.113.000016.

[CFS00] Jay N Cohn, Roberto Ferrari, and Norman Sharpe. *Cardiac Remodeling-Concepts and Clinical Implications: A Consensus Paper From an International Forum on Cardiac Remodeling*. 2000.

[Cha+21a] Brandon Y.H. Chan et al. “MMP inhibitors attenuate doxorubicin cardiotoxicity by preventing intracellular and extracellular matrix remodelling”. In: *Cardiovascular Research* 117 (1 Jan. 2021), pp. 188–200. issn: 17553245. doi: 10.1093/cvr/cvaa017.

[Cha+21b] Shambhabi Chatterjee et al. “Telomerase therapy attenuates cardiotoxic effects of doxorubicin”. In: *Molecular Therapy* 29 (4 Apr. 2021), pp. 1395–1410. issn:

15250024. doi: 10.1016/j.ymthe.
2020.12.035.

[Che+15] Bang Dang Chen et al. “Targeting transgene to the heart and liver with AAV9 by different pro- moters”. In: *Clinical and Experimental Pharmacology and Physiology* 42 (10 Oct. 2015), pp. 1108– 1117. issn: 14401681. doi: 10.1111/1440-1681.12453.

[Che+18] Chao Chen et al. *Autophagy and Doxorubicin resistance in cancer*. Jan. 2018. doi: 10.1097/CAD.
0000000000000572.

[Che+20] Yan Chen et al. “Traditional cardiovascular risk factors and individual prediction of cardiovascular events in childhood cancer survivors”. In: *Journal of the National Cancer Institute* 112 (3 2020). issn: 14602105. doi: 10.1093/JNCI/DJZ108.

[Chi+16] Dai Chihara et al. “Management strategies and outcomes for very elderly patients with diffuse large B-cell lymphoma”. In: *Cancer* 122 (20 Oct. 2016), pp. 3145–3151. issn: 0008543X. doi: 10.1002/cncr.30173.

[Cho+12] Jason C. Choi et al. *Temsirolimus activates autophagy and ameliorates cardiomyopathy caused by lamin A/C gene mutation*. July 2012. doi: 10.1126/scitranslmed.3003875.

[Cla+07] Brian A. Clarke et al. “The E3 Ligase MuRF1 Degrades Myosin Heavy Chain Protein in Dexamethasone- Treated Skeletal Muscle”. In: *Cell Metabolism* 6 (5 Nov. 2007), pp. 376–385. issn: 15504131. doi: 10.1016/j.cmet.2007.09.009.

[Coh+09] Shenhav Cohen et al. “During muscle atrophy, thick, but not thin, filament components are degraded by MuRF1-dependent ubiquitylation”. In: *Journal of Cell Biology* 185 (6 June 2009), pp. 1083–1095. issn: 00219525. doi: 10.1083/jcb.200901052.

[Con+01] Patrice Connell et al. *The co-chaperone CHIP regulates protein triage decisions mediated by heat- shock proteins*. 2001. url: http://cellbio.nature.com.

[Cor+19] Giovanni Corsetti et al. “Autophagy and Oncosis/Necroptosis Are Enhanced in Cardiomyocytes from Heart Failure Patients”. In: *Medical science monitor basic research* 25 (Feb. 2019), pp. 33–44. issn: 23254416. doi: 10.12659/MSMBR.913436.

[Cue+00] Ana Maria Cuervo et al. “Selective degradation of annexins by chaperone-mediated autophagy”. In: *Journal of Biological Chemistry* 275 (43 Oct. 2000), pp. 33329–33335. issn: 00219258. doi: 10.1074/jbc.M005655200.

[Cué+13] Jorge Cuéllar et al. “Structural insights into the chaperone activity of the 40-kDa heat shock protein DnaJ: Binding and remodeling of a native substrate”. In: *Journal of Biological Chemistry* 288 (21 May 2013), pp. 15065–15074. issn: 00219258. doi: 10.1074/jbc.M112.430595.

[Dam+16] Roberto Marques Damiani et al. *Pathways of cardiac toxicity: comparison between chemotherapeu- tic drugs doxorubicin and mitoxantrone*. Sept. 2016. doi: 10.1007/s00204-016-1759-y.

[DGW13] Shannon M. Doyle, Olivier Genest, and Sue Wickner. *Protein rescue from aggregates by powerful molecular chaperone machines*. 2013. doi: 10.1038/nrm3660.

[Dhi+14] Rimpy Dhingra et al. “Bnip3 mediates doxorubicin-induced cardiac myocyte necrosis and mortality through changes in mitochondrial signaling”. In: *Proceedings of the National Academy of Sciences of the United States of America* 111 (51 Dec. 2014), E5537–E5544. issn: 10916490. doi: 10.1073/ pnas.1414665111.

[Dia+00] Sophia Diamant et al. “Size-dependent disaggregation of stable protein aggregates by the DnaK chaperone machinery”. In: *Journal of Biological Chemistry* 275 (28 July 2000), pp. 21107–21113. issn: 00219258. doi: 10.1074/jbc.M001293200.

[DiM+12] Michael A. DiMattia et al. “Structural Insight into the Unique Properties of Adeno-Associated Virus Serotype 9”. In: *Journal of Virology* 86 (12 June 2012), pp. 6947–6958. issn: 0022-538X. doi: 10.1128/jvi.07232-11.

[DML21] Thamonwan Diteepeng, Federica del Monte, and Marco Luciani. *The long and winding road to target protein misfolding in cardiovascular diseases*. May 2021. doi: 10.1111/eci.13504.

[Doo+03] Howard Doong et al. "CAIR-1/BAG-3 abrogates heat shock protein-70 chaperone complex-mediated protein degradation. Accumulation of poly-ubiquitinated Hsp90 client proteins". In: *Journal of Bi- ological Chemistry* 278 (31 Aug. 2003), pp. 28490–28500. issn: 00219258. doi: 10.1074/jbc.M209682200.

[Dra+06] Zdravko Dragovic et al. "Molecular chaperones of the Hsp110 family act as nucleotide exchange factors of Hsp70s". In: *EMBO Journal* 25 (11 July 2006), pp. 2519–2528. issn: 02614189. doi: 10.1038/sj.emboj.7601138.

[EAH04] Claudia Esser, Simon Alberti, and Jörg Höhfeld. *Cooperation of molecular chaperones with the ubiquitin/proteasome system*. Nov. 2004. doi: 10.1016/j.bbamcr.2004.09.020.

[EKS00] Douglas P Easton, Yoshiyuki Kaneko, and John R Subjeck. *The Hsp110 and Grp170 stress proteins: newly recognized relatives of the Hsp70s*. 2000. pp. 276–290.

[ELM15] Slava Epelman, Peter P. Liu, and Douglas L. Mann. *Role of innate and adaptive immune mecha- nisms in cardiac injury and repair*. Jan. 2015. doi: 10.1038/nri3800.

[Eng+13] Nikolai Engedal et al. "Modulation of intracellular calcium homeostasis blocks autophagosome formation". In: *Autophagy* 9 (10 2013), pp. 1475–1490. issn: 15548635. doi: 10.4161/auto.25900.

[Eve+22] Martijn J.W. Evers et al. "Delivery of modified mRNA to damaged myocardium by systemic administration of lipid nanoparticles". In: *Journal of Controlled Release* 343 (Mar. 2022), pp. 207– 216. issn: 18734995. doi: 10.1016/j.jconrel.2022.01.027.

[Fan+17] Xi Fang et al. "Loss-of-function mutations in co-chaperone BAG3 destabilize small HSPs and cause cardiomyopathy". In: *Journal of Clinical Investigation* 127 (8 Aug. 2017), pp. 3189–3200. issn: 15588238. doi: 10.1172/JCI94310.

[Fan+20] Guorun Fan et al. "The expression profiles and prognostic values of HSPs family members in Head and neck cancer". In: *Cancer Cell International* 20 (1 June 2020). issn: 14752867. doi: 10.1186/s12935-020-01296-7.

[Fat+93] D M Fathallah et al. *chromosome 5. from a B cell line and its assignment to Molecular cloning of a novel human hsp70*. 1993. url: http://www.jimmunol.org/content/151/2/810.

[Fel+14] Arthur M. Feldman et al. "Decreased Levels of BAG3 in a Family With a Rare Variant and in Idiopathic Dilated Cardiomyopathy". In: *Journal of Cellular Physiology* 229 (11 2014), pp. 1697–
1702. issn: 10974652. doi: 10.1002/jcp.24615.

[Fen10] Feng. "Overexpression of Apg-2 increases cell proliferation and protects from oxidative damage in BaF3-BCR/ABL cells". In: *International Journal of Oncology* 36 (4 Mar. 2010). issn: 10196439. doi: 10.3892/ijo_00000568.

[Fer+17] María Rosario Fernández-Fernández et al. *Hsp70 – a master regulator in protein degradation*. Sept.
2017. doi: 10.1002/1873-3468.12751.

[Fra+17] Michael G Fradley et al. "Rates and risk of arrhythmias in cancer survivors with chemotherapy- induced cardiomyopathy compared with patients with other cardiomyopathies". In: *Open Heart* 4 (2 Dec. 2017), e000701. doi: 10.1136/openhrt-2017-000701.

[Fu+21] Xiao Fu et al. *Redox interactions-induced cardiac toxicity in cancer therapy*. Sept. 2021. doi: 10.1016/j.abb.2021.108952.

[Gab+07] Kathleen Gabrielson et al. "Heat shock protein 90 and ErbB2 in the cardiac response to doxorubicin injury". In: *Cancer Research* 67 (4 Feb. 2007), pp. 1436–1441. issn: 00085472. doi: 10.1158/0008- 5472.CAN-06-3721.

[Gam+09] Martin Gamerdinger et al. “Protein quality control during aging involves recruitment of the macroautophagy pathway by BAG3”. In: *EMBO Journal* 28 (7 Apr. 2009), pp. 889–901. issn: 02614189. doi: 10.1038/emboj.2009.29.

[Gio+12] Sharon H. Giordano et al. “Decline in the Use of Anthracyclines for Breast Cancer”. In: *Journal of Clinical Oncology* 30 (18 June 2012), pp. 2232–2239. issn: 0732-183X. doi: 10.1200/JCO.2011.
40.1273.

[GK17] Jiefei Geng and Daniel J. Klionsky. *Direct quantification of autophagic flux by a single molecule- based probe*. Apr. 2017. doi: 10.1080/15548627.2017.1280646.

[GM10] Roberta A. Gottlieb and Robert M. Mentzer. “Autophagy During Cardiac Stress: Joys and Frustra- tions of Autophagy”. In: *Annual Review of Physiology* 72 (1 Mar. 2010), pp. 45–59. issn: 0066-4278. doi: 10.1146/annurev-physiol-021909-135757.

[GM13] Roberta A. Gottlieb and Robert M. Mentzer. “Autophagy: An affair of the heart”. In: vol. 18.
Sept. 2013, pp. 575–584. doi: 10.1007/s10741-012-9367-2.

[Goe+20] Jens P. Goetze et al. *Cardiac natriuretic peptides*. Nov. 2020. doi: 10.1038/s41569-020-0381-0.

[Gog+19] Rajinikanth Gogiraju et al. “Endothelial Leptin Receptor Deletion Promotes Cardiac Autophagy and Angiogenesis Following Pressure Overload by Suppressing Akt/mTOR Signaling”. In: *Circu- lation. Heart failure* 12 (1 Jan. 2019), e005622. issn: 19413297. doi: 10.1161/CIRCHEARTFAILURE.
118.005622.

[Gon+22] Arantxa González et al. *Cardiac remodelling – Part 1: From cells and tissues to circulating biomark- ers. A review from the Study Group on Biomarkers of the Heart Failure Association of the European Society of Cardiology*. June 2022. doi: 10.1002/ejhf.2493.

[Goo+61] J. F. Goodwin et al. “Clinical Aspects of Cardiomyopathy”. In: *BMJ* 1 (5219 Jan. 1961), pp. 69–79.
issn: 0959-8138. doi: 10.1136/bmj.1.5219.69.

[Got+04] Kazuhisa Gotoh et al. “Apg-2 has a chaperone-like activity similar to Hsp110 and is overexpressed in hepatocellular carcinomas”. In: *FEBS Letters* 560 (1-3 Feb. 2004), pp. 19–24. issn: 00145793. doi: 10.1016/S0014-5793(04)00034-1.

[Goy07] Siddharth Singh Abha Goyal. *Texas Heart Institute Journal The Origin of Echocardiography A Tribute to Inge Edler Early Developments in Echocardiography*. Texas Heart Institute Journal, 2007. url: https://www.ncbi.nlm.nih.gov/pmc/articles/PMC2170493/pdf/20071200s00010p431. pdf.

[Gro+20] Amy Groenewegen et al. *Epidemiology of heart failure*. Aug. 2020. doi:
10.1002/ejhf.1858.

[Gu+19] Yan Gu et al. “Tumor-educated B cells selectively promote breast cancer lymph node metastasis by HSPA4-targeting IgG”. In: *Nature Medicine* 25 (2 Feb. 2019), pp. 312–322. issn: 1546170X. doi: 10.1038/s41591-018-0309-y.

[Gue+21] Magellan Guewo-Fokeng et al. “Heat Shock Protein 70 (HSP70) Protein-Protein Interactions and a Putative Mechanism for the Potential Benefits of Heat Therapy for Type 2 Diabetes Mellitus”. In: *Biochemistry and Molecular Biology* 6 (2 2021), p. 19. issn: 2575-5064. doi: 10.11648/j.bmb.
20210602.11.

[Gui+97] S Guillaumes et al. *Chloroquine Stabilizes Pancreatic Lysosomes and Improves Survival of Mice with Diet-Induced Acute Pancreatitis*. 1997, pp. 262–266. url: http://journals.lww.com/pancreasjournal.

[Guo+17] Yuxuan Guo et al. “Analysis of Cardiac Myocyte Maturation Using CASAAV, a Platform for Rapid Dissection of Cardiac Myocyte Gene Function in Vivo”. In: *Circulation Research* 120 (12 June 2017), pp. 1874–1888. issn: 15244571. doi:

10.1161/CIRCRESAHA.116.310283.

[Ha+05] Tuanzhu Ha et al. “Attenuation of cardiac hypertrophy by inhibiting both mTOR and NFkB activation in vivo”. In: *Free Radical Biology and Medicine* 39 (12 Dec. 2005), pp. 1570–1580. issn: 08915849. doi: 10.1016/j.freeradbiomed.2005.08.002.

[Han+20] Ying Han et al. “lncRNA RMRP Prevents Mitochondrial Dysfunction and Cardiomyocyte Apopto- sis via the miR-1-5p/hsp70 Axis in LPS-Induced Sepsis Mice”. In: *Inflammation* 43 (2 Apr. 2020), pp. 605–618. issn: 15732576. doi: 10.1007/s10753-019-01141-8.

[Han+21] Balvinder S. Handa et al. “Ventricular fibrillation mechanism and global fibrillatory organization are determined by gap junction coupling and fibrosis pattern”. In: *Cardiovascular Research* 117 (4 Apr. 2021), pp. 1078–1090. issn: 17553245. doi: 10.1093/cvr/cvaa141.

[Har+17] Justin Hartupee et al. “Impaired Protein Quality Control during Left Ventricular Remodeling in Mice with Cardiac Restricted Overexpression of Tumor Necrosis Factor”. In: *Circulation: Heart Failure* 10 (12 Dec. 2017). issn: 19413297. doi: 10.1161/CIRCHEARTFAILURE.117.004252.

[Has+18] Saamir A. Hassan et al. *Chemotherapeutic Agents and the Risk of Ischemia and Arterial Throm- bosis*. Feb. 2018. doi: 10.1007/s11883-018-0702-5.

[HBH11] F. Ulrich Hartl, Andreas Bracher, and Manajit Hayer-Hartl. *Molecular chaperones in protein folding and proteostasis*. July 2011. doi: 10.1038/nature10317.

[Hel+11] Torsten Held et al. “Heat-shock protein HSPA4 is required for progression of spermatogenesis”. In: *Reproduction* 142 (1 July 2011). HSP-KO mouse line generation, pp. 133–144. issn: 14701626. doi: 10.1530/REP-11-0023.

[Her+12] Daniel S. Herman et al. “Truncations of Titin Causing Dilated Cardiomyopathy”. In: *New England Journal of Medicine* 366 (7 Feb. 2012), pp. 619–628. issn: 0028-4793. doi: 10.1056/NEJMoa1110186.

[Her+14] David Heras-Sandoval et al. “The role of PI3K/AKT/mTOR pathway in the modulation of au- tophagy and the clearance of protein aggregates in neurodegeneration”. In: *Cellular Signalling* 26 (12 Dec. 2014), pp. 2694–2701. issn: 08986568. doi: 10.1016/j.cellsig.2014.08.019.

[Hie+20] Michinari Hieda et al. “Increased Myocardial Stiffness in Patients with High-Risk Left Ventricu- lar Hypertrophy: The Hallmark of Stage-B Heart Failure with Preserved Ejection Fraction”. In: *Circulation* (2020), pp. 115–123. issn: 15244539. doi: 10.1161/CIRCULATIONAHA.119.040332.

[HKT10] Akinori Hishiya, Toshio Kitazawa, and Shinichi Takayama. “BAG3 and Hsc70 interact with actin capping protein CapZ to maintain myofibrillar integrity under mechanical stress”. In: *Circulation Research* 107 (10 Nov. 2010), pp. 1220–1231. issn: 00097330. doi: 10.1161/CIRCRESAHA.110.
225649.

[HL14] Pamela A. Harvey and Leslie A. Leinwand. *Cardiac Atrophy and Remodeling*. 2014. doi: 10.1016/ B978-0-12-405206-2.00003-X.

[Hom+06] Sachiko Homma et al. “BAG3 deficiency results in fulminant myopathy and early lethality”. In: *American Journal of Pathology* 169 (3 2006). similar phenotype as HSPAKO, pp. 761–773. issn: 00029440. doi: 10.2353/ajpath.2006.060250.

[Hoo+17] Edgar T. Hoorntje et al. *Arrhythmogenic cardiomyopathy: Pathology, genetics, and concepts in pathogenesis*. Oct. 2017. doi: 10.1093/cvr/cvx150.

[Hop+09] Charles L. Hoppel et al. *Dynamic organization of mitochondria in human heart and in myocardial disease*. Oct. 2009. doi: 10.1016/j.biocel.2009.05.004.

[HPH14] Mark S. Hipp, Sae Hun Park, and Ulrich U. Hartl. *Proteostasis impairment in protein-misfolding and -aggregation diseases*. 2014. doi: 10.1016/j.tcb.2014.05.003.

[Hu+03] Ping Hu et al. “Minimally invasive aortic banding in mice: effects of altered cardiomyocyte insulin signaling during pressure overload”. In: *American Journal of Physiology-Heart and Circulatory Physiology* 285 (3 Sept. 2003), H1261–H1269. issn: 0363-6135. doi: 10.1152/ajpheart.00108.

2003.

[Hua+22] Junqi Huang et al. *Understanding Anthracycline Cardiotoxicity From Mitochondrial Aspect*. Feb. 2022. doi: 10.3389/fphar.2022.811406.

[Ina+06] Katsuya Inagaki et al. *Robust Systemic Transduction with AAV9 Vectors in Mice: Efficient Global Cardiac Gene Transfer Superior to That of AAV8*. AAV9 is good for gene transfer in heart (FIG 3). 2006.

[JAA18] Jonas Jarasunas, Audrius Aidietis, and Sigita Aidietiene. "Left atrial strain - An early marker of left ventricular diastolic dysfunction in patients with hypertension and paroxysmal atrial fibril- lation 11 Medical and Health Sciences 1102 Cardiorespiratory Medicine and Haematology". In: *Cardiovascular Ultrasound* 16 (1 Oct. 2018). issn: 14767120. doi: 10.1186/s12947-018-0147-6.

[Jac+18] Aasems Jacob et al. *Cardiovascular effects of Hodgkin's lymphoma: a review of literature*. Jan. 2018. doi: 10.1007/s00432-017-2560-x.

[Jas+09] Brian E. Jaski et al. "Calcium Upregulation by Percutaneous Administration of Gene Therapy in Cardiac Disease (CUPID Trial), a First-in-Human Phase 1/2 Clinical Trial". In: *Journal of Cardiac Failure* 15 (3 Apr. 2009), pp. 171–181. issn: 10719164. doi: 10.1016/j.cardfail.2009.01.013.

[JC20] Matthew Jankowich and Gaurav Choudhary. "Endothelin-1 levels and cardiovascular events". In: *Trends in Cardiovascular Medicine* 30 (1 Jan. 2020), pp. 1–8. issn: 10501738. doi: 10.1016/j. tcm.2019.01.007.

[JF90] Dice J.F. "Peptide Sequences that target cytosolic proteins for lysosomal proteolysis". In: *TIBS* (1990).

[JL11] Terje Johansen and Trond Lamark. *Selective autophagy mediated by autophagic adapter proteins*. 2011. doi: 10.4161/auto.7.3.14487.

[JWK98] Jennifer A. Johnston, Cristina L. Ward, and Ron R. Kopito. "Aggresomes: A Cellular Response to Misfolded Proteins". In: *Journal of Cell Biology* 143 (7 Dec. 1998), pp. 1883–1898. issn: 0021-9525. doi: 10.1083/jcb.143.7.1883.

[K+14] Katerina Naka K et al. "Hsp70 regulates the doxorubicin-mediated heart failure in Hsp70-transgenic mice". In: *Cell Stress and Chaperones* 19 (6 Nov. 2014). issn: 14661268. doi: 10.1007/s12192- 014-0509-4.

[Kam+09] Harm H. Kampinga et al. *Guidelines for the nomenclature of the human heat shock proteins*. Jan. 2009. doi: 10.1007/s12192-008-0068-7.

[Kan+17] Seol-Hee Kang et al. "Forkhead box O3 plays a role in skeletal muscle atrophy through expression of E3 ubiquitin ligases MuRF-1 and atrogin-1 in Cushing's syndrome". In: (2017). doi: 10.1152/ ajpendo.00389.2016.-Cush. url: http://www.ajpendo.org.

[Kan+97] Yoshiyuki Kaneko et al. *Cloning of apg-2 encoding a novel member of heat shock protein 110 family*. Structure of HSPA4. 1997, p. 810.

[Kan02] Kang. "Hspa4 (HSP70) is Involved in the Radioadaptive Response: Results from Mouse Spleno- cytes". In: *Radiation Research* VOL. 157 (NO 6 2002). doi: 10.1667/0033. url: https://doi. org/10.1667/0033-.

[Kaw+12] Tomonori Kawaguchi et al. "Prior starvation mitigates acute doxorubicin cardiotoxicity through restoration of autophagy in affected cardiomyocytes". In: *Cardiovascular Research* 96 (3 Dec. 2012), pp. 456–465. issn: 00086363. doi: 10.1093/cvr/cvs282.

[KC10] Harm H. Kampinga and Elizabeth A. Craig. *The HSP70 chaperone machinery: J proteins as drivers of functional specificity*. Aug. 2010. doi: 10.1038/nrm2941.

[Ke+11] Lei Ke et al. “HSPB1, HSPB6, HSPB7 and HSPB8 Protect against RhoA GTPase-Induced Re- modeling in Tachypaced Atrial Myocytes”. In: *PLoS ONE* 6 (6 2011). issn: 19326203. doi: 10. 1371/journal.pone.0020395.

[Kie+19] Jake M. Kieserman et al. *Current Landscape of Heart Failure Gene Therapy*. May 2019. doi: 10.1161/JAHA.119.012239.

[Kim+21] Soyeon Kim et al. “Stress-induced NEDDylation promotes cytosolic protein aggregation through HDAC6 in a p62-dependent manner”. In: *iScience* 24 (3 Mar. 2021). issn: 25890042. doi: 10. 1016/j.isci.2021.102146.

[Kit+22] Hiroki Kitakata et al. *Therapeutic Targets for DOX-Induced Cardiomyopathy: Role of Apoptosis vs. Ferroptosis*. Feb. 2022. doi: 10.3390/ijms23031414.

[KK12] Norimichi Koitabashi and David A. Kass. *Reverse remodeling in heart failure-mechanisms and therapeutic opportunities*. Mar. 2012. doi: 10.1038/nrcardio.2011.172.

[KK17] Navid Koleini and Elissavet Kardami. *Autophagy and mitophagy in the context of doxorubicin- induced cardiotoxicity*. 2017, pp. 46663–46680. url: www.impactjournals.com/oncotarget/.

[Kli+12] Daniel J Klionsky et al. *Guidelines for the use and interpretationof assays for monitoring au- tophagy*. 2012, p. 312. url: www.landesbioscience.com.[Kna+01] Michiel W M Knaapen et al. *Apoptotic versus autophagic cell death in heart failure a b c b c*. 2001, pp. 304–312. url: www.elsevier.com/locate/cardiores.

[Kne+16] Tijana Knezevic et al. *Adeno-Associated Virus Serotype 9-Driven Expression of BAG3 Improves Left Ventricular Function in Murine Hearts With Left Ventricular Dysfunction Secondary to a Myocardial Infarction*. 2016, pp. 647–56.

[Kob+10] Satoru Kobayashi et al. “Transcription factor GATA4 inhibits doxorubicin-induced autophagy and cardiomyocyte death”. In: *Journal of Biological Chemistry* 285 (1 Jan. 2010), pp. 793–804. issn: 00219258. doi: 10.1074/jbc.M109.070037.

[Koc+10] Robb D. Kociol et al. *Troponin elevation in heart failure: Prevalence, mechanisms, and clinical implications*. Sept. 2010. doi: 10.1016/j.jacc.2010.06.016.

[Kon+22] Chun Yan Kong et al. *Underlying the Mechanisms of Doxorubicin-Induced Acute Cardiotoxicity: Oxidative Stress and Cell Death*. 2022. doi: 10.7150/ijbs.65258.

[Kus+20] Kenya Kusunose et al. *Erratum: The evaluation of aortic stenosis, how the new guidelines are implemented across Europe: a survey by EACVI (European Heart Journal - Cardiovascular Imaging (2020) 21 (357-362) DOI: 10.1093/ehjci/jeaa009)*. July 2020. doi: 10.1093/ehjci/jez235.

[LA13] Min Luo and Mark E. Anderson. “Mechanisms of altered Ca2+ handling in heart failure”. In:*Circulation Research* 113 (6 2013), pp. 690–708. issn: 00097330. doi: 10.1161/CIRCRESAHA.113.301651.

[Lan+20] Yin Lan et al. “Heat Shock Protein 22 Attenuates Doxorubicin-Induced Cardiotoxicity via Regulat- ing Inflammation and Apoptosis”. In: *Frontiers in Pharmacology* 11 (Mar. 2020). issn: 16639812. doi: 10.3389/fphar.2020.00257.

[Lan88] Douglas J. Lanska. “Conditions Associated With Huntington’s Disease at Death”. In: *Archives of Neurology* 45 (8 Aug. 1988), p. 878. issn: 0003-9942. doi: 10.1001/archneur.1988.00520320068017.

[LDH00] Jens Lüders, Jens Demand, and Jörg Höhfeld. “The ubiquitin-related BAG-1 provides a link be- tween the molecular chaperones Hsc70/Hsp70 and the proteasome”. In: *Journal of Biological Chem- istry* 275 (7 Feb. 2000), pp. 4613–4617. issn: 00219258. doi: 10.1074/jbc.275.7.4613.

[LE14] Longjian Liu and Howard J. Eisen. “Epidemiology of Heart Failure and Scope of the Problem”. In:
Cardiology Clinics 32 (1 Feb. 2014), pp. 1–8. issn: 07338651. doi: 10.1016/j.ccl.2013.09.009.

[Lee+02] Mun-Yong Lee et al. *An immunohistochemical study of APG-2 protein in the rat hippocampus after transient forebrain ischemia a b a c a*. 2002, pp. 237–241. url: www.elsevier.com/locate/bres.

[Lee+95] D. Lee-Yoon et al. "Identification of a major subfamily of large hsp70-like proteins through the cloning of the mammalian 110-kDa heat shock protein". In: *Journal of Biological Chemistry* 270 (26 1995), pp. 15725–15733. issn: 00219258. doi: 10.1074/jbc.270.26.15725.

[Li+06] Duanxiang Li et al. *ARTICLE Mutations of Presenilin Genes in Dilated Cardiomyopathy and Heart Failure*. 2006, pp. 1030–1039. url: www.ajhg.org.

[Li+14] Siying Li et al. "Nrf2 deficiency exaggerates doxorubicin-induced cardiotoxicity and cardiac dys- function". In: *Oxidative Medicine and Cellular Longevity* 2014 (2014). issn: 19420994. doi: 10. 1155/2014/748524.

[Li+16a] Bao Li et al. "Distinct changes of myocyte autophagy during myocardial hypertrophy and heart failure: association with oxidative stress". In: *Experimental Physiology* 101 (8 Aug. 2016), pp. 1050– 1063. issn: 1469445X. doi: 10.1113/EP085586.

[Li+16b] Dan L. Li et al. "Doxorubicin Blocks Cardiomyocyte Autophagic Flux by Inhibiting Lysosome Acidification". In: *Circulation* 133 (17 Apr. 2016), pp. 1668–1687. issn: 15244539. doi: 10.1161/ CIRCULATIONAHA.115.017443.

[Li+17] Kai Li et al. "Tetrameric Assembly of K+ Channels Requires ER-Located Chaperone Proteins". In: *Molecular Cell* 65 (1 Jan. 2017), pp. 52–65. issn: 10974164. doi: 10.1016/j.molcel.2016.10.027.

[Li+20] Wen Li et al. *Selective autophagy of intracellular organelles: Recent research advances*. 2020. doi:

[Li+22] Sung-Chou Li et al. "HSPA4 Is a Biomarker of Placenta Accreta and Enhances the Angiogenesis Ability of Vessel Endothelial Cells". In: *International Journal of Molecular Sciences* 23 (10 May 2022), p. 5682. doi: 10.3390/ijms23105682.

[Lim+15] Junghyun Lim et al. "Proteotoxic Stress Induces Phosphorylation of p62/SQSTM1 by ULK1 to Regulate Selective Autophagic Clearance of Protein Aggregates". In: *PLoS Genetics* 11 (2 2015), pp. 1–28. issn: 15537404. doi: 10.1371/journal.pgen.1004987.[LKK20] Pierre Loap, Krassen Kirov, and Youlia Kirova. "Cardiotoxicity in breast cancer patients treated with radiation therapy: From evidences to controversies". In: *Critical Reviews in Oncology/Hematology* 156 (Dec. 2020), p. 103121. issn: 10408428. doi: 10.1016/j.critrevonc.2020.103121.

[Lóp+15] Begoña López et al. *Circulating Biomarkers of Myocardial Fibrosis The Need for a Reappraisal*.2015.

[Lóp+21] Begoña López et al. "Diffuse myocardial fibrosis: mechanisms, diagnosis and therapeutic ap- proaches". In: *Nature Reviews Cardiology* 18 (7 July 2021), pp. 479–498. issn: 1759-5002. doi: 10.1038/s41569-020-00504-1.

[LRM01] Do Sun Lim, Robert Roberts, and Ali J. Marian. "Expression profiling of cardiac genes in human hypertrophic cardiomyopathy: Insight into the pathogenesis of phenotypes". In: *Journal of the American College of Cardiology* 38 (4 2001), pp. 1175–1180. issn: 07351097. doi: 10.1016/S0735-1097(01)01509-1.

[Lv+12] Xiuxiu Lv et al. “Berberine Inhibits Doxorubicin-Triggered Cardiomyocyte Apoptosis via Atten- uating Mitochondrial Dysfunction and Increasing Bcl-2 Expression”. In: *PLoS ONE* 7 (10 Oct. 2012). issn: 19326203. doi: 10.1371/journal.pone.0047351.

[LW06] Huiyun Liang and Walter F Ward. “Staying Current PGC-1: a key regulator of energy metabolism”.
In: *Advanced Physiological Education* (2006). doi: 10.1152/advan.00052.2006.-Peroxisome.

[LYM11] Wenming Li, Qian Yang, and Zixu Mao. *Chaperone-mediated autophagy: Machinery, regulation and biological consequences*. Mar. 2011. doi: 10.1007/s00018-010-0565-6.

[Ma+15] Sai Ma et al. *The role of the autophagy in myocardial ischemia/reperfusion injury*. Feb. 2015. doi:10.1016/j.bbadis.2014.05.010.

[Ma+17] Yanyan Ma et al. “Rutin attenuates doxorubicin-induced cardiotoxicity via regulating autophagy and apoptosis”. In: *Biochimica et Biophysica Acta - Molecular Basis of Disease* 1863 (8 Aug. 2017), pp. 1904–1911. issn: 1879260X. doi: 10.1016/j.bbadis.2016.12.021.

[Mac+15] Christophe Macri et al. “Modulation of deregulated chaperone-mediated autophagy by a phospho- peptide”. In: *Autophagy* 11 (3 Jan. 2015), pp. 472–486. issn: 15548635. doi: 10.1080/15548627.
2015.1017179.

[Mae+13] Yasuhiro Maejima et al. “Mst1 inhibits autophagy by promoting the interaction between beclin1 and Bcl-2”. In: *Nature Medicine* 19 (11 Nov. 2013), pp. 1478–1488. issn: 10788956. doi: 10.1038/ nm.3322.

[Mag+18] Chantal M. Maghames et al. “NEDDylation promotes nuclear protein aggregation and protects the Ubiquitin Proteasome System upon proteotoxic stress”. In: *Nature Communications* 9 (1 Dec. 2018). issn: 20411723. doi: 10.1038/s41467-018-06365-0.

[Mam+07] Cristina Mammucari et al. “FoxO3 Controls Autophagy in Skeletal Muscle In Vivo”. In: *Cell Metabolism* 6 (6 Dec. 2007), pp. 458–471. issn: 15504131. doi: 10.1016/j.cmet.2007.11.001.

[Man+22] Palanisamy Manikandan et al. “Exploring the biological behavior of Heat shock protein (HSPs) for understanding the Anti-ischemic stroke in humans”. In: *Journal of Infection and Public Health* 15 (4 Apr. 2022), pp. 379–388. issn: 1876035X. doi: 10.1016/j.jiph.2022.03.001.

[Mar+00] Barry J. Maron et al. “Efficacy of Implantable Cardioverter–Defibrillators for the Prevention of Sudden Death in Patients with Hypertrophic Cardiomyopathy”. In: *New England Journal of Medicine* 342 (6 Feb. 2000), pp. 365–373. issn: 0028-4793. doi: 10.1056/NEJM200002103420601.

[Mar+06] Carla Marques et al. “The triage of damaged proteins: degradation by the ubiquitin-proteasome pathway or repair by molecular chaperones”. In: *The FASEB Journal* 20 (6 Apr. 2006), pp. 741– 743. issn: 0892-6638. doi: 10.1096/fj.05-5080fje.

[Mat+09] Kohichi Matsunaga et al. “Two Beclin 1-binding proteins, Atg14L and Rubicon, reciprocally reg- ulate autophagy at different stages”. In: *Nature Cell Biology* 11 (4 2009), pp. 385–396. issn: 14657392. doi: 10.1038/ncb1846.

[Mau+18] Mario Mauthe et al. “Chloroquine inhibits autophagic flux by decreasing autophagosome-lysosome fusion”. In: *Autophagy* 14 (8 Aug. 2018), pp. 1435–1455. issn: 15548635. doi: 10.1080/15548627.
2018.1474314.

[May13] Matthias P. Mayer. *Hsp70 chaperone dynamics and molecular mechanism*. Oct. 2013. doi: 10.1016/j.tibs.2013.08.001.

[MB05] M. P. Mayer and B. Bukau. *Hsp70 chaperones: Cellular functions and molecular mechanism*. Mar. 2005. doi: 10.1007/s00018-004-4464-6.

[MC02] Melanie Maytin and Wilson S. Colucci. “Molecular and cellular mechanisms of myocardial remod- eling”. In: *Journal of Nuclear Cardiology* 9 (3 2002), pp. 319–327. issn: 10713581. doi: 10.1067/ mnc.2002.123207.

[McG+17] John V. McGowan et al. “Anthracycline Chemotherapy and Cardiotoxicity”. In: *Cardiovascular Drugs and Therapy* 31 (1 Feb. 2017), pp. 63–75. issn: 15737241. doi: 10.1007/s10557-016-6711-0.

[McT+07] C. F. McTiernan et al. “Myocarditis following adeno-associated viral gene expression of human sol- uble TNF receptor (TNFRII-Fc) in baboon hearts”. In: *Gene Therapy* 14 (23 Dec. 2007), pp. 1613– 1622. issn: 09697128. doi: 10.1038/sj.gt.3303020.

[MGC09] Eirini Meimaridou, Sakina B. Gooljar, and J. Paul Chapple. *From hatching to dispatching: The multiple cellular roles of the Hsp70 molecular chaperone machinery*. 2009. doi: 10.1677/JME-08- 0116.

[MH13] Federico Mingozzi and Katherine A. High. *Immune responses to AAV vectors: Overcoming barriers to successful gene therapy*. July 2013. doi: 10.1182/blood-2013-01-306647.

[MMO95] Toshiaki MIURA, Sanae MURAOKA, and Taketo OGISO. “Adriamycin-Fe3+-Induced Mitochon- drial Protein Damage with Lipid Peroxidation.” In: *Biological and Pharmaceutical Bulletin* 18 (4 1995), pp. 514–517. issn: 0918-6158. doi: 10.1248/bpb.18.514.

[MMT17] William J. McKenna, Barry J. Maron, and Gaetano Thiene. “Classification, Epidemiology, and Global Burden of Cardiomyopathies”. In: *Circulation Research* 121 (7 Sept. 2017), pp. 722–730. issn: 0009-7330. doi: 10.1161/CIRCRESAHA.117.309711.

[Moh+12] Belal A. Mohamed et al. “Targeted disruption of Hspa4 gene leads to cardiac hypertrophy and fibrosis”. In: *Journal of Molecular and Cellular Cardiology* 53 (4 Oct. 2012), pp. 459–468. issn: 00222828. doi: 10.1016/j.yjmcc.2012.07.014.

[Moh+14] Belal A. Mohamed et al. “Respiratory distress and early neonatal lethality in Hspa4l/Hspa4 double- mutant mice”. In: *American Journal of Respiratory Cell and Molecular Biology* 50 (4 2014), pp. 817–824. issn: 15354989. doi: 10.1165/rcmb.2013-0132OC.

[Moo+11] Brioni R. Moore et al. “Pharmacokinetics, pharmacodynamics, and allometric scaling of chloro- quine in a murine malaria model”. In: *Antimicrobial Agents and Chemotherapy* 55 (8 Aug. 2011), pp. 3899–3907. issn: 00664804. doi: 10.1128/AAC.00067-11.

[MOY02] Noboru Mizushima, Yoshinori Ohsumi, and Tamotsu Yoshimori. *Autophagosome Formation in Mammalian Cells*. 2002, pp. 421–429.

[MR15] Patrick M. McLendon and Jeffrey Robbins. *Proteotoxicity and cardiac dysfunction*. May 2015. doi:10.1161/CIRCRESAHA.116.305372.

[MS17] Abhisek Mukherjee and Claudio Soto. *Prion-like protein aggregates and type 2 diabetes*. May 2017.doi: 10.1101/cshperspect.a024315.

[Mur+01] Shigeo Murata et al. “CHIP is a chaperone-dependent E3 ligase that ubiquitylates unfolded pro- tein”. In: (2001). issn: 1133-1138.

[Nab+15] Chadi Nabhan et al. “Disease characteristics, treatment patterns, prognosis, outcomes and lymphoma- related mortality in elderly follicular lymphoma in the United States”. In: *British Journal of Haematology* 170 (1 July 2015), pp. 85–95. issn: 00071048. doi: 10.1111/bjh.13399.

[Nak+04] Mitsunari Nakajima et al. “Presenilin 1 is essential for cardiac morphogenesis”. In: *Developmental Dynamics* 230 (4 Aug. 2004), pp. 795–799. issn: 10588388. doi:

10.1002/dvdy.20098.

[Nak+07] Atsuko Nakai et al. “The role of autophagy in cardiomyocytes in the basal state and in response to hemodynamic stress”. In: *Nature Medicine* 13 (5 May 2007), pp. 619–624. issn: 10788956. doi: 10.1038/nm1574.

[Nis+09] K. Nishida et al. *The role of autophagy in the heart*. 2009. doi: 10.1038/cdd.2008.163.

[NO16] Kazuhiko Nishida and Kinya Otsu. *Autophagy during cardiac remodeling*. June 2016. doi: 10.1016/j.yjmcc.2015.12.003.

[Nog+20] Masayuki Noguchi et al. *Autophagy as a modulator of cell death machinery*. July 2020. doi: 10.1038/s41419-020-2724-5.

[Non+99] Kohsuke Nonoguchi et al. *Cloning of human cDNAs for Apg-1 and Apg-2, members of the Hsp110 family, and chromosomal assignment of their genes*. 1999, pp. 21–28. url: www.elsevier.com/ locate/gene.

[Nor+02] Gavin R. Norton et al. “Heart failure in pressure overload hypertrophy: The relative roles of ventric- ular remodeling and myocardial dysfunction”. In: *Journal of the American College of Cardiology* 39 (4 Feb. 2002), pp. 664–671. issn: 07351097. doi: 10.1016/S0735-1097(01)01792-2.

[NQW14] Thao P. Nguyen, Zhilin Qu, and James N. Weiss. *Cardiac fibrosis and arrhythmogenesis: The road to repair is paved with perils*. 2014. doi: 10.1016/j.yjmcc.2013.10.018.

[OC10] Samantha J. Orenstein and Ana Maria Cuervo. *Chaperone-mediated autophagy: Molecular mecha- nisms and physiological relevance*. 2010. doi: 10.1016/j.semcdb.2010.02.005.

[OCS97] Hyun Ju Oh, Xing Chen, and John R. Subjeck. “hsp110 protects heat-denatured proteins and con- fers cellular thermoresistance”. In: *Journal of Biological Chemistry* 272 (50 Dec. 1997), pp. 31636– 31640. issn: 00219258. doi: 10.1074/jbc.272.50.31636.

[Odn+97] R Odney et al. *Review Articles Medical Progress*. 1997.

[Olz+11] Heidi Olzscha et al. “Amyloid-like aggregates sequester numerous metastable proteins with essential cellular functions”. In: *Cell* 144 (1 Jan. 2011), pp. 67–78. issn: 00928674. doi: 10.1016/j.cell.2010.11.050.

[Ost+13] Moritz Osterholt et al. “Alterations in mitochondrial function in cardiac hypertrophy and heart failure”. In: vol. 18. Sept. 2013, pp. 645–656. doi: 10.1007/s10741-012-9346-7.

[Oya+13] Jota Oyabu et al. “Autophagy-mediated degradation is necessary for regression of cardiac hyper- trophy during ventricular unloading”. In: *Biochemical and Biophysical Research Communications* 441 (4 Nov. 2013), pp. 787–792. issn: 0006291X. doi: 10.1016/j.bbrc.2013.10.135.

[Oya12] Oka Takafumi Shungo Hikoso Osamu Yamaguchi Manabu Taneike Toshihiro Takeda Takahito Tamai Jota Oyabu. “Mitochondrial DNA that escapes from autophagy causes inflammation and heart failure”. In: *Nature* 485 (7397 May 2012), pp. 251–255. issn: 00280836. doi: 10.1038/nature10992.

[Pac+06] Christina A. Pacak et al. “Recombinant adeno-associated virus serotype 9 leads to preferential cardiac transduction in vivo”. In: *Circulation Research* 99 (4 Aug. 2006). issn: 00097330. doi: 10.1161/01.RES.0000237661.18885.f6.

[Pan+07] Serhiy Pankiv et al. “p62/SQSTM1 binds directly to Atg8/LC3 to facilitate degradation of ubiq- uitinated protein aggregates by autophagy*[S]”. In: *Journal of Biological Chemistry* 282 (33 Aug. 2007), pp. 24131–24145. issn: 00219258. doi: 10.1074/jbc.M702824200.

[Pan+19] Jian An Pan et al. “miR-146a attenuates apoptosis and modulates autophagy by

targeting TAF9b/P53 pathway in doxorubicin-induced cardiotoxicity". In: *Cell Death and Disease* 10 (9 Sept. 2019). issn: 20414889. doi: 10.1038/s41419-019-1901-x.

[Par+11] Ah Mee Park et al. "Mechanism of anthracycline-mediated down-regulation of GATA4 in the heart". In: *Cardiovascular Research* 90 (1 Apr. 2011), pp. 97–104. issn: 00086363. doi: 10.1093/ cvr/cvq361.

[PBP90] Marc A Pfeffer, Eugene Braunwald, and Asso-ciate Professor. *Ventricular Remodeling After My- ocardial Infarction Experimental Observations and Clinical Implications*. 1990. url: http : // ahajournals.org.

[Ped+13] Zully Pedrozo et al. "Cardiomyocyte ryanodine receptor degradation by chaperone-mediated au- tophagy". In: *Cardiovascular Research* 98 (2 May 2013), pp. 277–285. issn: 00086363. doi: 10. 1093/cvr/cvt029.

[Pfe+87] U Pfeifer et al. *Short-term Inhibition of Cardiac Cellular Autophagy by Isoproterenol*. 1987, pp. 1179– 184.

[Pil+18] Björn Pilebro et al. "Positron emission tomography (PET) utilizing Pittsburgh compound B (PIB) for detection of amyloid heart deposits in hereditary transthyretin amyloidosis (ATTR)". In: *Jour- nal of Nuclear Cardiology* 25 (1 Feb. 2018), pp. 240–248. issn: 15326551. doi: 10.1007/s12350-016-0638-5.

[Pin+20] Zhang Ping et al. *Oxidative Stress in Radiation-Induced Cardiotoxicity*. 2020. doi: 10.1155/2020/ 3579143.

[Pis+10] Andrew Pistner et al. "Murine echocardiography and ultrasound imaging". In: *Journal of Visualized Experiments* (42 Aug. 2010). issn: 1940-087X. doi: 10.3791/2100. url: http://www.jove.com/ index/Details.stp?ID=2100.

[PKH15] Jong Min Park, Ju Whan Kim, and Ki Baik Hahm. *HSPA4, the "Evil Chaperone" of the HSP Family, Delays Gastric Ulcer Healing*. Apr. 2015. doi: 10.1007/s10620-015-3597-9.

[Ple+07] Sven T. Pleger et al. "Stable myocardial-specific AAV6-S100A1 gene therapy results in chronic functional heart failure rescue". In: *Circulation* 115 (19 May 2007), pp. 2506–2515. issn: 00097322. doi: 10.1161/CIRCULATIONAHA.106.671701.

[PM18] Elizabeth Potter and Thomas H. Marwick. *Assessment of Left Ventricular Function by Echocar- diography: The Case for Routinely Adding Global Longitudinal Strain to Ejection Fraction*. Feb. 2018. doi: 10.1016/j.jcmg.2017.11.017.

[PML19] Rithu Pattali, Yongchao Mou, and Xue Jun Li. *AAV9 Vector: a Novel modality in gene therapy for spinal muscular atrophy*. Aug. 2019. doi: 10.1038/s41434-019-0085-4.

[Pol+11] Cécile Polge et al. "Muscle actin is polyubiquitinylated in vitro and in vivo and targeted for breakdown by the E3 ligase MuRF1". In: *The FASEB Journal* 25 (11 Nov. 2011), pp. 3790–3802. issn: 0892-6638. doi: 10.1096/fj.11-180968.

[PR08] J. Scott Pattison and Jeffrey Robbins. "Protein misfolding and cardiac disease: Establishing cause and effect". In: *Autophagy* 4 (6 Aug. 2008), pp. 821–823. issn: 15548635. doi: 10.4161/auto.6502.

[PTP20] Dulce Peris-Moreno, Daniel Taillandier, and Cécile Polge. "MuRF1/TRIM63, master regulator of muscle mass". In: *International Journal of Molecular Sciences* 21 (18 Sept. 2020), pp. 1–39. issn: 14220067. doi: 10.3390/ijms21186663.

[Qi+14] Guan Ming Qi et al. "Adiponectin suppresses angiotensin II-induced inflammation and cardiac fibrosis through activation of macrophage autophagy". In: *Endocrinology* 155 (6 2014), pp. 2254–2265. issn: 19457170. doi: 10.1210/en.2013-2011.

[Ram+12] Heike Rampelt et al. "Metazoan Hsp70 machines use Hsp110 to power protein disaggregation". In:*EMBO Journal* 31 (21 Oct. 2012), pp. 4221–4235. issn: 02614189. doi: 10.1038/emboj.2012.264.

[Ren+09] Giuseppe Rengo et al. “Myocardial adeno-associated virus serotype 6-ARKct gene therapy improves cardiac function and normalizes the neurohormonal axis in chronic heart failure”. In: *Circulation* 119 (1 Jan. 2009), pp. 89–98. issn: 00097322. doi: 10.1161/CIRCULATIONAHA.108.803999.

[RG97] Stefan Rüand Lothar Germeroth. *Substrate specificity of the DnaK chaperone determined byreening cellulose-bound peptide libraries respect to the bound folding conformer are only partly*. 1997, pp. 1501–1507.

[RH12] Oktay F. Rifki and Joseph A. Hill. *Cardiac autophagy: Good with the bad*. Sept. 2012. doi: 10.1097/FJC.0b013e3182646cb1.

[RJA10] Glenn C. Rowe, Aihua Jiang, and Zolt Arany. *PGC-1 coactivators in cardiac development and disease*. Oct. 2010. doi: 10.1161/CIRCRESAHA.110.223818.

[Roc+91] H A Rockman et al. “Segregation of atrial-specific and inducible expression of an atrial natriuretic factor transgene in an in vivo murine model of cardiac hypertrophy.” In: *Proceedings of the National Academy of Sciences* 88 (18 Sept. 1991), pp. 8277–8281. issn: 0027-8424. doi: 10.1073/pnas.88.18.8277.

[Rot+04] David M Roth et al. “Indirect intracoronary delivery of adenovirus encoding adenylyl cyclase increases left ventricular contractile function in mice Indirect intracoronary delivery of adenovirus encoding adenylyl cy-clase increases left ventricular contractile function in mice”. In: *Am J Physiol Heart Circ Physiol* 287 (2004), pp. 172–177. doi: 10.1152/ajpheart.01009.2003.-We. url: www.ajpheart.org.

[Ruj+06] María A Rujano et al. “Polarised Asymmetric Inheritance of Accumulated Protein Damage in Higher Eukaryotes”. In: *PLoS Biology* 4 (12 Dec. 2006), e417. issn: 1545-7885. doi: 10.1371/journal.pbio.0040417.

[Sak+15] Toshiharu Sakurai et al. “Heat Shock Protein A4 Controls Cell Migration and Gastric Ulcer Heal- ing”. In: *Digestive Diseases and Sciences* 60 (4 Apr. 2015), pp. 850–857. issn: 15732568. doi: 10.1007/s10620-015-3561-8.

[SB14] Gabriel Sayer and Geetha Bhat. “The Renin-Angiotensin-Aldosterone System and Heart Failure”. In: *Cardiology Clinics* 32 (1 Feb. 2014), pp. 21–32. issn: 07338651. doi: 10.1016/j.ccl.2013.09.002.

[SBE08] Paul Saftig, Wouter Beertsen, and Eeva Liisa Eskelinen. “LAMP-2: A control step fot phagosome and autophagosome maturation”. In: *Autophagy* 4 (4 May 2008), pp. 510–512. issn: 15548635. doi: 10.4161/auto.5724.

[SC12] Rajat Singh and Ana Maria Cuervo. *Lipophagy: Connecting autophagy and lipid metabolism*. 2012.

doi: 10.1155/2012/282041.[SCC20] Mark Sweeney, Ben Corden, and Stuart A Cook. “Targeting cardiac fibrosis in heart failure with preserved ejection fraction: mirage or miracle?” In: *EMBO Molecular Medicine* 12 (10 Oct. 2020). issn: 1757-4676. doi: 10.15252/emmm.201910865.

[Sch+08] Jonathan P. Schuermann et al. “Structure of the Hsp110:Hsc70 Nucleotide Exchange Machine”. In: *Molecular Cell* 31 (2 July 2008), pp. 232–243. issn: 10972765. doi: 10.1016/j.molcel.2008.05.006.

[Sch+12] O Schakman et al. “Role of IGF-I and the TNF/NF-B pathway in the induction of muscle atrogenes by acute inflammation”. In: *Am J Physiol Endocrinol Metab* 303 (2012), pp. 729–739. doi: 10. 1152/ajpendo.00060.2012.-Several. url: http://www.ajpendo.org.

[Sch+20] Rachel A. Schlaak et al. *Advances in preclinical research models of radiation-induced cardiac toxi- city*. Feb. 2020. doi: 10.3390/cancers12020415.

[SCJ82] J R Subjeck J J Sciandra, C F Chao, and R J Johnson. *HEAT SHOCK PROTEINS AND BIO- LOGICAL RESPONSE TO HYPERTHERMIA*. 1982, p. 127.

[Sel+10] Zachary M. Sellers et al. “Cardiomyocytes with disrupted CFTR function require CaMKII and Ca2+-activated Cl- channel activity to maintain contraction rate”. In: *Journal of Physiology* 588 (13 July 2010), pp. 2417–2429. issn: 00223751. doi:

10.1113/jphysiol.2010.188334.

[She+22] Mohammad Sheibani et al. *Doxorubicin-Induced Cardiotoxicity: An Overview on Pre-clinical Ther- apeutic Approaches*. Apr. 2022. doi: 10.1007/s12012-022-09721-1.

[Sho11] James Shorter. "The mammalian disaggregase machinery: Hsp110 synergizes with Hsp70 and Hsp40 to catalyze protein disaggregation and reactivation in a cell-free system". In: *PLoS ONE* 6 (10 2011). issn: 19326203. doi: 10.1371/journal.pone.0026319.

[Shu+19] Zeyu Shu et al. *The role of microvesicles containing microRNAs in vascular endothelial dysfunction*.Dec. 2019. doi: 10.1111/jcmm.14716.

[SMK96] Roland E Schmieder, Peter Martus, and Arnfried Klingbeil. *Reversal of Left Ventricular Hyper- trophy in Essential Hypertension A Meta-analysis of Randomized Double-blind Studies*. 1996. url: http://jama.jamanetwork.com/.

[SN18] Filip K. Swirski and Matthias Nahrendorf. *Cardioimmunology: the immune system in cardiac home- ostasis and disease*. Dec. 2018. doi: 10.1038/s41577-018-0065-8.

[Son01] Sondermann. "Structure of a Bag/Hsc70Complex: ConvergentFunctional Evolution of Hsp70Nucleotide Exchange Factors". In: *Sciencemag* 291 (2001).

[Spa+09] Paolo Spallarossa et al. "Doxorubicin induces senescence or apoptosis in rat neonatal cardiomy- ocytes by regulating the expression levels of the telomere binding factors 1 and 2". In: *Am J Physiol Heart Circ Physiol* 297 (2009), pp. 2169–2181. doi: 10.1152/ajpheart.00068.2009.-Low. url: www.ajpheart.org.

[SR14] Ayala Shiber and Tommer Ravid. *Chaperoning proteins for destruction: Diverse roles of Hsp70 chaperones and their co-chaperones in targeting misfolded proteins to the proteasome*. Sept. 2014. doi: 10.3390/biom4030704.

[SSW18] Jianjian Shi, Michelle Surma, and Lei Wei. *Disruption of ROCK1 gene restores autophagic flux and mitigates doxorubicin-induced cardiotoxicity*. 2018. url: www.impactjournals.com/oncotarget.

[Sta+18] Christoffer Stark et al. "Pegylated and liposomal doxorubicin is associated with high mortality and causes limited cardiotoxicity in mice". In: *BMC Research Notes* 11 (1 Feb. 2018). issn: 17560500. doi: 10.1186/s13104-018-3260-6.

[Ste+20] Sabine Steffens et al. *Stimulating pro-reparative immune responses to prevent adverse cardiac re- modelling: Consensus document from the joint 2019 meeting of the ESC working groups of cellular biology of the heart and myocardial function*. Sept. 2020. doi: 10.1093/cvr/cvaa137.

[Str+03] Beate K. Straub et al. *A novel cell-cell junction system: The cortex adhaerens mosaic of lens fiber cells*. Dec. 2003. doi: 10.1242/jcs.00815.

[Sum+20] Georg Summer et al. "A directed network analysis of the cardiome identifies molecular pathways contributing to the development of HFpEF". In: *Journal of Molecular and Cellular Cardiology* 144 (July 2020), pp. 66–75. issn: 00222828. doi: 10.1016/j.yjmcc.2020.05.008.

[Swy99] Bernard Swynghedauw. *Molecular Mechanisms of Myocardial Remodeling*. 1999.

[Tak+05] Toshihiro Takeda et al. "Presenilin 2 regulates the systolic function of heart by modulating Ca 2+ signaling". In: *The FASEB Journal* 19 (14 Dec. 2005), pp. 2069–2071. issn: 0892-6638. doi: 10.1096/fj.05-3744fje.

[Tak+18] Genzou Takemura et al. *Anti-apoptosis in nonmyocytes and pro-autophagy in cardiomyocytes: two strategies against postinfarction heart failure through regulation of cell death/degeneration*. Sept. 2018. doi: 10.1007/s10741-018-9708-x.

[Tan+08a] Paul Tannous et al. *Autophagy is an adaptive response in desmin-related cardiomyopathy*. 2008.

[Tan+08b] Paul Tannous et al. "Intracellular protein aggregation is a proximal trigger of

cardiomyocyte au- tophagy". In: *Circulation* 117 (24 June 2008), pp. 3070–3078. issn: 00097322. doi: 10.1161/CIRCULATIONAHA.107.763870.

[TB14] Guido Tarone and Mara Brancaccio. *Keep your heart in shape: Molecular chaperone networks for treating heart disease*. June 2014. doi: 10.1093/cvr/cvu049.

[Ter+92] Stanley R Terleckys et al. *Protein and Peptide Binding and Stimulation of in Vitro Lysosomal Proteolysis by the 73-kDa Heat Shock Cognate Protein**. 1992, pp. 9202–9209.

[TF85] Robert C Tarazi and Fetnat M Fouad. *REVERSAL OF CARDIAC HYPERTROPHY BY MED- ICAL TREATMENT*. 1985, pp. 407–421. url: www.annualreviews.org.

[TH17] Barry H. Trachtenberg and Joshua M. Hare. "Inflammatory Cardiomyopathic Syndromes". In: *Circulation Research* 121 (7 Sept. 2017), pp. 803–818. issn: 0009-7330. doi: 10.1161/CIRCRESAHA.117.310221.

[TM10] Fujiko Tsukahara and Yoshiro Maru. "Bag1 directly routes immature BCR-ABL for proteasomal degradation". In: *Blood* 116 (18 Nov. 2010), pp. 3582–3592. issn: 00064971. doi: 10.1182/blood-2009-10-249623.

[TM12] Oliver Trüe and Patrick Matthias. "Interplay between histone deacetylases and autophagy - from cancer therapy to neurodegeneration". In: *Immunology I& Cell Biology* 90 (1 Jan. 2012), pp. 78–84. issn: 0818-9641. doi: 10.1038/icb.2011.103.

[TMB06] Anna Tsapara, Karl Matter, and Maria S Balda. "The Heat-Shock Protein Apg-2 Binds to the Tight Junction Protein ZO-1 and Regulates Transcriptional Activity of ZONAB". In: *Molecular Biology of the Cell* 17 (2006), pp. 1322–1330. doi: 10.1091/mbc.E05-06. url: http://www.molbiolcell.org/cgi/doi/10.1091/mbc.E05-06.

[Tok+10] Malgorzata Tokarska-Schlattner et al. "Early effects of doxorubicin in perfused heart: transcrip- tional profiling reveals inhibition of cellular stress response genes". In: *Am J Physiol Regul Integr Comp Physiol* 298 (2010), pp. 1075–1088. doi: 10.1152/ajpregu.00360.2009.-Doxorubicin. url: http://www.broad.mit..

[Tsa+03] W.P Tsang et al. "Reactive oxygen species mediate doxorubicin induced p53-independent apopto- sis". In: *Life Sciences* 73 (16 Sept. 2003), pp. 2047–2058. issn: 00243205. doi: 10.1016/S0024-3205(03)00566-6.

[TSD13] Oktay Tacar, Pornsak Sriamornsak, and Crispin R. Dass. *Doxorubicin: An update on anticancer molecular action, toxicity and novel drug delivery systems*. Feb. 2013. doi: 10.1111/j.2042-7158.2012.01567.x.

[Tus+19] Marina Tusup et al. "Design of in vitro transcribed mRNA vectors for research and therapy". In: *Chimia* 73 (5 2019), pp. 391–394. issn: 00094293. doi: 10.2533/chimia.2019.391.

[Uca+12] Ahmet Ucar et al. "The miRNA-212/132 family regulates both cardiac hypertrophy and car- diomyocyte autophagy". In: *Nature Communications* 3 (2012). issn: 20411723. doi: 10.1038/ncomms2090.

[VAR05] Olli Vuolteenaho, Minna Ala-Kopsala, and Heikki Ruskoaho. "BNP as a biomarker in heart dis- ease." In: *Advances in clinical chemistry* 40 (2005), pp. 1–36. issn: 0065-2423.

[Vel+11] Joyce M. Velez et al. "p53 regulates oxidative stress-mediated retrograde signaling: A novel mech- anism for chemotherapy-induced cardiac injury". In: *PLoS ONE* 6 (3 2011). issn: 19326203. doi: 10.1371/journal.pone.0018005.

[Ver+00] Rati Verma et al. *Proteasomal Proteomics: Identification of Nucleotide-sensitive Proteasome-interacting Proteins by Mass Spectrometric Analysis of Affinity-purified Proteasomes*. 2000. pp. 3425–3439.

[VG22] Elisa Vitiello and Fanni Gergely. *Centrosomes grow aggresomes to clear waste*. Apr. 2022. doi: 10.1038/s41556-022-00891-2.

[Vos+08] Michel J. Vos et al. *Structural and functional diversities between members of the human HSPB, HSPH, HSPA, and DNAJ chaperone families*. July 2008. doi: 10.1021/bi800639z.

[VS21] Sander Verheule and Ulrich Schotten. *Electrophysiological consequences of cardiac fibrosis*. Nov.2021. doi: 10.3390/cells10113220.

[VSD14] David Vilchez, Milos S. Simic, and Andrew Dillin. *Proteostasis and aging of stem cells*. Mar. 2014. doi: 10.1016/j.tcb.2013.09.002.

[Wan+21] Yong Wang et al. "Atg7 -Based Autophagy Activation Reverses Doxorubicin-Induced Cardiotox- icity". In: *Circulation Research* (2021), E166–E182. issn: 15244571. doi: 10.1161/CIRCRESAHA. 121.319104.

[Wen+19] Nadine Wenningmann et al. *Insights into doxorubicin-induced cardiotoxicity: Molecular mecha- nisms, preventive strategies, and early monitoring*. 2019. doi: 10.1124/mol.119.115725.

[WHB16] Marit Wiersma, Robert H. Henning, and Bianca J.J.M. Brundel. "Derailed Proteostasis as a De- terminant of Cardiac Aging". In: *Canadian Journal of Cardiology* 32 (9 Sept. 2016), 1166.e11– 1166.e20. issn: 0828282X. doi: 10.1016/j.cjca.2016.03.005.

[Wil+19] Monte S. Willis et al. "Doxorubicin Exposure Causes Subacute Cardiac Atrophy Dependent on the Striated Muscle-Specific Ubiquitin Ligase MuRF1". In: *Circulation: Heart Failure* 12 (3 Mar. 2019). issn: 19413297. doi: 10.1161/CIRCHEARTFAILURE.118.005234.

[WMG92] Sue Wickner, Michael R Maurizi, and Susan Gottesman. *66. M. Molinari and A. Helenius, unpub- lished data. 67. F. Melchers*. 1992, p. 687. url: https://www.science.org.

[WP13] Monte S. Willis and Cam Patterson. "Proteotoxicity and Cardiac Dysfunction — Alzheimer's Disease of the Heart?" In: *New England Journal of Medicine* 368 (5 Jan. 2013), pp. 455–464. issn: 0028-4793. doi: 10.1056/NEJMra1106180.

[WPJ20] Marian Wesseling, Julius H.C. de Poel, and Saskia C.A. de Jager. *Growth differentiation factor 15 in adverse cardiac remodelling: from biomarker to causal player*. Aug. 2020. doi: 10.1002/ehf2. 12728.

[WR14] Xuejun Wang and Jeffrey Robbins. "Proteasomal and lysosomal protein degradation and heart dis- ease". In: *Journal of Molecular and Cellular Cardiology* 71 (June 2014), pp. 16–24. issn: 00222828. doi: 10.1016/j.yjmcc.2013.11.006.

[WRH10] Zhao V. Wang, Beverly A. Rothermel, and Joseph A. Hill. *Autophagy in hypertensive heart disease*.Mar. 2010. doi: 10.1074/jbc. R109.025023.

[Wu+11] Chung Yin Wu et al. "Induction of HSPA4 and HSPA14 by NBS1 overexpression contributes to NBS1-induced in vitro metastatic and transformation activity". In: *Journal of Biomedical Science* 18 (1 2011). issn: 10217770. doi: 10.1186/1423-0127-18-1.

[XBR13] Xihui Xu, Richard Bucala, and Jun Ren. "Macrophage migration inhibitory factor deficiency aug- ments doxorubicin-induced cardiomyopathy." In: *Journal of the American Heart Association* 2 (6 2013). issn: 20479980. doi: 10.1161/JAHA.113.000439.

[Xia+19] Bin Xiao et al. *The true colors of autophagy in doxorubicin-induced cardiotoxicity (Review)*. Sept.2019. doi: 10.3892/ol.2019.10576.

[Yam19] Osamu Yamaguchi. "Autophagy in the heart". In: *Circulation Journal* 83 (4 Apr. 2019), pp. 697– 704. issn: 13474820. doi: 10.1253/circj.CJ-18-1065.

[Yan+15] Zongguo Yang et al. "Upregulation of heat shock proteins (HSPA12A, HSP90B1, HSPA4, HSPA5 and HSPA6) in tumour tissues is associated with poor outcomes from HBV-related early-stage hepatocellular carcinoma". In:

International Journal of Medical Sciences 12 (3 Feb. 2015), pp. 256– 263. issn: 14491907. doi: 10.7150/ijms.10735.

[Yan+16] Jin Yang et al. "Targeting LOXL2 for cardiac interstitial fibrosis and heart failure treatment". In:*Nature Communications* 7 (Dec. 2016). issn: 20411723. doi: 10.1038/ncomms13710.

[Yi+07] Lisa Lyu Yi et al. "Topoisomerase IIb-mediated DNA double-strand breaks: Implications in dox- orubicin cardiotoxicity and prevention by dexrazoxane". In: *Cancer Research* 67 (18 Sept. 2007), pp. 8839–8846. issn: 00085472. doi: 10.1158/0008-5472.CAN-07-1649.

[YK10] Zhifen Yang and Daniel J. Klionsky. *Eaten alive: A history of macroautophagy*. 2010. doi: 10.1038/ncb0910-814.

[YM17] Saori R. Yoshii and Noboru Mizushima. *Monitoring and measuring autophagy*. Sept. 2017. doi:10.3390/ijms18091865.

[Yu+20] Wei Yu et al. "Curcumin suppresses doxorubicin-induced cardiomyocyte pyroptosis via a PI3K/Akt/mTOR- dependent manner". In: *Cardiovascular Diagnosis and Therapy* 10 (4 Aug. 2020), pp. 752–769. issn: 22233652. doi: 10.21037/cdt-19-707.

[Zec+20] Antonia T.L. Zech et al. *Autophagy in cardiomyopathies*. Mar. 2020. doi: 10.1016/j.bbamcr.2019.01.013.

[Zha+07] Jinghui Zhao et al. "FoxO3 Coordinately Activates Protein Degradation by the Autophagic/Lysosomal and Proteasomal Pathways in Atrophying Muscle Cells". In: *Cell Metabolism* 6 (6 Dec. 2007), pp. 472–483. issn: 15504131. doi: 10.1016/j.cmet.2007.11.004.

[Zha+14] Deli Zhang et al. "Activation of histone deacetylase-6 induces contractile dysfunction through derailment of a-tubulin proteostasis in experimental and human atrial fibrillation". In: *Circulation* 129 (3 Jan. 2014), pp. 346–358. issn: 00097322. doi: 10.1161/CIRCULATIONAHA.113.005300.

[Zha+21] Mingliang Zhang et al. "Hspa4 knockdown retarded progression and development of colorectal cancer". In: *Cancer Management and Research* 13 (2021), pp. 4679–4690. issn: 11791322. doi: 10.2147/CMAR.S310729.

[Zhu+07] Hongxin Zhu et al. "Cardiac autophagy is a maladaptive response to hemodynamic stress". In: *Journal of Clinical Investigation* 117 (7 July 2007), pp. 1782–1793. issn: 00219738. doi: 10.1172/ JCI27523.

[Zil+18] Rita Zilinyi et al. "The cardioprotective effect of metformin in doxorubicin-induced cardiotoxicity: The role of autophagy". In: *Molecules* 23 (5 2018). issn: 14203049. doi: 10.3390/molecules23051184.

[Zor+09] Leonardo A M Zornoff et al. *Ventricular Remodeling after Myocardial Infarction: Concepts and Clinical Implications*. 2009.

[ZQ11] Xingqian Zhang and Shu Bing Qian. "Chaperone-mediated hierarchical control in targeting mis- folded proteins to aggresomes". In: *Molecular Biology of the Cell* 22 (18 Sept. 2011), pp. 3277–3288. issn: 10591524. doi: 10.1091/mbc.E11-05-0388.

[ZRI10] Faiez Zannad, Patrick Rossignol, and Wafae Iraqi. *Extracellular matrix fibrotic markers in heart failure*. July 2010. doi: 10.1007/s10741-009-9143-0.

Acknowledgements

I would like to extend my heartfelt appreciation and gratitude to Dr. med. Belal Mohamed for his invaluable contributions to my research project. Dr. Mohamed's expertise, dedication, and collaborative spirit have played a pivotal role in advancing my work and achieving meaningful results.

I am grateful to Prof. Karl Toischer for providing me with the opportunity to work in his laboratory on this intriguing project. My sincere thanks also go to my thesis committee members Prof. Susanne Lutz and Prof. Michael Thumm for their active support, valuable scientific criticism, and the friendly atmosphere in our annual meetings. Additionally, I express my gratitude to Prof. Ralf Dressel, Prof. Elisabeth Heßmann, and Dr. Shiv Singh for agreeing to join my extended examination board.

Furthermore, I am thankful to the German Research Foundation (DFG) under grant number MO 3373/1-1 for funding this project and to the Göttingen Graduate Center for Neurosciences, Biophysics, and Molecular Biosciences (GGNB) for awarding me the end of project bridging fund.

I would like to express my appreciation to the entire Toischer-Schnelle-Seidler-Lab for their support and the positive working atmosphere. I am grateful to the SFB1002 Service Unit, including Sabrina, Sarah, and Marcel, for their excellent work with all the surgeries and echoes. I would also like to acknowledge the caretakers for their diligent care of the mice throughout the years, and I am thankful to all the students who have come to the Toischer lab to learn and have provided assistance.

I am deeply grateful to my family and friends for their continuous support in my studies. I would like to thank Dawid for his teachings, and my friends Eric and Lennard for reviewing the drafts of this thesis. I express my gratitude to Tamara and Friedi for always being there to listen, and special thanks to Arya for her unwavering support during challenging times. Lastly, I would like to thank Valentina for always believing in me and for all that she has given me.